Extension of Viscoplasticity Based on Overstress to Capture the Effects of Prior Aging on the Time Dependent Deformation Behavior of a High-Temperature Polymer: Experiments and Modeling

DISSERTATION

Amber J.W. McClung, Civ

AFIT/DS/ENY/08-D15

DEPARTMENT OF THE AIR FORCE
AIR UNIVERSITY

AIR FORCE INSTITUTE OF TECHNOLOGY

Wright-Patterson Air Force Base, Ohio

The views expressed in this work are those of the author and do not reflect the official policy or position of the United States Air Force, Department of Defense, or the United States Government.

AFIT/DS/ENY/08-D15

Extension of Viscoplasticity Based on Overstress to Capture the Effects of Prior Aging on the Time Dependent Deformation Behavior of a High-Temperature Polymer: Experiments and Modeling

DISSERTATION

Presented to the Faculty

Department of Aeronautics and Astronautics

Graduate School of Engineering and Management

Air Force Institute of Technology

Air University

Air Education and Training Command

In Partial Fulfillment of the Requirements for the

Degree of Doctor of Philosophy in Aeronautical Engineering

Amber J.W. McClung, B.S.M.E., M.S.E.

Civ

October 2008

AFIT/DS/ENY/08-D15

Extension of Viscoplasticity Based on Overstress to Capture the Effects of Prior Aging on the Time Dependent Deformation Behavior of a High-Temperature Polymer: Experiments and Modeling

Amber J.W. McClung, B.S.M.E., M.S.E.

Civ

Approved:

/signed/	15 Oct 08
Dr. Marina B. Ruggles-Wrenn Committee Chairman	date
/signed/	15 Oct 08
Dr. Robert A. Canfield Committee Member	date
/signed/	15 Oct 08
Dr. Robert L. Hengehold Committee Member	date
/signed/	15 Oct 08
Dr. Richard B. Hall Committee Member	date
/signed/	15 Oct 08
Dr. Greg A. Schoeppner Committee Member	date

Accepted:

/signed/	30 Oct 08
Dr. M. U. THOMAS Dean, Graduate School of Engineering and Management	date

Abstract

The inelastic deformation behavior of PMR-15 neat resin, a high-temperature thermoset polymer, was investigated at 288 $^{\circ}C$. The experimental program was designed to explore the influence of strain rate on tensile loading, unloading, and strain recovery behaviors. In addition, the effect of the prior strain rate on the relaxation response of the material, as well as on the creep behavior following strain controlled loading were examined. The material exhibits positive, nonlinear strain rate sensitivity in monotonic loading. Nonlinear, "curved" stress-strain behavior during unloading is observed at all strain rates. The recovery of strain at zero stress is strongly affected by prior strain rate. The prior strain rate also has a profound influence on relaxation behavior. The rest stresses measured at the termination of relaxation tests form the relaxation boundary which resembles a nonlinear stress-strain curve. Likewise, creep response is significantly influenced by prior strain rate. The experimental results suggest that the inelastic behavior of the PMR-15 solid polymer at 288 $^{\circ}C$ can be represented using a unified constitutive model with an overstress dependence of the inelastic rate of deformation. The experimental data were modeled with the Viscoplasticity Based on Overstress (VBO) theory. A systematic procedure for determining model parameters was developed and the model was employed to predict the response of the material under various test histories. Additionally the effects of prior aging at 288 $^{\circ}C$ in argon on the time (rate)-dependent behavior of the PMR-15 poly-

mer were evaluated in a series of strain and load controlled experiments. Based on experimental results, the VBO theory was extended to capture the environmentally induced changes in the material response. Several of the VBO material parameters were expanded as functions of prior aging time. The resulting model was used to predict the high-temperature behavior of the PMR-15 polymer subjected to prior aging of various durations.

Acknowledgements

First and foremost, I owe a large debt of gratitude to Dr. Ruggles-Wrenn for her enthusiastic guidance and support throughout my studies at AFIT. I have been truly fortunate to have such an exceptional mentor. I would like to thank Dr. Robert Canfield, Dr. Robert Hengehold, Dr. Richard Hall, and Dr. Greg Schoeppner for serving as members of my advisory committee. Whether in the classroom, in discussions directly related to my research subject, or general considerations of state-of-the-art research, their willingness to share their vast knowledge in their respective areas of expertise has been of valuable assistance.

I would also like to thank the AFIT Materials Testing Laboratory staff for their assistance; Jay Anderson and Barry Page for supporting the first operation of the MTS equipment at AFIT in strain control, John Hixenbaugh for his assistance with the argon gas and aging, and Chris Zickefoose and Sean Miller for their assistance keeping the experimental equipment operational.

And of course, I would like to convey my gratitude to my husband. Without his constant willingness to assist in the realm of Linux and cluster computing, the modeling portion of this research would not have been completed in such a timely fashion. His companionship along this scholarly journey has continuously reinforced my ambition to pursue this research.

Amber J.W. McClung

Table of Contents

Page

List of Figures

List of Tables

List of Symbols

Symbol		Page
k	Viscosity Function	42
A	Isotropic Stress	42
Ψ	Shape Function	42
f	Kinematic Stress	42
k_1	Material Constants of the Viscosity Function	42
k_2	Material Constants of the Viscosity Function	42
k_3	Material Constants of the Viscosity Function	42
A_f	Saturated Value of Isotropic Stress	42
C_1	Constant of the Shape Function	43
C_2	Constant of the Shape Function	43
C_3	Constant of the Shape Function	43
E_t	Tangent Modulus	43
A_o	Initial Value of Isotropic Stress	47
T_g	Glass Transition Temperature	49
$u(t)$	Controller Output Signal	60
$e(t)$	Control System Error	60
t_a	Aging Time	149

List of Abbreviations

Extension of Viscoplasticity Based on Overstress to Capture the Effects of Prior Aging on the Time Dependent Deformation Behavior of a High-Temperature Polymer: Experiments and Modeling

I. Introduction

1.1 Motivation

The drive to develop aircraft that have a reduced weight while maintaining structural integrity has positioned engineering materials with a higher specific strength as a sought-after commodity. Polymer matrix composites (PMC's) fit well into this role, and are in fact used in many aircraft components today. However, reliable life prediction methods for the PMC structural components do not currently exist. Experimentally-based, durability-driven predictive models are critical to assuring structural integrity and safe operation of the aircraft structural components utilizing PMC's.

The growing interest in the use of PMC's in critical load-bearing structures commands extensive knowledge of the mechanical behavior as well as of the durability of these materials. To analyze or predict the behavior of the composite material, it is essential to evaluate the contribution of the matrix to the overall mechanical response of the composite. Current design and analysis methods utilized for polymer matrix materials rely mainly on elastic and/or linear viscoelastic models of material behavior.

Because most structural polymers exhibit elastic or linear viscoelastic response only over a small portion of the material's load bearing capacity, high safety factors are applied and the material is not used to its full potential. In order to reduce the safety factors and greatly reduce the weight of PMC components, the inelastic material response must be incorporated into design and analysis procedures.

Recent efforts at the Air Force Institute of Technology demonstrated that polymers exhibit rate-dependent behavior [15, 16, 62, 75]. It was also shown that this behavior is not represented by linear or nonlinear viscoelasticity. Therefore, to represent the mechanical behavior of these polymers, rate-dependent viscoplasticity is needed. While several viscoplastic models exist, the Viscoplasticity Based on Overstress (VBO) has been demonstrated to account for some aspects of the deformation behavior of solid polymers [4, 5, 11, 12, 20, 23, 25–28, 42, 43, 45]. Based on experimental findings, a specialization of this model for polymers, the Viscoplasticity Based on Overstress for Polymers (VBOP), has been developed [20, 26–28, 41]. Despite the capability to represent inelastic material behavior, most viscoplastic models are not used by designers because of a lack of clear, consistent, experimentally-based model characterization procedures. Unfortunately, the VBOP is not exempt from this trend.

Thermal aging has been shown to notably affect the mechanical properties of polymers [6, 7, 63, 71] and PMC's [19, 48, 66]. Given that aerospace components must operate at high temperatures for extended periods of time, thermal aging of polymer containing components becomes a vital issue. To assure environmental durability of

polymer matrix materials, the effects of prior aging must be incorporated into the material constitutive equations and life prediction models.

Thus in order to develop the needed experimentally-based, durability-driven predictive models two major obstacles must be overcome: (1) a comprehensive, systematic characterization scheme must be developed and (2) aging must be incorporated into the model formulation. Both of these key issues for the VBOP are addressed in this research effort.

This research combines experimental investigations with the numerical modeling of the inelastic material behavior. A Polymerization of Monomeric Reactants-15 (PMR-15) polymer is investigated in the experimental studies. Among the various types of polymer resins, this polyimide resin is of particular interest because of its enhanced high-temperature properties and ease of processing [6, 57]. Designed for use at temperatures near its glass transition temperature, the PMR-15 polymer is extensively used as a matrix material in high-temperature structural composites for aerospace applications. Composites utilizing PMR-15 as matrix material are capable of service temperatures up to 300 $^{\circ}C$ [52]. Because PMR-15 is designed for use in high-temperature structural components, the need for a model capable of predicting the effects of aging on the mechanical performance of this material cannot be overestimated. It should be noted that introducing aging into the constitutive model does not equate to simply predicting changes in basic material properties such as elastic modulus, E. More accurately, the final model should be able to predict the response of material to various types of loading as a function of its aging history. With en-

Table 1.1: Free Standing Post Cure Cycle for PMR-15 Neat Resin

Step	Description
1	Heat to 204 $^{\circ}C$ in 2 h and hold for 1 h
2	Heat to 260 $^{\circ}C$ in 1 h and hold for 1 h
3	Heat to 316 $^{\circ}C$ in 2 h and hold for 16 h
4	Cool to room temperature at a rate of 1 $^{\circ}C/min$

hancement of life prediction methods in mind, the current research aims to answer the following questions. What are the qualitative and quantitative effects of prior aging on the mechanical deformation behavior of PMR-15? How can the existing VBOP formulation be expanded to account for these changes?

1.2 Material Description

This research focuses on PMR-15 solid polymer which is a thermosetting polyimide used as a matrix material for high-temperature Polymer Matrix Composites (PMC's). The PMR-15 polyimide has a glass transition temperature of 347 $^{\circ}C$ [7] and a long-term use temperature of 288 $^{\circ}C$ [57]. This highly cross-linked polyimide resin was developed by NASA specifically for use in high-temperature aerospace structural applications. The post-cured PMR-15 neat resin samples were supplied by HyComp, Inc. (Cleveland, OH). The standard free standing post cure cycle used by the Air Force Research Laboratory is shown in Table 1.1. It is assumed that the specimens were exposed to this post cure cycle.

1.3 Polymer Aging

All polymers experience some degree of degradation when subjected to temperatures at which their covalent bonds start to break down. Chain scission and additional cross-linking take place, not only degrading the polymer chain, but also changing its morphology and mechanical material properties. Polymer degradation occurs rapidly when it is exposed to temperatures well above its glass transition temperature [6]. At lower temperatures, degradation occurs at a much slower rate, consequently the mechanical properties and material behaviors change slowly over time as well [7, 63]. This can be commonly observed as a material becomes brittle and stiff after prolonged exposure to elevated temperatures.

Researchers in the field of the inelastic constitutive models offer several definitions of aging. Lemaitre [49] described aging as the change of the characteristic properties of a material with time. Krempl [34, 37] differentiated between "prior aging" (diffusion processes with chemical reactions which occur in the absence of deformation and which proceed independently of it) and "strain aging" (diffusion processes with chemical reactions which are influenced by deformation).

For the purpose of the current research, the following definitions are be adopted:

- prior aging: mechanical property/behavior changes induced by exposure to elevated temperature prior to deformation
- strain aging: property changes induced by deformation

- environmental stability: material properties and deformation behavior are not affected by either prior aging or strain aging [34]

The current effort focuses on the effects of prior aging on the material properties and mechanical responses of PMR-15. Hence, material properties and deformation behavior of the material are analyzed as a function of prior aging time. As a result, dependence on prior aging time is incorporated into the constitutive model. This approach assumes that deformation induced aging, or strain aging, does not occur. Recent experimental evidence [7,63] revealed that the effects of strain aging (i.e. aging due to deformation at elevated temperature) were negligible provided the duration of deformation/loading was less than 50 h. Because the current experiments are of less than 50 h duration, a simplifying assumption that the strain aging can be neglected is reasonable.

1.4 Problem Statement

Previous experimental investigations into the high temperature mechanical response of polymers revealed that these materials exhibit rate-dependent deformation behavior [3, 15, 16, 62, 75]. The Viscoplasticity Based on Overstress for Polymers (VBOP) was shown to qualitatively represent the rate-dependent behaviors observed in experiments [20, 26–28, 41]. However, the procedure for characterizing material constants and functions included in the VBOP formulation is lacking. The currently available model characterization method relies extensively on experience and intu-

ition as well as on the "trial-and-error" approach [25, p. 138] rather than on a clearly defined set of short-term experiments and data reduction procedures.

The objective of this effort is two-fold. First, a systematic experimentally-based model characterization scheme for the VBOP is developed. Development of a clearly defined model characterization procedure enables wide utilization of the VBOP in practical design analysis. This systematic characterization procedure is a significant contribution toward extending current life prediction methodologies to include inelastic material behavior. Second, the effects of prior aging on high-temperature inelastic deformation behaviors of a solid polymer is investigated experimentally. Based on the results of this experimental study, the VBOP constitutive formulation is extended to account for the effects of prior aging on the time-dependent deformation response of solid polymers. The research focuses on PMR-15 neat resin in a laboratory air environment.

The following problem statement summarizes the objectives of this research:

> *Develop a systematic, experimentally-based model characterization procedure for Viscoplasticity Based on Overstress for Polymers. Identify the effects of prior aging at elevated temperature on PMR-15 neat resin. Develop an analytical capability to account for the observed effects within the constitutive framework of Viscoplasticity Based on Overstress for Polymers.*

1.5 Methodology

The key objectives outlined in the problem statement were accomplished by the following tasks:

1. Develop/validate a computer code for the VBOP.
2. Demonstrate the ability of the VBOP to qualitatively model PMR-15 behavior using data from current and past work at AFIT.
3. Elucidate the effects of prior aging on the deformation behavior of PMR-15 neat resin.
4. Develop and validate a comprehensive procedure for characterizing the VBOP.
5. Develop an analytical capability within the VBOP to account for effects of prior aging.
6. Demonstrate the VBOP with prior aging.

1.6 Dissertation Outline

Chapter II gives a general background. Results of several experimental investigations into the time-dependent deformation of solid polymers as well as experimental studies of the effects of prior aging on the subsequent material response are presented. Linear and nonlinear viscoelastic constitutive modeling approaches are discussed. The concept of viscoplastic material behavior is introduced and a historical development of the VBO and the VBOP is described. Chapter III gives a detailed description of the mathematical formulations of the VBO and the VBOP. The differences between the VBO and the VBOP are explained. Chapter IV presents experimental procedures. The experimental tools and techniques developed specifically to reveal the rate (time)-dependent behavior of the solid polymer are discussed in detail. The

experiments outlined in Chapter IV are conducted for the unaged material as well as the material subjected to various degrees of prior aging. This chapter also describes the aging procedure and equipment. Chapter V is devoted to the experimental observations of the unaged material mechanical behavior and Chapter VI discusses the implications for modeling the observed material behavior. Chapter VII is devoted to modeling of the unaged material behavior utilizing VBOP. This chapter includes a detailed description of the systematic characterization procedure which was developed within this research to find the constants from experimental data. Chapters VIII, IX, and X discuss the aged material behaviors. Chapter VIII focuses on the experimentally observed effects of the aging on the material mechanical behavior while Chapter IX discusses the implications for including the effects of prior aging in the modeling of the material behavior. Chapter X discusses the extension of the VBOP to account for the effects of prior thermal aging. Suggested directions of future research as well as concluding remarks are offered in Chapter XI.

II. Background and Previous Research

This chapter describes experimental and modeling efforts that have been reported in literature, as well as how these findings set the groundwork for the current research.

2.1 Prior Work: Experimental Investigations

This sections outlines previous experimental work sorted by the material behavior feature that was under examination.

2.1.1 Deformation Behavior of Polymers. This section discusses some aspects of the deformation behavior of polymers. Experimental results were examined.

2.1.1.1 Various Polymers – Mechanical Behavior in the 15 *to* 40 $°C$ *Range.* Kitagawa and Matsutani [29] examined the time-dependent mechanical behavior of Polypropylene (PP) in compression at 15, 25, and 40 $°C$. Kitagawa, Zhou, and Qiu [30] also examined the mechanical behavior of several polymers, specifically crystalline Polyoxymethylene (POM), amorphous Polycarbonate (PC), and amorphous Polymethyl Methacrylate (PMMA) in tension and compression at 25 $°C$. In these tests, they found that the initial slope of the stress-strain curves was independent of the strain rate. They also found that as the strain increased, the stress-strain curves became dependent on the strain rate and were finally parallel to each other. Note that similar mechanical behavior is exhibited by engineering alloys. Kitagawa and co-workers also observed evidence confirming existence of an equilibrium stress in

relaxation. (The equilibrium stress can be viewed as the stress that the material can sustain as all rates approach zero.) They reported that the stress (strain) rate may change signs during relaxation (creep) during unloading, referred to as rate reversal. Constitutive modeling of polymer mechanical behavior carried out by Kitagawa et al. using an overstress model is discussed in Section 2.2.2.1.

Bordonaro [5] expanded the study of rate-dependent mechanical behavior into the realm of thermoplastics. Her research focused primarily on Nylon-66 using both stress and strain-controlled experiments. Bordonaro also investigated Polyetheretherketone (PEEK) and Polyetherimide (PEI). Results demonstrated that the solid polymers exhibited similar mechanical response to that exhibited by engineering alloys. Bordonaro also identified some key differences in mechanical responses of polymers and that of engineering alloys. Those differences include:

- higher relaxation rates
- increased strain recovery after unloading to zero stress
- curved unloading in stress control
- reduced rate-dependence of the unloading curves
- merging of stress-strain curves produced at different strain rates

Khan [25] further extended Bordonaro's study to include PC, High Density Polyethylene (HDPE), Polyethylene Terephthalate (PET), Polyphenylene Oxide (PPO), and Polyether Sulfone (PES). Khan divided the polymers in his study into two groups amorphous and crystalline. The amorphous materials are PC, PPO, and PES and the

crystalline are Nylon-66, HDPE, PET. He found that all of these materials exhibited four key behavior features:

- positive non-linear rate sensitivity in loading,
- nonlinear dependence of the response in creep, relaxation, and recovery tests on the prior loading rate,
- the stress drop in relaxation tests conducted in the region where inelastic flow is fully established was found to be independent of the test strain value,
- reversal of stress (strain) rate in the case of relaxation (creep) during unloading.

("Rate reversal" refers to the change in sign of the rate of change of stress or strain. "Inelastic flow" is another name given to plastic flow.)

Collectively, these investigations demonstrate that solid polymers exhibit mechanical behaviors that are similar to those exhibited by engineering alloys. They also showed that the VBO can be utilized to model not only the mechanical response of the engineering alloys, but also the mechanical response of polymers [4,5,25,29,30]. Khan [25] pointed out that the standard VBO shows the capability to qualitatively capture some of the material behavior features reported in References [5] and [25]. Khan also reported that the VBO did not capture the curved unloading or the rate reversal.

2.1.1.2 PMR-15 – Mechanical Behavior at Room and Elevated Temperatures. The time-dependent behavior of PMR-15 was studied by Westberry [75] at room temperature and at 288 $^{\circ}C$. Westberry conducted tests using using different stress rates at 23 and 288 $^{\circ}C$. Westberry reported that at 288 $^{\circ}C$, PMR-15 polymer exhibits behavior that is dependent upon the prior stress rate in both creep and recovery tests. Westberry pointed out the need for a rate history dependent constitutive equation to describe the deformation behavior of PMR-15 at elevated temperatures. Falcone and Ruggles-Wrenn [15] conducted further experiments on PMR-15 neat resin at 288 $^{\circ}C$. These results also showed that the creep and relaxation behaviors of the material are dependent upon the prior stress rate. Creep response of PMR-15 at 288 $^{\circ}C$ reported in Reference [16] is reproduced in Figure 2.1. Both Westberry [75] and Falcone and Ruggles-Wrenn [15] also observed a creep rate reversal in creep tests conducted on the unloading path in a stepwise creep test. Falcone and Ruggles-Wrenn [15] also conducted monotonic loading/unloading tests at various constant stress rates and reported that the material response was also dependent upon the rate of loading/unloading. Section 2.2.1.1 illustrates the use of viscoelastic models to predict the PMR-15 behavior at 288 $^{\circ}C$.

2.1.2 Prior Aging – Effects on Mechanical Behavior. Prior aging in materials that exhibit time-dependent behavior has been addressed in a very limited way. Krempl [36, 37] called for a separation of the effects of aging from other factors in order to obtain valid conclusions. He borrowed much of his reasoning and process

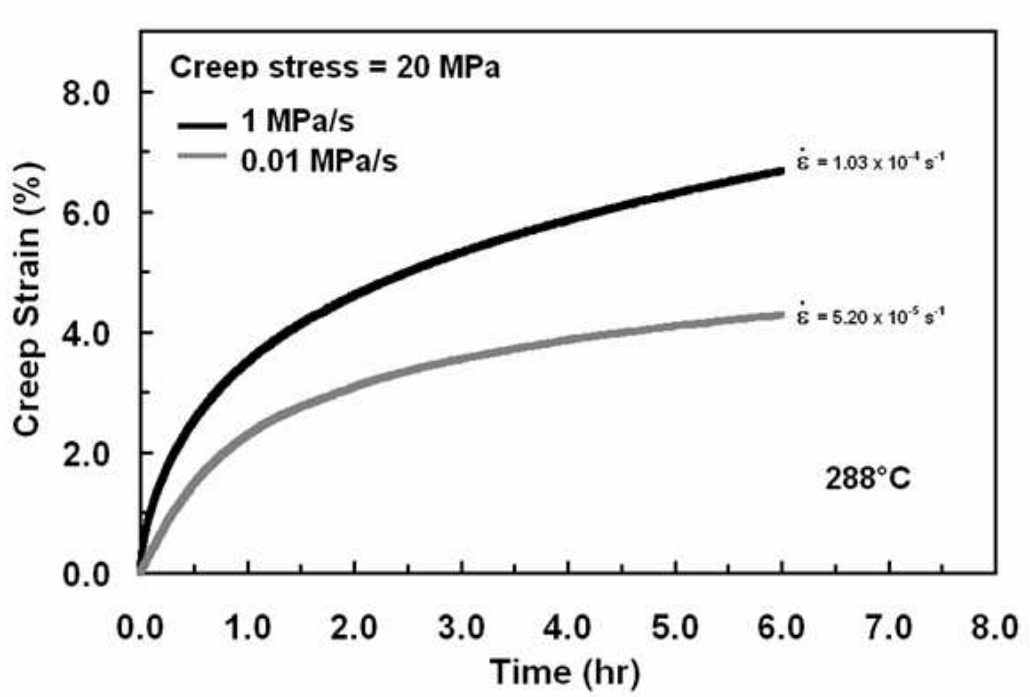

Figure 2.1: Creep Behavior of PMR-15 Following Stress-Controlled Loading at 288 $^{\circ}C$ Reproduced from Falcone [16]. Loading Rates of 0.01 and 1 MPa/s, Loading Rate Dependence is Evident.

from concrete technology, pointing out that tests must be repeated with specimens that have seen different durations of prior aging in order to examine the effects of exposure. He described a procedure to test for prior aging effects, in which the material is exposed to step changes in strain rate. He drew up the hypothesis stating that if at a constant strain rate, flow stress increases or decreases, then aging affects work hardening. (The flow stress is the applied stress in the region of fully developed plastic flow.) If a change in the spacing of the stress-strain curves obtained at different strain rates occurs, then aging affects the rate-dependence of the material.

Ruggles and Krempl [61] examined the effects of prior aging on AISI Type 304 stainless steel and found that it did not have a significant influence on the material behavior. Instead the material response was more influenced by strain aging.

Ruggles-Wrenn and Broeckert [63] investigated the effects of prior aging in air and in argon at 288 $^{\circ}C$ on PMR-15 polymer. They examined the weight loss, changes in dynamic modulus, and the growth of the oxidative layer with prior aging time. It was found that the material develops an oxidative layer when aged in air, but not in argon. They also investigated the effects of prior aging on the elastic modulus and the creep behavior. Despite the differences in oxidative layer growth, it was found that specimens aged in air and those aged in argon exhibited similar changes in elastic modulus and creep behavior. They reported that the elastic modulus increased with prior aging time and also observed that accumulated creep strain decreased with an increase in prior aging time.

2.2 Prior Work: Constitutive Modeling

This modeling review is sorted according to the type of model utilized.

2.2.1 Viscoelastic Constitutive Models. The first class of models considered is viscoelastic. This behavior is easiest to understand when compared and contrasted with simple linear elastic behavior. Figure 2.2 shows a graphical comparison of true stress, σ, versus true strain, ϵ, for (a) perfectly linear elastic behavior and for (b) viscoelastic behavior.

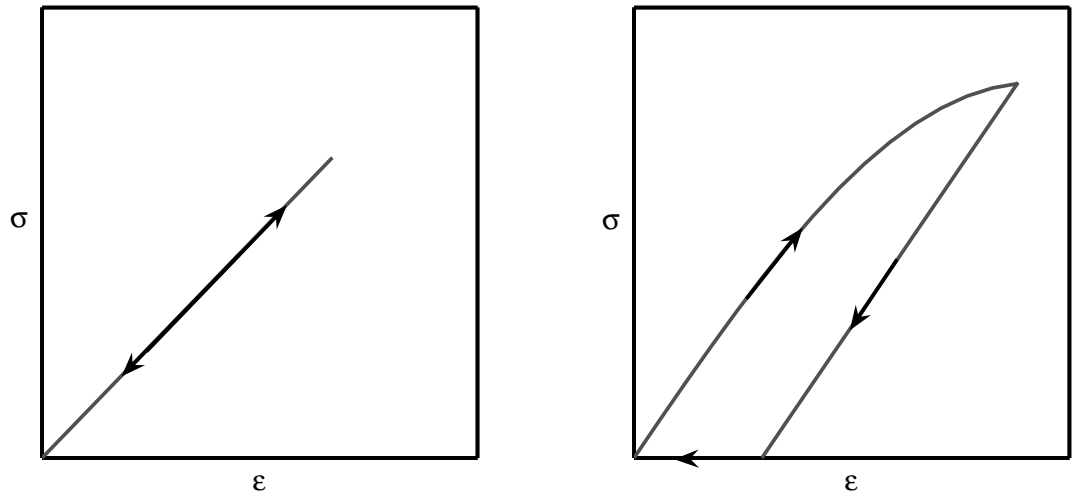

(a) Linear Elasticity (b) Viscoelasticity

Figure 2.2: Linear Elastic and Viscoelastic Stress-Strain Behavior. Viscoelastic Material Exhibits a Nonzero Strain Upon Unloading to Zero Stress. It Recovers this Strain If Given Time to Do So.

When a material exhibits perfectly elastic behavior, the unloading path is exactly the same as the loading path. The material also returns to zero strain after complete unloading to zero stress.

The viscoelastic material on the other hand does not necessarily have the same unloading path as the loading path. The material also exhibits a nonzero strain immediately after unloading to zero stress. However, the strain returns to zero with time.

The two general types of mathematical formulations used in viscoelastic models are integral and differential.

2.2.1.1 Integral Models. Schapery's Formulation is selected as an example of an Integral Model. This model is widely used largely because a sys-

tematic approach to material characterization exists which is based on creep and recovery tests. Weitsman's models are also presented in this section as they build upon Schapery's formulation.

Schapery's Model. Schapery [17] developed a constitutive model for nonlinear viscoelastic materials. This approach was originally empirically based, but is also consistent with the thermodynamics of irreversible processes. The nonlinearity is captured in a "reduced time". The resulting model is often referred to as the Standard Schapery's Model.

The equations formulate the stress-strain relationship using the term $D(t)$ which is called the creep compliance. The creep compliance is defined as the ratio of the strain response to a constant applied stress and is a function of time t.

$$D(t) = \frac{\epsilon(t)}{\sigma} \tag{2.1}$$

Schapery's [17,64] constitutive equations for constant temperature and uniaxial stress are as follows

$$\epsilon = \int_{0-}^{t} D(t-\tau)\frac{d\sigma}{d\tau}d\tau. \tag{2.2}$$

or

$$\epsilon(t) = g_o D_o \sigma + g_1 \int_{0-}^{t} \Delta D(\psi - \psi')\frac{dg_2\sigma}{d\tau}d\tau \tag{2.3}$$

where D_o is the initial linear compliance value

$$D_o \equiv D(0) \tag{2.4}$$

and ΔD is the transient compliance

$$\Delta D \equiv D(t) - D_o \tag{2.5}$$

ψ is the reduced time

$$\psi \equiv \int_0^t \frac{dt'}{a_\sigma[\sigma(t')]} \tag{2.6}$$

and

$$\psi' \equiv \psi(\tau) \equiv \int_0^\tau \frac{dt'}{a_\sigma[\sigma(t')]}. \tag{2.7}$$

The material properties g_o, g_1, g_2 and a_σ are functions of stress. Schapery [64] explains that changes in g_o, g_1, or g_2 reflect high-order thermodynamic dependencies. The property a_σ is a shift factor. These four material properties are functions that are characterized for a particular material by curve fitting procedures applied to creep and recovery data. Here creep is defined as a continuous deformation occurring under constant stress. Recovery is defined as continuously decreasing strain after the removal of stress (stress is held at zero). Schematics of creep and recovery tests are shown in Figure 2.3 for (a) viscoelastic and (b) viscoplastic material behaviors. Figure 2.3 illustrates that in viscoelastic creep and recovery, strain returns to zero with time, t. In viscoplastic creep and recovery, strain does not fully return to zero.

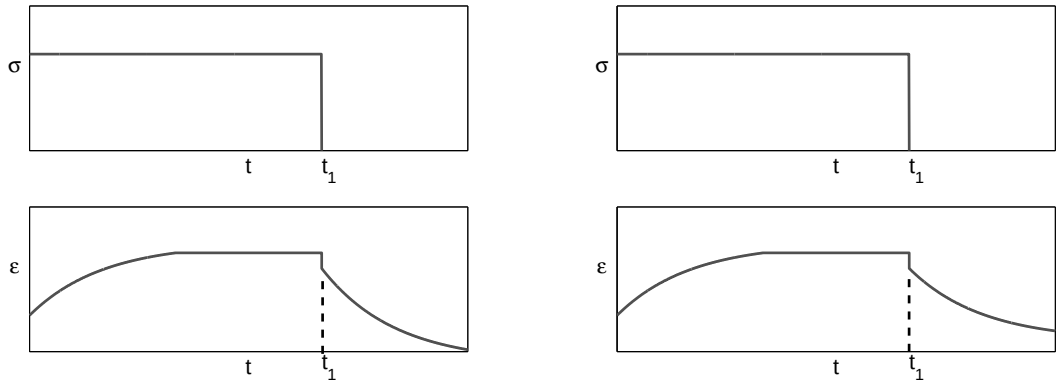

(a) Viscoelasticity (b) Viscoplasticity

Figure 2.3: Schematic of Viscoelastic and Viscoplastic Creep and Recovery Behavior. Viscoelastic Material Recovers All Strain Given Time to Do So. Viscoplastic Does Not Fully Recover.

Falcone and Ruggles-Wrenn [15] applied Schapery's model to PMR-15 at 288 $°C$. They demonstrated that this model is capable of capturing only some of the characteristic behaviors of the material. One aspect that Schapery's model represents qualitatively is the strain reversal in creep shown in Figures 2.4 and 2.5. However, the model does not account for the dependence of the creep strain on the rate history of the loading applied to the material.

Falcone also considered the addition of a viscoplastic term to Schapery's model following the approach suggested by Zaoutsos, Papanicolaou, and Cardon [81] and Papanicolaou and S.P. Zaoutsos and A.H. Cardon [58]. In this formulation the viscoplastic term was simply added to the creep and recovery equations. The form of the viscoplastic term was defined based on Cardon, Qin, and Vossole [8] as a power law strain. The parameters of Schapery's model with the added viscoplastic term were characterized by Falcone based on her experimental data on PMR-15. As part of

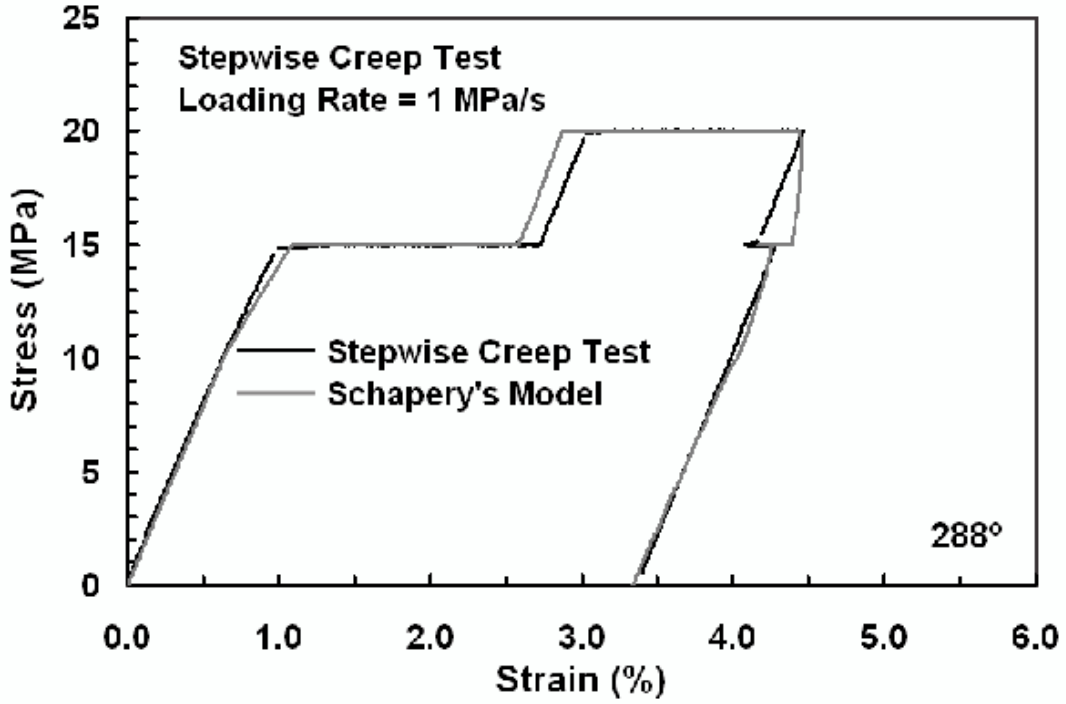

Figure 2.4: Stress-Strain Response in a Stepwise Creep Test of PMR-15 at 288 $^{\circ}C$: Experiment and Schapery's Model Reproduced from Falcone [16].

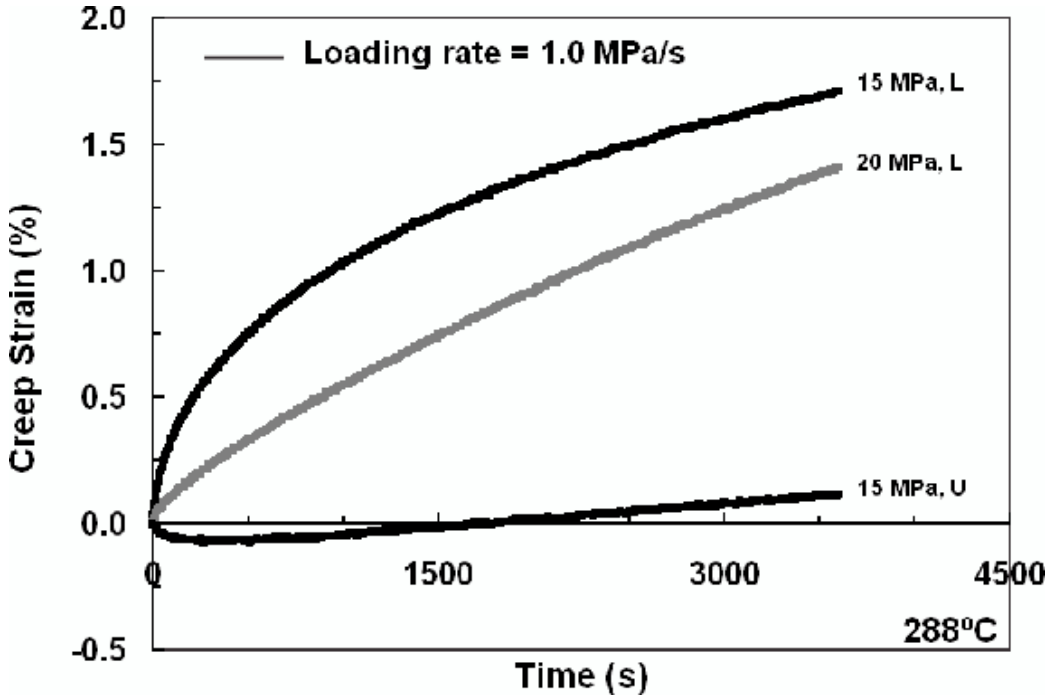

Figure 2.5: Creep Strain as a Function of Time for the Stepwise Creep Test of PMR-15 at 288 $^{\circ}C$ Reproduced from Falcone [16].

the current effort, the Schapery's model MATLAB code was expanded to include the viscoplastic term. Predictions were obtained using Schapery's model with the added viscoplastic term. The resulting simulations show improved predictive capability in recovery following stepwise creep (see Figure 2.6). However, the modified model still has no mechanism to account for rate effects. This is seen in Figure 2.7 where model predictions are compared with the experimental creep and recovery data for the case of a prior loading rate of 0.01 MPa/s. Notice that the shape of the predictions of the creep strain and of the recovered strain are the same regardless of the prior loading/unloading rate, while the experimental results show a difference in shape for the creep and recovery response following different loading/unloading rates. Note that the standard model characterization procedure is based on creep and recovery tests, where loading and unloading occurs at a fast rate of 1.0 MPa/s (ideally approaching step loading and step unloading).

Schapery [65] added a damage function to his original model which can also be used to account for aging. However, he proposed accounting for aging by measuring the length of the cracks that are formed in the material during the aging process. These cracks can then evaluated using the principles of fracture mechanics by means of the Gibbs free energy for viscoelastic material. When all of the cracks in the material are accounted for, their effect on the material behavior can be combined into a damage tensor α which is defined as

$$\alpha_{ij} \equiv \sum_{c} \frac{(l^2 n_i n_j)_c}{A_{ip}} \tag{2.8}$$

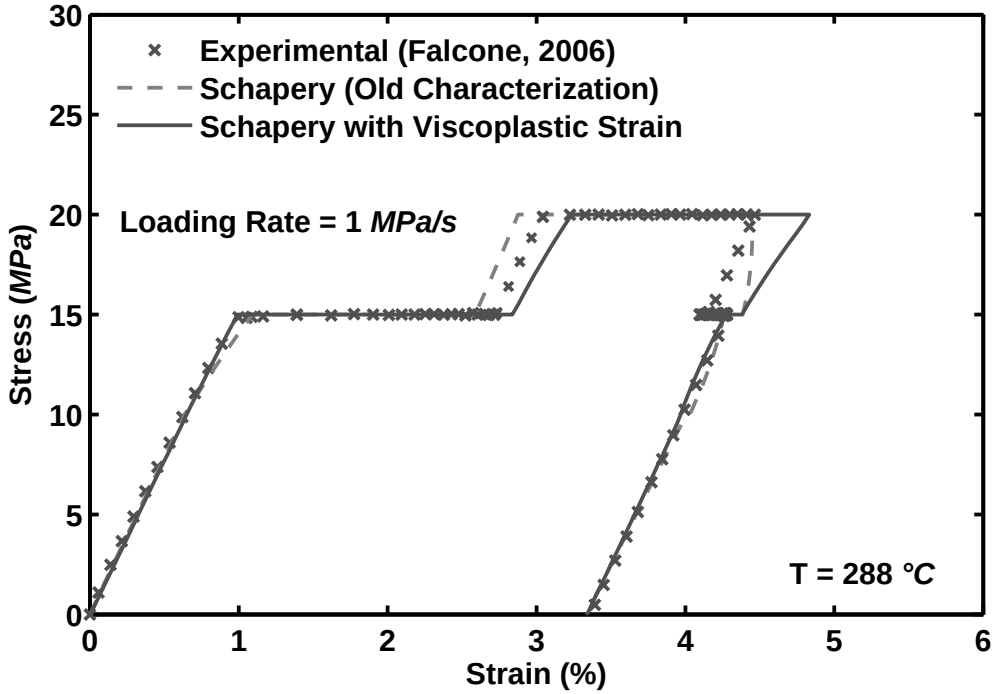

(a) Stepwise Creep

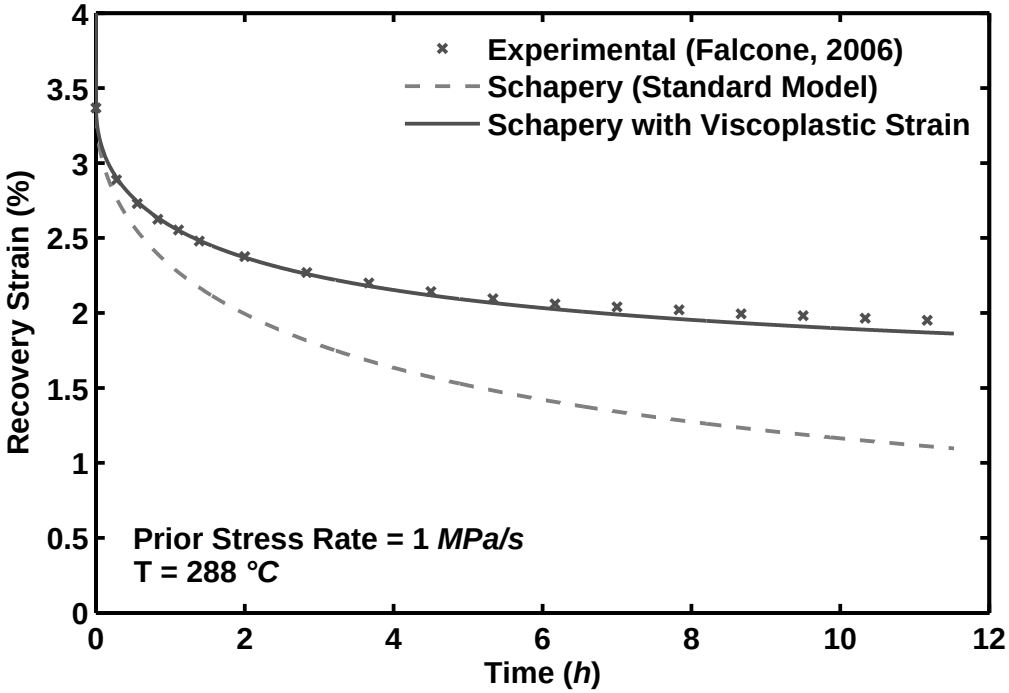

(b) Recovery Following Stepwise Creep

Figure 2.6: Step Creep Behavior of PMR-15 at 288 $°C$: Experiment, Schapery's Model, and Schapery's Model with Viscoplastic Addition. Viscoplastic Addition Does Improve the Fit in Recovery.

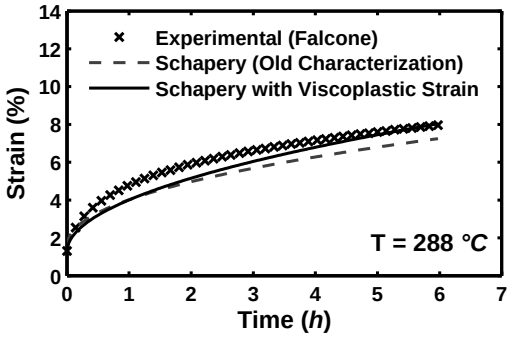

(a) Creep Following 1 MPa/s Loading Rate

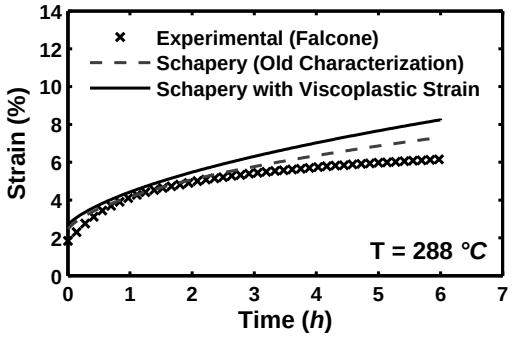

(b) Creep Following 0.01 MPa/s Loading Rate

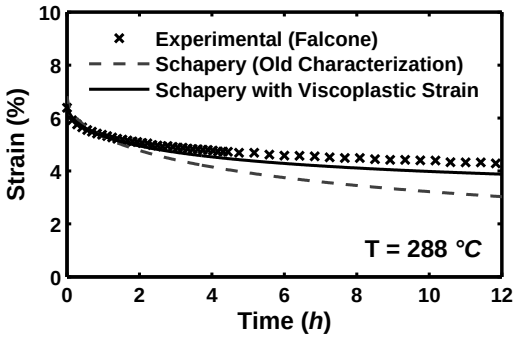

(c) Recovery Following 1 MPa/s Unloading Rate

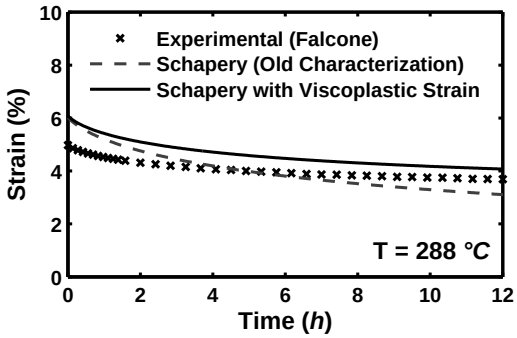

(d) Recovery Following 0.01 MPa/s Unloading Rate

Figure 2.7: Creep at 20 MPa and Recovery: Experiment, Schapery's Standard Model, and Schapery's Model with Viscoplastic Terms Added. Both Forms of Schapery's Model Fail to Account for the Rate Effects.

where $2l$ is the length of an individual crack, $\mathbf{n}$ is the local normal vector of the crack, and A_{ip} is the in-plane area of the material characteristic cell. For the uniaxial case, Schapery's model with the damage function has the form:

$$\epsilon(t) = g_o D_o \sigma + g_1 \int_{0-}^{t} \Delta D(\psi - \psi') \frac{dg_2\sigma}{d\tau} d\tau + 2\pi \int_{0-}^{t} D(t,\tau) \frac{d(\alpha_{11}\sigma)}{d\tau} d\tau \qquad (2.9)$$

which expands to

$$\begin{aligned}\epsilon(t) = \quad & g_o D_o \sigma + g_1 \int_{0-}^{t} \Delta D(\psi - \psi') \frac{dg_2\sigma}{d\tau} d\tau + \\ & 2\pi g_o D_o \alpha_{11} \sigma + 2\pi g_1 \int_{0-}^{t} \Delta D(\psi - \psi') \frac{dg_2\alpha_{11}\sigma}{d\tau} d\tau.\end{aligned} \tag{2.10}$$

Although Falcone and Ruggles-Wrenn [15] have shown that Schapery's standard model may not be appropriate for modeling PMR-15, Schapery's techniques for including damage effects provides a useful example of introducing prior aging effects into the VBOP. However, this method is not directly applicable because each crack has to be accounted for individually. This means that individual cracks would have to be identifiable. In the case of the PMR-15 polymer, prior aging causes the formation of a layer of oxidation instead of cracking in the material.

Weitsman's Model. Weitsman [73] investigated environmental (moisture) effects on fiber-reinforced polymeric composite properties. He coupled damage with moisture-transport into the material. Weitsman used a "representative damaged cell" and correlated damage to the amount of moisture absorbed. This theory is not limited to small damage. Weitsman [74] applied the concept to Schapery's standard model to develop a continuum damage viscoelastic model. The model accounts for both open and closed crack regions, and employs a damaged compliance (A_d). The uniaxial creep response is described by the following equation:

$$\epsilon/\sigma_o = D_o D_d + \int_0^t D_d \left[\frac{\partial(D + A_d)}{\partial a} \frac{\partial a}{\partial \tau} d\tau + \frac{\partial(D + A_d)}{\partial a^*} \frac{\partial a^*}{\partial \tau} d\tau \right] \tag{2.11}$$

where a and a^* are the open crack lengths and closed crack lengths respectively, D_d is a damage surface tensor of the open cracks, and D is the "classical" compliance and A_d is the damaged compliance. The model also includes a damage surface tensor of the closed cracks, D_d^*, which does not appear in the final equations. Weitsman does not explain in this work how to find a, a^*, D_d, or A_d experimentally. He does explain that a, D_d, a^*, and D_d^* are related in the following way:

$$a = \frac{\sum_{k=1}^{K} D_d D_d}{\Delta^2}, \quad a^* = \frac{\sum_{k}^{K} D_d^* D_d^*}{\Delta^2}, \tag{2.12}$$

where Δ is a characteristic area such as that of a wall of the Representative Volume Element (RVE), and K is the number of cracks in the material. Therefore, this method requires some way of counting the number of cracks.

Abdel-Tawab and Weitsman [1] expanded this formulation to include plastic behavior. The strain was divided into viscoelastic and plastic parts, and a tensor that accounts for damage (ω) is introduced. These damage tensors are fit into the uniaxial viscoelastic strain as follows. In the uniaxial case, the damage reduces to a scalar provided it does not depend on time or stress. Strain response to constant temperature and uniaxial stress given in Eq. (2.2) (Schapery' standard model) is now augmented by an additional term ϵ^v.

$$\epsilon^v = \int_{0-}^{t} D(t-\tau) \frac{d}{d\tau} \left(\frac{\sigma}{1-\omega} \right) d\tau. \tag{2.13}$$

However, no specific guidance is provided for the form of plastic strain. The example presented in Reference [1] covers only linear viscoelastic behavior and does not include the plastic strain term.

Smith and Weitsman [69] considered polymer matrix composites and correlated damage level to maximum applied stress. This in essence introduces a type of damage surface similar to a yield surface in plastic theory. The damage concentration factor (K), which is a function of stress, can be placed into Schapery's equation. Strain response to uniaxial stress is then given by:

$$\epsilon(t) = \int_0^t KD(t-\tau)\frac{d\sigma}{d\tau}d\tau. \tag{2.14}$$

Elahi and Weitsman [14] developed a relation between ω and K in the form

$$\omega = 1 - K_\sigma^{-1}. \tag{2.15}$$

This relation shows how Eq. (2.13) can be utilized if the concentration factor K is known.

Since Weitsman's approach is based on Schapery's standard model, it is not directly applicable to PMR-15. However, his methods for including damage effects into the model provides a useful example of the incorporation of damage effects into a constitutive model.

2.2.1.2 Differential Models. Ellyin and co-workers developed a Differential Nonlinear Viscoelastic model. Xia and Ellyin [76] began their work with the goal of developing a constitutive model that, once characterized, would accurately predict the mechanical response of all types of loading (e.g. creep, relaxation, compression, tension, biaxial, etc.). They started with a finite number of Kelvin elements connected in series coupled with an elastic spring and formulated the constitutive equations in differential form. They also allowed the spring elements to enter the nonlinear regime and used a power law to describe creep behavior.

In Reference [76], Xia and Ellyin utilized two Kelvin elements and had partial success in modeling stress-rate-dependent behavior. However, the resulting model, when characterized by one set of tests, did not model another type of tests successfully. The lack of capability to model loading and unloading within the same equation may be partially responsible for this shortcoming.

Hu, Xia, and Ellyin [24] and Xia, Hu, and Ellyin [77] added a function that accounted for loading and unloading. This model was expanded to include six Kelvin elements. A procedure for determining the material constants experimentally was outlined which includes tension and compression tests as well as axial creep tests. A nonlinear least squares fit procedure was recommended for the curve fitting. For the majority of the tests reported in References [24] and [77], this differential model predicts the Epoxy behavior more accurately than Schapery's standard model. Shen, Xia, and Ellyin [68] and Xia, Shen, and Ellyin [78] modified the switching rule for loading versus unloading and then used the differential model to simulate cyclic load-

ing of an epoxy polymer. This model had some success in modeling ratcheting strain. However, it did not successfully capture the recovery of ratcheting strain.

Zhang, Xia, and Ellyin [82, 83] approached the subject of damage evolution in polymer matrix composites with the differential model. In their composite model, the fiber material was assumed to behave elastically, the matrix was assumed to behave in a nonlinear viscoelastic fashion following Xia and Ellyin [76]. Ellyin and co-workers were concerned with strain aging resulting in the formation of cracks. A strain damage criterion was introduced, postulating that once the principal strain reaches a critical value, a crack is assumed to be present. Once this crack has formed, the constitutive equation for the matrix is simply set so that the stress level within the matrix will quickly decay to zero stress, thereby simulating the inability of the cracked matrix to transfer any stress. The critical value of strain for damage onset was based on test results on pure epoxy specimens. While this work represents an example of utilizing experimental evidence to create a damage criterion, it is concerned specifically with strain aging, which is not the focus of the current research.

2.2.2 Viscoplastic Constitutive Models. The concepts of mechanical material behavior can be expanded to include viscoplastic behavior. (This is the type of behavior that can be observed in the laboratory with PMR-15.) Figure 2.8 shows a graphical comparison of (a) viscoelastic behavior and (b) viscoplastic behavior.

Viscoelastic behavior is characterized by nonzero strain immediately after unloading to zero stress. The strain, however, returns to zero with time. Viscoplastic

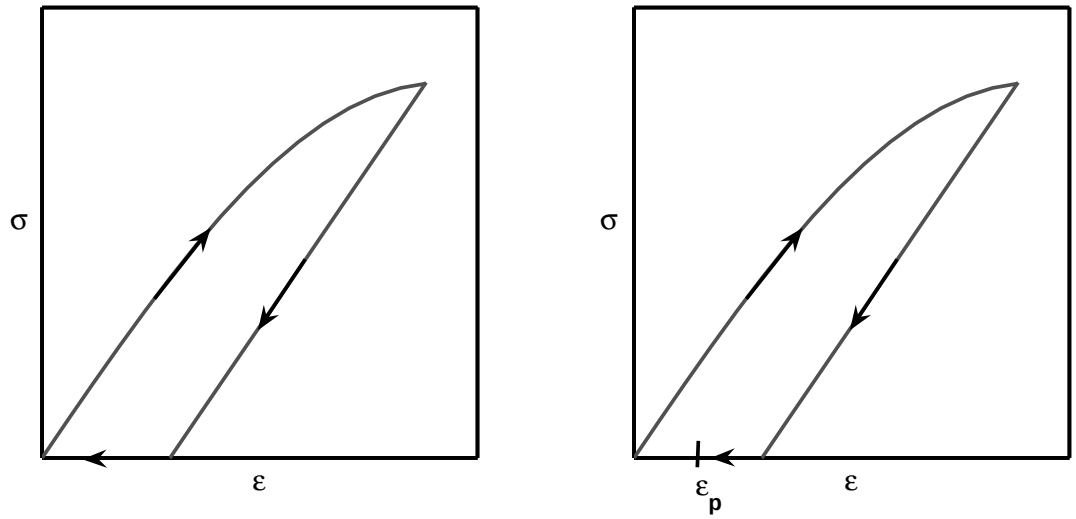

(a) Viscoelasticity (b) Viscoplasticity

Figure 2.8: Viscoelastic and Viscoplastic Stress-Strain Behavior. Both Types of Material Exhibit Inelastic Strain Upon Unloading to Zero Stress. The Viscoelastic Material Fully Recovers this Strain if Given Time. The Viscoplastic Material Does Not Fully Recover, Exhibiting a Permanent Strain ϵ_p.

behavior is also characterized by nonzero strain immediately after unloading to zero stress. However, the strain does not return completely to zero even if given infinite time to recover (a permanent strain ϵ_p remains).

Many viscoplastic models have been formulated based on varying microstructural or phenomenological bases. The current discussion focuses on Viscoplasticity Based on Overstress (VBO). For an overview of viscoplastic models, the reader is referred to Krempl [31].

2.2.2.1 Viscoplasticity Based on Overstress. The VBO is a constitutive model developed by Krempl and co-workers. The VBO is a unified viscoplastic constitutive model, meaning that inelastic strain is not separated into creep strain

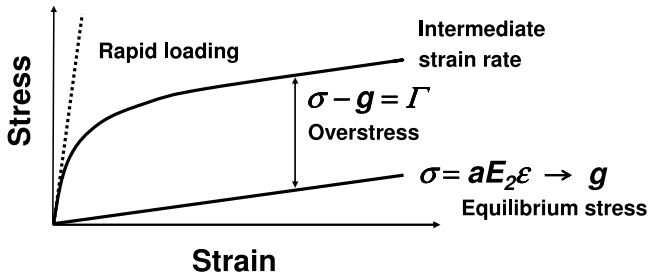

Figure 2.9: Standard Linear Solid Range of Rate-Dependent Stress-Strain Behavior [39]. Stress and Equilibrium Stress Are Shown Versus Strain.

and plastic strain. The VBO model also includes the overstress concept. Overstress is defined as the difference between the flow stress and the equilibrium stress. (The flow stress is the applied stress in the region of fully developed plastic flow. The equilibrium stress is a theoretical stress-strain curve conducted at an infinitesimally small strain rate.) Figure 2.9 shows a schematic depicting the flow stress and the equilibrium stress as functions of strain as well as the overstress for the standard linear solid which forms the basis for VBO. A historical background of the development of the VBO is given in this section, the details of the mathematical formulation are discussed in Section 3.2.

In the early 1970's Krempl [34] emphasized the need to develop valid constitutive equations for engineering alloys. He pointed out that without a set of constitutive equations we would have to develop extensive databases on material behaviors for each individual material at each possible temperature. Krempl advocated phenomenological models based on the experimental results observed in the laboratory.

Cernocky and Krempl [9,10] developed a framework using the following constitutive law as the foundation:

$$m[\sigma,\epsilon]\dot{\epsilon} + g[\epsilon] = \sigma + k[\sigma,\epsilon]\dot{\sigma} \tag{2.16}$$

where square brackets signify "function of", $\dot{\epsilon}$ is the strain rate, $\dot{\sigma}$ is the stress rate, and g is the equilibrium stress. The material functions m and k must be determined from experiments.

Cernocky and Krempl [9] went on to derive an integral form of Eq. (2.16). Of particular interest to this report is the observation made in Reference [9] regarding a "useful specialization (A)" of Eq. (2.16). The specialization represents the case where $m[\ ]$ and $k[\ ]$ are selected to depend upon overstress $\sigma - g[\epsilon]$ and on $\frac{d\mathring{g}[\epsilon]}{d\epsilon} = E$, where $\mathring{g}$ is defined as the equilibrium stress $g[\ ]$ for extremely fast loading. For this case, the stress-strain curves for different strain rates are equidistant in the region where plastic flow is fully established, as shown in Figure 2.10. (Or as stated by Cernocky and Krempl [9] discussing Eq. (2.16), "every solution curve ... for constant or variable strain must become parallel to $g[\epsilon]$". Also see Figure 10 of Reference [9].) Note that this case is an overstress model that is unique in that it does not decompose the strains into elastic and plastic parts. Reference [9] presents numerical data that suggest that the model appropriately mirrors the experimentally observed behavior of engineering alloys. One notable desired feature of the model is an initial elastic region. The second feature is that the stresses at high strains are rate-dependent but

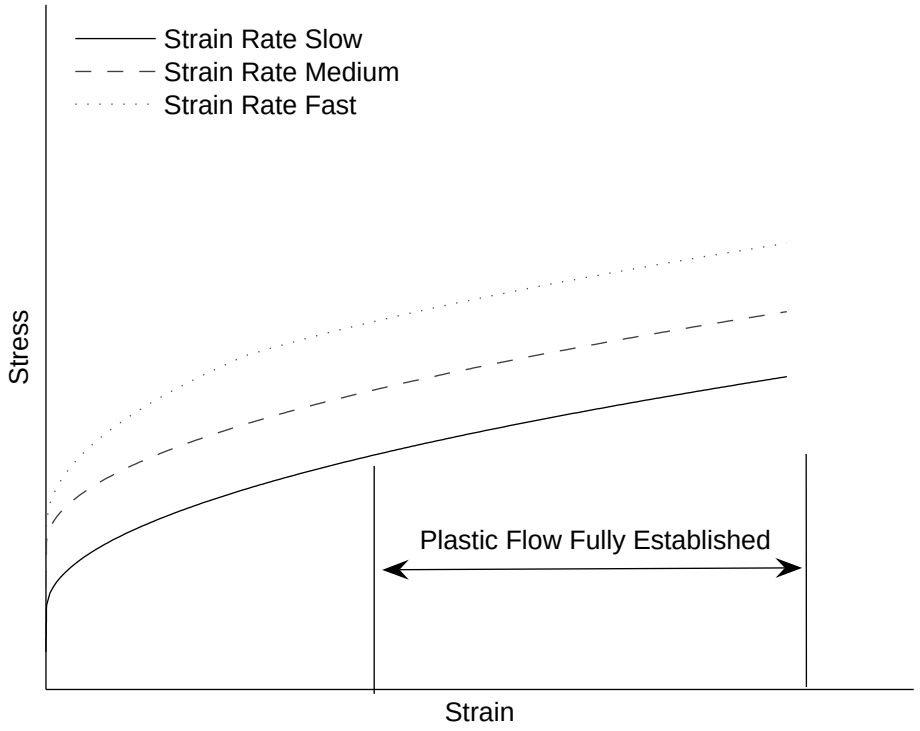

Figure 2.10: Stress Strain Curve Schematic Showing Equidistance of Response at the Different Strain Rates in the Region of Fully Established Plastic Flow.

stress-strain curves follow parallel paths. Also, the model is shown to be capable of representing shear stress as well as axial stress.

Liu and Krempl [50] utilized the differential constitutive equations discussed by Cernocky and concentrated on specializing them into the overstress form. They demonstrated how the model can be utilized for a specific material by deriving material constants from tests carried out on AISI type 304 stainless steel by Yamada and Li [79]. These constants were then used in numerical tests showing the capabilities of the VBO. Liu and Krempl reported qualitatively accurate material behavior provided

the overstress $\sigma - g[\epsilon]$ does not change sign. Unfortunately, the model characterization discussed in Reference [50] only lays out a procedure for finding the equilibrium stress g and viscosity function k. This procedure obviously does not account for the functions which were added later in order to better capture material behavior (specifically, isotropic stress A and shape function Ψ). Liu and Krempl also demonstrated that the model can represent complex loading such as a Strain Rate Jump Test with intermittent periods of relaxation. This capability to handle a complex history is an important feature for a constitutive model developed for life predictions of engineering alloys.

Krempl and Kallianpur [32] gave a brief description of the process that they used to characterize the VBO along with an explanation of the role of servocontrolled testing. Reference [32] listed some experimental procedures that are useful for characterization of engineering alloys especially emphasizing the strain rate change test. They did not, however, provide a sufficiently detailed description to enable another researcher to repeat this characterization. Krempl, McMahon, and Yao [33] and Yao and Krempl [80] also briefly discussed characterization. These references gave definitive information about finding the elastic modulus and the tangent modulus. However, they are vague about finding the other parameters listing "trial and error with judgement" [33, p. 39] as the suggested approach. While these papers offer some insight into characterizing the VBO constants and functions, they do not come close to providing a detailed, methodical characterization scheme that would enable researchers to readily utilize the VBO.

The concepts of the VBO developed for engineering alloys have been shown to be invaluable as they can be applied to a large variety of loading scenarios. These scenarios can include strain rate changes and stress rate changes. For instance, uniaxial creep, cyclic creep, relaxation, Bauschinger effect, and ratchetting behavior (with strain aging) of stainless steel have been investigated experimentally [32,38,46,60]. A titanium alloy (Ti-7Al-2Cb-1Ta) has been investigated under monotonic axial loading, cyclic axial loading, and Bauschinger effect tests [32,38,47]. An aluminum alloy (6061-T6) was subjected to tests of uniaxial creep, biaxial loading, and cyclic loading [80].

As solid polymers began replacing engineering alloys in some load bearing structures, the need to accurately predict their behavior increased. In many cases it is true that the behavior of solid polymers does not follow time-independent, linear elastic relations, leading to the need to employ more complex constitutive relations.

Kitagawa and Matsutani [29] pointed out evidence of an equilibrium stress in polymers specifically in Polypropylene (PP). Kitagawa, Zhou, and Qiu [30] also reported evidence of an equilibrium stress for Polyoxymethylene (POM), Polycarbonate (PC), and Polymethyl Methacrylate (PMMA). Kitagawa et al. [29,30] used the VBO to model the mechanical behavior of these materials. However, since Kitagawa et al. were using the early version of the VBO theory described in References [36,50], they were only able to model monotonic loading with success.

Inspired by the partial success of Kitagawa and co-workers, Bordonaro [5] and Krempl and Bordonaro [42] began to investigate the deformation behavior of polymers to determine if the overstress concept would fully apply. Their work was carried out on Nylon 66, PEI, and PEEK at room temperature. This research showed that non-linear elasticity is not a proper model for the polymers in question, and further demonstrated that the VBO was capable of reproducing the experimentally observed deformation behavior of these solid polymers. The qualitative match achieved with the VBO led to the conclusion that the VBO is a proper candidate model for the polymers in question.

However, Bordonaro [5] and Krempl and Bordonaro [42] also demonstrated specific features of mechanical behavior of polymers (specifically Nylon-66, PEEK, and PEI) which the standard VBO could not capture. These features include higher relaxation rates, increased strain recovery after unloading to zero stress, curved unloading in stress control, reduced rate-dependence in unloading, and merging of the stress-strain curves produced at different strain rates. Khan [25] also reported the need to capture curved unloading for HDPE as well as higher relaxation rates for PPO, and confirmed the need to model rate reversal during unloading. Khan demonstrated that the standard VBO can successfully capture some, but not all of the essential features of polymer mechanical behavior at room temperature. No comprehensive systematic procedure was given in any of these references for characterizing model constants and functions for a given material. Instead, "seed" values were chosen from a previously

characterized material for the various constants, then a "trial-and-error approach" was utilized to tune the model to match the desired material behavior [25, p. 138].

Based on the findings of Bordonaro's research, the VBO for Polymers (VBOP) was developed, see Ho [20] and Krempl and Ho [43]. This version was shown to predict the behaviors of Nylon-66 [20, 43], PC [27, 28], PPO [27], and HDPE [28] better than standard the VBO. Note that the VBOP was used to model the behavior of both amorphous (PC, PPO, and PES) and crystalline (Nylon-66, HDPE, PET) polymers. A detailed description of the VBOP mathematical formulation is given in Section 3.3. Still no procedure was given for a systematic characterization of the VBOP. Aging was also not taken into account in the formulation of the VBOP.

Colak [11] and Colak and Dusunceli [12, 13] developed an alternate version of the VBO aimed at modeling the behaviors of polymer materials. This version introduced a new unloading function to better represent the unloading path displayed by polymers at room temperature. Comparisons with experimental data showed that this model predicts unloading of PPO and HDPE better than the VBO proposed by Krempl and Ho [43]. However, the model developed by Colak et al. does not account for all of the behavioral features reported by Bordonaro [5] which are accounted for in the VBOP. The behaviors which are not accounted for in Colak's formulation include higher relaxation rates and merging of the stress-strain curves obtained at different strain rates. Furthermore, Colak's formulation does not account for cyclic softening or hardening. This suggests that the addition of the unloading function to the VBO model is a valid option, but that it would be more appropriately added to the VBOP

if the need arose to further enhance representations of the unloading behavior for polymers.

2.2.3 Viscoplasticity Based on Overstress with Prior Aging. Krempl [36] suggested that the VBO can be adapted to account for prior aging. He proposed an approach of determining aging effects using creep and relaxation results. For stable material, certain constants exist within the VBO. When dealing with a material that does exhibit dependence on prior aging, those constants would be forced to explicitly depend on prior aging time. According to Reference [36], the same equations and assumptions would hold that were used for the standard VBO, with the exception that the equilibrium stress g and the viscosity function k would become functions of prior aging time. Since we assume that the effects of prior aging are separate from the deformation induced effects, separation of variables would be used in the development of the constitutive equations. While specifying that g and k have to be slowly varying functions of time, Krempl offers no mathematical form to describe this dependence on time. Yet, the assumption that these functions vary slowly with time is consistent with the assumption that aging is a diffusion process. Krempl did not attempt to apply of these concepts to any experimental results. Krempl did set the stage for adding the analytical capability within the VBO to account for aging, however this capability remained to be developed.

2.3 Objectives of Current Work

The previous experimental and theoretical studies lay the groundwork for examining the deformation behavior of high temperature polymers. The current research pursues two major purposes. A systematic characterization procedure for the VBOP is developed and validated. At the same time, effects of prior aging on the deformation behavior of PMR-15 neat resin are characterized. Based on experimental findings, the predictive capability of the VBOP is extended to account for the effects of prior aging.

III. Theoretical Formulation of Viscoplasticity Based on Overstress for Polymers

This chapter describes the theory of Viscoplasticity Based on Overstress for Polymers (VBOP). The VBOP is chosen as the framework to model the behavior of PMR-15 with and without prior aging. The current research also extends the VBOP to include prior aging. A thorough understanding of the intricate details of the VBOP is needed before the introduction of aging into the model formulation can be discussed.

Note that both the VBO and the VBOP are unified viscoplastic constitutive models. The underlying concept of a so called "unified model" is that all of the observed inelastic effects are "intrinsically coupled" [51]. This suggests, for example, that creep strain and plastic strain are not represented by separate terms in the constitutive equations.

3.1 Basis of Viscoplasticity Based on Overstress – Standard Linear Solid

This section briefly explains the Standard Linear Solid (SLS) model upon which the VBO is based. The SLS model, schematically shown in Figure 3.1, consists of two springs and a dashpot (all elements are linear). This is a simple linear viscoelastic solid, classified as a solid since it can maintain a nonzero stress while the strain rate is zero [18, 39].

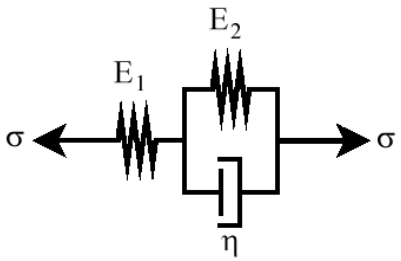

Figure 3.1: Schematic of a Standard Linear Solid

The constitutive equation of the SLS is

$$\dot{\epsilon} + \frac{E_2}{\eta}\epsilon = \frac{\dot{\sigma}}{E_1} + \left(\frac{E_1 + E_2}{E_1}\right)\frac{\sigma}{\eta} \tag{3.1}$$

where E_i is the elastic constant of spring "i" and η is the viscosity constant of a dashpot. This model is capable of representing both creep and relaxation.

3.2 Viscoplasticity Based on Overstress

The strain rate in the standard linear solid constitutive equation can be divided into elastic, $\dot{\epsilon}^{el}$, and inelastic, $\dot{\epsilon}^{in}$, parts. The constitutive equation can then be re-arranged into the following overstress form,

$$\dot{\epsilon} = \dot{\epsilon}^{el} + \dot{\epsilon}^{in} = \frac{\dot{\sigma}}{E_1} + \left[\frac{\sigma}{a\eta} - \frac{E_2}{\eta}\epsilon\right] \tag{3.2}$$

or

$$\dot{\epsilon} = \frac{\dot{\sigma}}{E_1} + \frac{\sigma - aE_2\epsilon}{a\eta}, \tag{3.3}$$

where

$$a = \frac{E_1}{E_1 + E_2}. \tag{3.4}$$

The term $\sigma - aE_2\epsilon$, then referred to as the overstress, leads to the name Viscoplasticity Based on Overstress. The term

$$g = aE_2\epsilon \tag{3.5}$$

is called the equilibrium stress. The equilibrium stress can be viewed as the stress that the material can sustain as all rates approach zero.

The material behaves differently depending on loading rate, as illustrated in Figure 2.9. Extremely slow loading corresponds to the equilibrium stress curve which is governed by the two springs in series $\frac{E_1E_2}{E_1+E_2}$. Extremely fast loading provides a linear upper bound to the material behavior and is governed by E_1 [39].

The constitutive equations are made nonlinear by making the spring modulus E_2 a nonlinear function of strain and by making the viscosity η a function of overstress [39]. The final step needed to develop the standard VBO is to change the equilibrium stress to have a "proper hysteretic behavior" [39]. The proper behavior is dependent on the specific material to which the model is applied.

The governing equation of the standard VBO is as follows [40]:

$$\dot{\epsilon} = \frac{\dot{\sigma}}{E} + \frac{\sigma - g}{Ek}, \tag{3.6}$$

where E is the elastic modulus, g is the equilibrium stress, and k is the viscosity function.

The evolution of the equilibrium stress is

$$\dot{g} = \Psi \frac{\dot{\sigma}}{E} + \frac{\Psi}{E}\left[\frac{\sigma - g}{k} - \frac{g - f}{A}\frac{(\sigma - g)}{k}\right] + \left(1 - \frac{\Psi}{E}\right)\dot{f}, \tag{3.7}$$

where A is the isotropic (rate independent) stress, Ψ is the shape function, and f is the kinematic (rate dependent) stress.

The basic form of the viscosity function [5] is

$$k = k_1 \left(1 + \frac{|\sigma - g|}{k_2}\right)^{-k_3}, \tag{3.8}$$

where k_1, k_2, and k_3 are material constants. This function acts as a repository for nonlinear viscous behavior [10].

The isotropic stress A establishes the difference between the kinematic stress and the equilibrium stress [51] and is responsible for modeling cyclic hardening or softening [21]. The evolution of the isotropic stress is [44]:

$$\dot{A} = A_c[A_f - A]\left|\frac{\sigma - g}{Ek}\right|, \tag{3.9}$$

where A_c is a constant that controls how quickly saturation of cyclic hardening or softening is reached and A_f is the saturated value of A [44].

The shape function governs the shape of the "knee" in the stress-strain diagram. The recommended basic form is given as

$$\Psi = C_1 + (C_2 - C_1)e^{-C_3|\epsilon^{in}|}, \tag{3.10}$$

where C_1, C_2, and C_3 are material constants.

The kinematic (rate dependent) stress f governs the slope of the stress-strain curve in the plastic flow region (where inelastic flow is fully established) [33]. The evolution of the kinematic stress is given by [40]:

$$\dot{f} = E_t \frac{(\sigma - g)}{Ek}, \tag{3.11}$$

where E_t is the slope of the stress-strain curve in the region where the inelastic (plastic) flow is fully established. The kinematic stress was introduced as a repository for modeling the ultimate tangent modulus of the stress strain curve [20].

A yield surface is not employed in this theory, which implies that inelastic deformation is always present at least to a small degree.

Several versions of the VBO exist, each having its own specialized application or purpose. The different versions share the existence of a flow law and three state variables (equilibrium stress g, isotropic stress A, and kinematic stress f). The VBO with nonstandard rate-dependence allows for unusual trends such as dynamic strain aging [20, 22, 23]. The Simplified VBO (SVBO) reduces the number of material pa-

rameters to a minimum, making the model more manageable to characterize [51, 70]. The Improved Simplified VBO (ISVBO) removes some of the simplifications introduced in the SVBO to allow the model to be applicable to a wider range of materials [51]. The VBO for Polymers has added rate-dependence in the equilibrium growth law (Eq. (3.7)) and reconfigures some of the functions to better fit typical behavior of the investigated polymers at room temperature [20].

For the proposed research, the VBO for Polymers is an appropriate choice since it is formulated for the class of material that are under investigation. The functions and variables of the VBOP are explained in further detail in Section 3.3.

3.3 Viscoplasticity Based on Overstress for Polymers

Ho [20] developed the VBOP to address the needs reported by Bordonaro and Krempl [4], Bordonaro [5], and Krempl and Bordonaro [42]. This model was subsequently used to model the behaviors of various polymers [26, 28, 43]. In the VBOP formulation, Eq. (3.6) retains the form

$$\dot{\epsilon} = \dot{\epsilon}^{el} + \dot{\epsilon}^{in} = \frac{\dot{\sigma}}{E} + \frac{\sigma - g}{Ek}. \tag{3.12}$$

The growth (or evolution) of the equilibrium stress given by Eq. (3.7) for the standard VBO becomes dependent not only on the overstress, but also on the over-

stress rate,

$$\dot{g} = \Psi \frac{\dot{\sigma}}{E} + \Psi \left[\frac{(\sigma - g)}{Ek} - \frac{(g - f)}{A} \left| \frac{(\sigma - g)}{Ek} \right| + \frac{(\dot{\sigma} - \dot{g})}{E} \right] + \left[1 - \frac{\Psi}{E} \right] \dot{f}. \tag{3.13}$$

The difference between this formulation and the standard VBO is the inclusion of the term $\Psi \frac{(\dot{\sigma} - \dot{g})}{E}$. This term influences the rate of equilibrium stress and in turn influences the relaxation rate, allowing the model to capture the higher relaxation rates commonly observed in relaxation of polymers. This modification specifically addresses the behavior observed by Bordonaro [5] for Nylon-66. This additional term is optional, depending on the specific material behavior in question. If the term is not appropriate for the particular polymer, then it is simply not included. For the PMR-15 at 288 $^{\circ}C$ modeling was conducted both with and without this term. This modeling elucidated that the term is not appropriate for the mechanical behavior of the PMR-15 at 288 $^{\circ}C$. For more information see Appendix A.

The evolution of the kinematic stress is modified to the form

$$\dot{f} = \left[\frac{|\sigma|}{\Gamma + |g|} \right] E_t \frac{(\sigma - g)}{Ek}, \tag{3.14}$$

where Γ is the overstress invariant, which has the form

$$\Gamma = |\sigma - g|, \tag{3.15}$$

for the uniaxial case. The addition of the term $\left[\frac{|\sigma|}{\Gamma+|g|}\right]$ increases the strain recovery after unloading to zero stress [20]. This increase in recovery is achieved by slowing the rate at which the equilibrium stress decreases. This term is also optional depending on the behavior of the particular material of interest.

The isotropic stress evolution for polymers remains the same as that in the standard VBO

$$\dot{A} = A_c[A_f - A]\left|\frac{\sigma - g}{Ek}\right|. \tag{3.16}$$

In the case of many solid polymers, this is simplified by setting $A_c = 0$ and making A a constant [11, 12, 23, 25–28] if the material is cyclically neutral. However, this simplification cannot always be made. One such case is Nylon-66 [20, 43], which exhibits cyclic softening.

The shape function governs the shape of the knee in the stress-strain diagram as well as the curvature of the unloading curve. The recommended form for the VBOP is given by Ho [20] and Krempl and Ho [43] as

$$\Psi = C_1^* + (C_2 - C_1^*)e^{-C_3|\epsilon^{in}|} \tag{3.17}$$

$$C_1^* = C_1\left[1 + C_4\left(\frac{|g|}{A + |f| + \Gamma^2}\right)\right], \tag{3.18}$$

where C_1 to C_4 are material constants. The shape function not only reproduces the curved unloading exhibited by polymers, it more importantly reduces the rate-

dependence of the unloading curves. Both of these behaviors are characteristic for some polymers at room temperature [5, 20]. This term is also optional depending on the behavior of the particular material in question. For the PMR-15 at 288 $^{\circ}C$ it was determined that this term is not appropriate because the unloading behavior of the PMR-15 exhibits a strong rate dependence. For more information see Appendix A.

The viscosity function for polymers [20, 43] is

$$k = k_1 \left[1 + \left(1 + \frac{A_0 - A}{A_0 - A_f} \right) \frac{\Gamma}{k_2} \right]^{-k_3}, \tag{3.19}$$

where A_o is the initial value of A, and k_1, k_2, and k_3 are material constants. The addition of a dependence on the isotropic stress allows for the stress-strain curves at different strain rates to merge. This merging is "correlated with the strain dependence of the stress relaxation time" [20].

The modifications discussed above were initially introduced to meet the needs for modeling the behavior of Nylon-66 as discussed by Bordonaro [5] and Ho [20]. This form has become known as the VBOP and has been successfully utilized to model the behaviors of other solid polymers at room temperature including PC by Khan and Krempl [27, 28], HDPE by Khan and Krempl [28], and PPO by Khan [26]. The rate reversal effect that is typically observed for polymers is not captured by the VBOP or the standard VBO. Khan [26] discussed possible modifications to the model that would enable the prediction of the rate reversal. However, while the rate reversal effect is an observed feature of the material behavior, it is postulated here that the

rate reversal is not critical to creating an accurate life prediction for components manufactured with solid polymer materials.

The VBOP model lends itself as an appropriate choice of a constitutive framework for modeling the behavior of the solid polymer PMR-15 in the current research. A major contribution of this research is the development of a systematic model characterization scheme for the VBOP. A systematic experimental characterization scheme for this model is outlined in Chapter IV. Another major contribution is the development of the analytical capability to account for prior aging within the VBOP framework. The modifications to the VBOP are discussed in Chapter X.

IV. Experimental Methods

This chapter discusses the experimental arrangements and procedures needed to examine the strain rate-dependent behavior of the PMR-15 at 288 $^{\circ}C$ as well as the effects of prior aging on the inelastic deformation of the material.

4.1 Test Material and Experimental Arrangements

The material studied was PMR-15 solid polymer, a thermosetting polyimide. The PMR-15 polyimide has a T_g of 347 $^{\circ}C$ and a long-term use temperature of 288 $^{\circ}C$. The PMR-15 neat resin panels were supplied by HyComp Inc. (Cleveland, OH). The free standing post cure cycle is shown in Table 1.1. Dog bone-shaped test specimens of 150-mm total length with a 7.6-mm wide gage section were machined from the 3.18-mm thick panels using diamond-grinding. All as-received specimens must be processed to ensure that they have a common starting point with low moisture content. All specimens were washed with a common household soap and thoroughly rinsed with distilled water to remove contaminants from the machining process. The specimens were then dried in a vacuum oven at 105 $^{\circ}C$ for at least 24 h, and subsequently stored in a dry-air-purged desiccator until testing to prevent any moisture re-absorption.

Specimens were aged at 288 $^{\circ}C$, which is the design maximum sustained service temperature of PMR-15 based composites in aerospace applications. The isothermal aging was accomplished in a Blue M model 7780 air-circulating oven that provided continuous replenishment of argon by convection through the oven inlet. High purity

argon gas (99.999% pure) was supplied to the Blue M oven from a liquid argon tank. When specimens were taken out for periodic inspection and/or testing, the oven was opened without cooling and closed immediately. Then the oven automatically entered the 18-min purge cycle to flush out any ambient atmosphere that had entered the chamber. The flow rate of argon was $\sim$30 $SCFH$ during the steady state operation and 150 $SCFH$ during the purge cycle. Each group of test specimens isothermally aged for a given duration included a rectangular sample for the purpose of monitoring weight change with aging time. The aged rectangular specimens were removed from the oven and allowed to cool in the desiccator prior to obtaining weight measurement.

A servo-hydraulic MTS machine equipped with water-cooled hydraulic wedge grips, a compact resistance-heated furnace, and a temperature controller were used in all tests. A TestStar II digital controller was used for input signal generation and data acquisition. An MTS low contact force, high-temperature uniaxial extensometer of 12.5-mm gage length was used for measurement of strain. This set-up allowed for strain-controlled testing, as well as immediate control mode switching. Unless otherwise indicated, loading/unloading was performed under strain control mode at rates of $|\dot{\epsilon}| = 10^{-6}$ to 10^{-3} s^{-1}, and of course $|\dot{\epsilon}| = 0$ s^{-1} for any relaxation intervals. The capability of immediate control mode switching allowed for creep and recovery following loading/unloading in strain control. Naturally, for creep and recovery intervals $|\dot{\sigma}| = 0$ MPa/s.

For elevated temperature testing, thermocouples were attached to the specimens using Kapton Tape to calibrate the furnace on a periodic basis. The furnace controller

(using a non-contacting thermocouple exposed to the ambient environment near the test specimen) was adjusted to determine the power setting needed to achieve the desired temperature of the test specimen. Thermocouples were not bonded to the test specimens after the furnace was calibrated. All tests were carried out at 288 $^{\circ}C$ in a laboratory air environment. In all tests, the specimen was heated to 288 $^{\circ}C$ at the rate of 2 $^{\circ}C/min$, and held at 288 $^{\circ}C$ for an additional 45 min prior to testing.

4.2 Experimental Procedures

The test procedures that are necessary to explore the strain rate-dependent behavior of the PMR-15 at 288 $^{\circ}C$ are outlined in this section. The results of these tests are used for the characterization of the VBOP parameters and for model verification as described in detail in Section 7.2.

4.2.1 Monotonic Tensile Test at Constant Strain Rate. The type of experiment used for setting a baseline for the material strain rate dependent behavior is a Monotonic Tensile Test at Constant Strain Rate. Specimens from each aging group were subjected to tensile tests at constant strain rates of 10^{-6}, 10^{-5}, 10^{-4}, and 10^{-3} s^{-1}. This type of test is depicted schematically in Figure 4.1. The purpose of monotonic testing at multiple constant strain rates is to determine if and how the flow stress, elastic modulus, and tangent modulus depend on the strain rate. An example of the effect of strain rate on the stress-strain behavior of the solid polymer PPO is presented in the loading portion of Figure 4.2 reproduced from Khan [25].

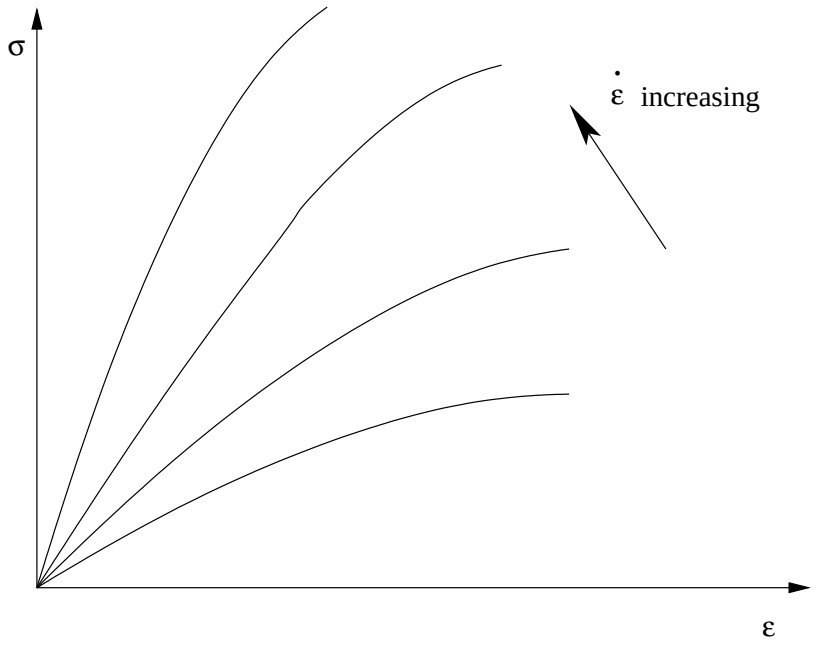

Figure 4.1: Schematic of a Set of Monotonic Tension Tests

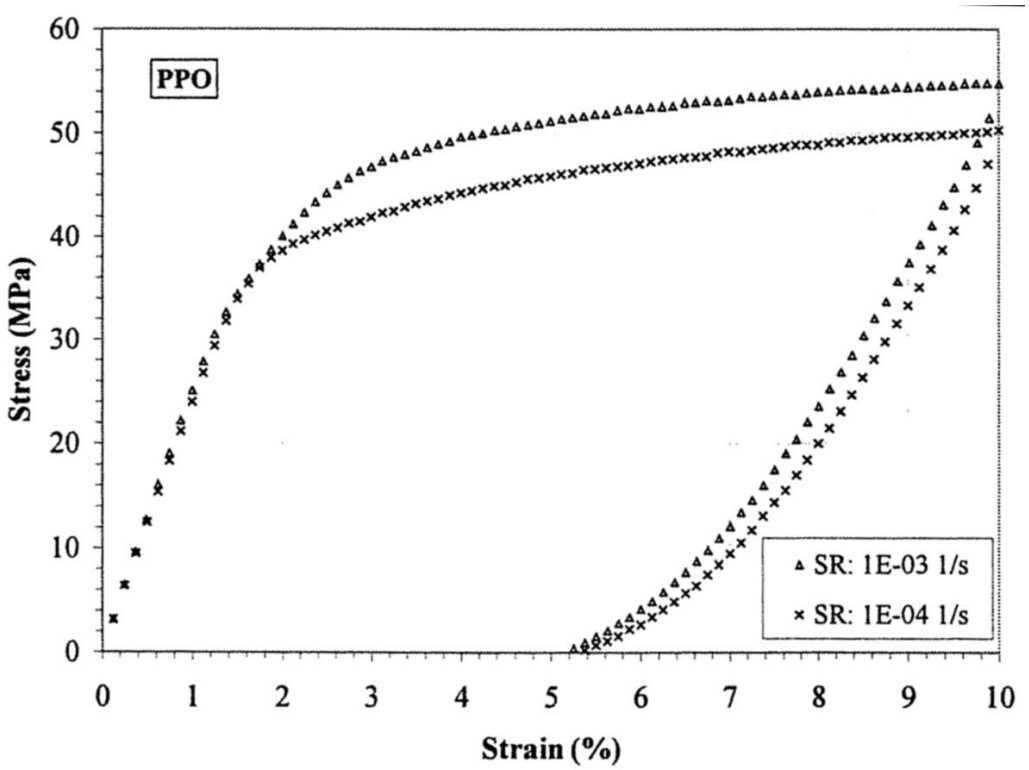

Figure 4.2: Example of a Loading Followed by Unloading at Constant Strain Rate on PPO Reproduced from Khan [25] Figure 4.14.

4.2.2 Loading Followed by Unloading at Constant Strain Rate. To assess the effect of strain rate on the unloading stress-strain behavior, strain-controlled tests consisting of loading to a fixed strain of 3% and unloading to zero stress at constant strain rate magnitude were carried out. Strain rate magnitudes ranging from 10^{-6} to 10^{-3} s^{-1} were employed. An example of this type of test to a fixed strain of 10% is shown in Figure 4.2 (reproduced from Khan [25]).

4.2.3 Recovery of Strain at Zero Stress. A recovery test is carried out after a load has been applied and then removed. The material is kept at zero load and the accumulated strain is monitored until an asymptotic point has been achieved. (The strain in the material is no longer reducing.)

In the current work, this test is carried out following loading and unloading to zero stress at constant strain rate magnitude. After unloading, the control mode is switched from strain to load, and the load is controlled to stay at zero for at least 10 h to observe the subsequent strain recovery.

4.2.4 Constant Strain Rate Test with Intermittent Periods of Relaxation. A relaxation test is carried out by imposing a constant strain while recording the change in stress. The "relaxation" is defined as the change in stress level with time as the strain is held constant. The relaxation stress is close to the equilibrium stress at the end of relaxation if the relaxation duration is long enough [60]. These tests are carried out as part of the constant strain rate tests with intermittent periods of relaxation, similar to that shown in Figures 4.3 and 4.4. It is important to ensure

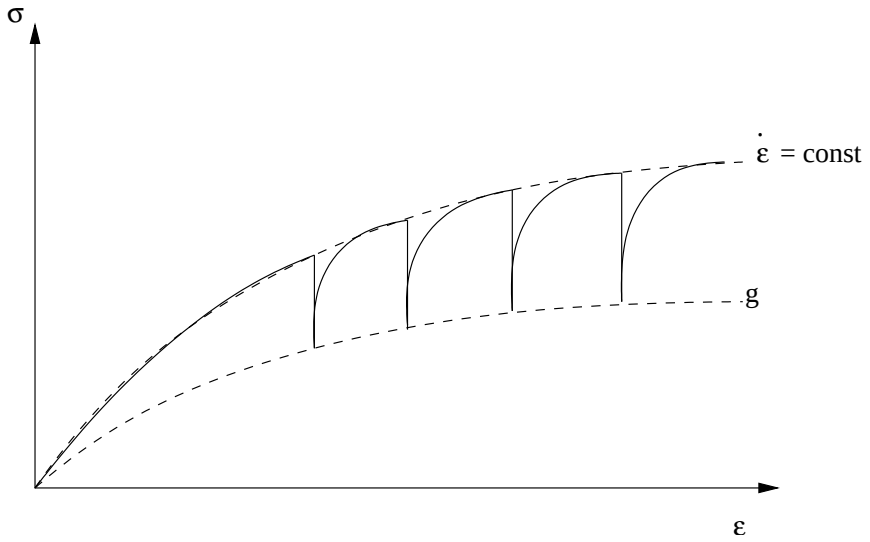

Figure 4.3: Schematic of a Constant Strain Rate Test with Intermittent Periods of Relaxation.

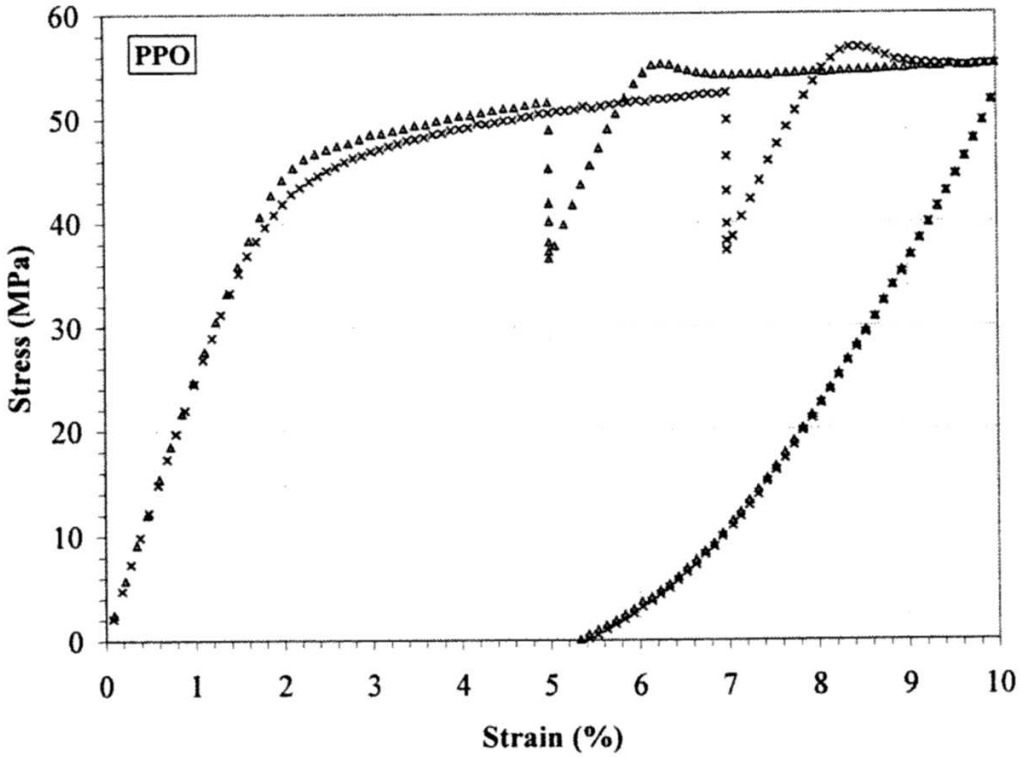

Figure 4.4: Example of a Constant Strain Rate Test with Intermittent Relaxation Periods on on PPO Reproduced from Khan [25] Figure 6.10.

that the periods of relaxation are long enough to reach the point when the stress rate approaches zero.

The relaxation tests (along with the creep tests) are used to verify the existence of an equilibrium stress [43]. By carrying out the constant strain rate test with intermittent periods of relaxation at different constant strain rates, one can detect the dependence of the stress drop during relaxation on the prior strain rate. By carrying out the relaxation tests for the same prior strain rate but at different strain levels, one can detect the dependence of the stress drop during relaxation on stress and strain at the beginning of the relaxation period.

4.2.5 Strain Rate Jump Test. The Strain Rate Jump Test (SRJT) [59, 61] consisting of segments of monotonic loading at two different strain rates was performed to assess whether the PMR-15 polymer exhibits the strain rate history effect at 288 $^{\circ}C$. The strain rates were 10^{-5} and 10^{-3} s^{-1}. The results are compared to the stress-strain curves obtained in constant strain rate tests conducted at 10^{-5} and 10^{-3} s^{-1}. A schematic of the expected material behavior during the strain rate jump test is shown in Figure 4.5. An example of the strain rate jump test is shown in Figure 4.6 (Reproduced from Khan [25]). This test can provide a better understanding of the effects of the strain rate history on the material behavior.

4.2.6 Creep. Influence of prior strain rate on creep behavior was explored in creep tests of 6 h duration preceded by uninterrupted loading to a target creep stress of 21 MPa at constant strain rates of 10^{-6} and 10^{-4} s^{-1}. The capability of

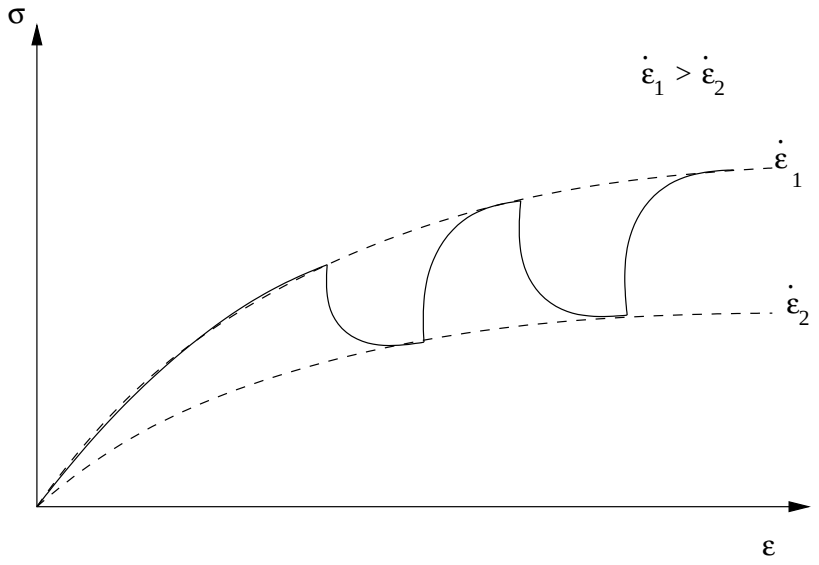

Figure 4.5: Schematic of a Strain Rate Jump Test

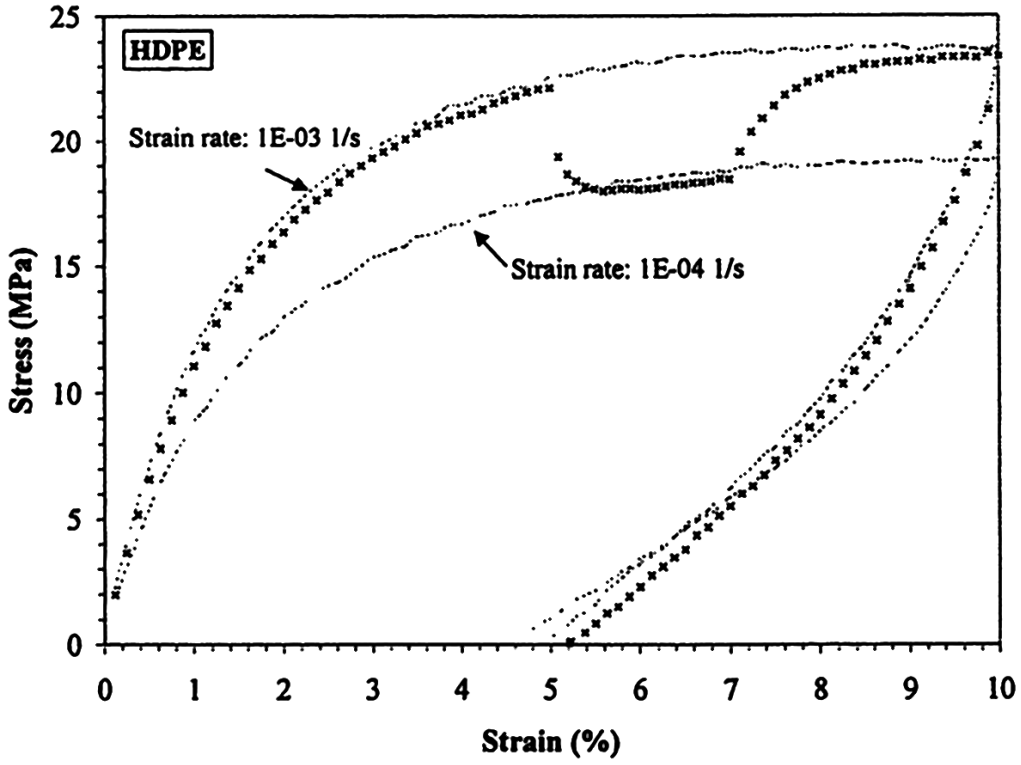

Figure 4.6: Strain Rate Jump Test with Unloading on HDPE Reproduced from Khan [25] Figure 4.8.

the testing system to instantaneously switch control mode made it possible to load a specimen to a target stress of 21 MPa at a constant strain rate under strain control, then switch mode to load control to perform a creep test.

4.3 Isothermal Aging Procedure

In order to investigate the effects of prior aging on the deformation behaviors of PMR-15, specimens that have been aged for various durations were subjected to the exploratory experiments outlined in Section 4.2. The results provide information on the effects of aging on the rate-dependent deformation behaviors of PMR-15.

The material was aged for durations of 50, 100, 250, 500, 1000, and 2000 h. Theses durations are the same as those used by Ruggles-Wrenn and Broeckert [63] with the 2000-h duration added. Hence, results obtained by Broeckert may be used together with the results obtained in the current research.

An important assumption is that the aging of PMR-15 is negligible at ambient temperatures. This allows us to assume that aging effects can be attributed completely to prior aging at high temperatures. Another critical assumption is that thermal cycling of the samples during heating and cooling periods does not contribute to degradation. In order to make this assumption, the number of thermal cycles is restricted to a minimum. Both of these assumptions are common for this type of research [7].

It is worth noting that prior to aging the room temperature elastic modulus of each specimen is measured and recorded in order to document the specimen-to-

specimen variability inherent in the material. The tests are carried out in the laboratory air environment at room temperature. Tests conducted for the purpose of elastic modulus measurement are limited to loads and stresses in the linear region of the material in order to not introduce permanent strain. Following the procedure outlined by Broeckert [7], each specimen is loaded to 3 MPa at a rate of approximately 1 MPa/s and unloaded at the same rate to zero stress. The measured modulus of each specimen represents its individual "signature" that can be useful in reducing data scatter due to specimen-to-specimen variability.

4.4 Tuning for Strain Control

It is established in Section 4.2 that various strain-controlled tests such as the constant strain rate, the strain rate jump, and relaxation tests are required for the current research. Both strain-controlled and stress-controlled tests conducted in this research require accurate control of the rate of loading. While modern servo controlled testing equipment boasts such control capability, the testing system must be calibrated for each specific material tested. This calibration procedure is called "tuning".

Tuning is performed to minimize the error between the command and the feedback signal. Successful tuning assures that the testing machine does what it is told to do. For example, consider a test in which the axial load imposed on a specimen increases at a constant rate of 100 N/s. The controller sends a command signal to the machine actuator. The axial motion of the actuator produces an increasing load

on the specimen. The load cell monitors the changing load and provides a feedback signal to the controller, which compares the command and feedback signals and evaluates the error between command (what the machine is told to do) and feedback (the action of the machine). The error is then minimized by adjusting the command signal to the servo-valve so that the feedback converges to the desired rate of 100 N/s. This is a closed loop control process. This process is continually taking place throughout each test. Several process parameters must be adjusted to establish a quick, but stable feedback loop.

The MTS testing system permits closed loop control using three different control channels:

1. the actuator displacement sensor – displacement control
2. the extensometer mounted directly on the test specimen – strain control
3. the load cell – load control

To successfully conduct both stress (load)- and strain-controlled tests, each control channel must be tuned individually.

Tuning of the test equipment in strain control specifically for the PMR-15 neat resin is key to this research. Yet, strain-controlled testing is not commonly performed due to the level of difficulty involved in tuning the testing system in this control mode. Strain-controlled tests are also not needed for characterizing most simplified material models. However, strain-controlled testing is critical to successful characterization of the VBOP (or the VBO). Prior to this research, strain-controlled testing had not

been accomplished in the Air Force Institute of Technology laboratories for any type of material.

The current experimental research was carried out on an MTS servo-hydraulic testing machine equipped with the TestStar II digital controller. Tuning of the test system in either stress control or strain control mode involves adjustment of the two critical parameters: the proportional gain (P) and the integral gain (I). The specifics of the MTS control system are proprietary. However, the basic theory of Proportional and Integral control can be discussed.

The P gain is the primary value that has to be adjusted for the types of tests proposed in this research. A proportional controller produces a signal that is proportional to the error. The steady-state performance and speed of response of a system improves as the P gain is increased [67]. However, setting the P gain too high can cause instabilities in the system.

The control signal for a Proportional Control system can be expressed as

$$u(t) = Pe(t), \tag{4.1}$$

where $u(t)$ is the controller output signal, P is the gain value, and $e(t)$ is the error between the command and the feedback [67].

The proportional gain has the following effects [56]:

- As P gain increases, the error between the command and the feedback decreases.

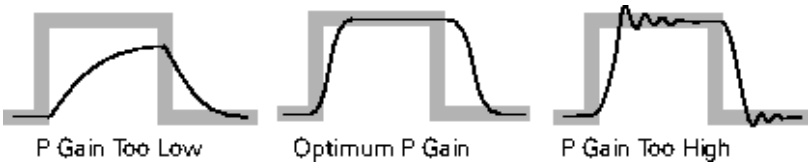

Figure 4.7: Effect of P Gain [56] on System Response

- A higher P gain increases the speed of the system response.
- Setting the P gain too low can cause the system to be sluggish.
- Setting the P gain too high can cause the system to become unstable.

A simple schematic of the effect of the P gain on a square wave form is shown in Figure 4.7, where a gray line represents the command and a black line represents the feedback (or the system response to the command).

Adjustments to the I gain can also improve the steady-state performance of a control system, creating a Proportional-Integral Control [56]. The control signal for this case can be represented as:

$$u(t) = P\left[e(t) + \frac{1}{I}\int_0^t e(\tau)d\tau\right], \tag{4.2}$$

where I is the integral gain value [67]. As can be seen in Eq. (4.2), the integral gain acts on the integral of the history of the error over time. Adding this integral to the control signal may lead to oscillatory response. A simple schematic of the effect of the I gain on a square wave form is shown in Figure 4.8.

MTS [56] suggests that a square waveform be utilized for tuning in displacement control or force control. However, a sinusoidal waveform is recommended for tuning in

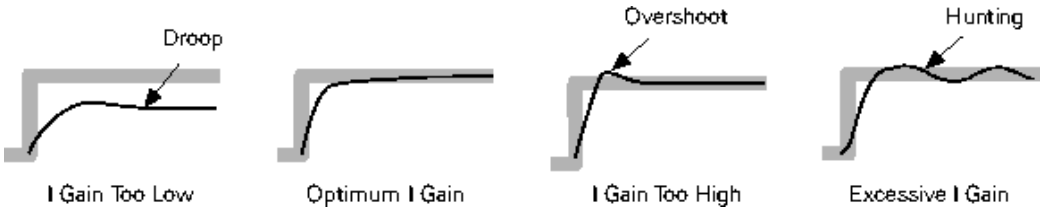

Figure 4.8: Effect of I Gain [56] on System Response

strain control, since the discrete changes in strain inherent in a square waveform can cause the extensometer to slip or fall off the specimen. Loss of contact between the extensometer, which provides the feedback signal in strain control, and the specimen would cause the system to go unstable.

Tuning of the strain control mode was first carried out at room temperature using an aluminum alloy specimen and an MTS high contact force uniaxial extensometer. A sinusoidal waveform with a mean axial strain of 0.5% and a strain amplitude of 0.2% was employed. The frequency was set to 0.1 Hz. The values of the P and I gains were set low initially and then gradually increased. Once good agreement between the command and feedback signals was achieved, the frequency was increased to 0.25 Hz where the P and I gains were further adjusted. The frequency was incrementally increased and values of P and I adjusted until the final frequency of 1 Hz was reached (tests planned in this research would not require tuning at higher frequencies). The final values of the P and I gains were 2100 and 80, respectively. To validate these gain settings, monotonic tests at several constant strain rates, a constant strain rate test with intermittent periods of relaxation, a strain rate jump test, and a stepwise creep test were carried out using an aluminum alloy specimen. The objective of these validation tests was to check the agreement between command

and feedback signals under complex loading histories. The results of all tests revealed that the P and I gain settings were adequate and that tuning was successful.

Next the tuning procedure was repeated using an aluminum alloy specimen and an MTS high-temperature low contact force extensometer, which would be used in actual tests. The tuning was also conducted using the testing system with the 3 Kip load cell, which would be used in actual tests. Successful completion of this step was not guaranteed. Because of the low-contact force design, this particular extensometer can easily lose contact with the test specimen, causing the testing system to become unstable. Yet with significant effort, the successful tuning was accomplished. At the final frequency of 1 Hz, good agreement between command and strain feedback was achieved at a P gain of 2400 an I gain of 35. Several strain-controlled tests were carried out to validate the tuning. The results demonstrated that the gain settings were adequate.

Then the tuning procedure was repeated using a PMR-15 specimen and an MTS high-temperature low contact force extensometer. The gain settings of P=2400 and I=35 produced good agreement between the command and feedback for the case of cyclic loading with the sinusoidal waveform with the mean tensile strain of 0.5%, strain amplitude of 0.3%, and a frequency of 0.75 Hz. The gain settings were further validated in several strain-controlled tests. Evaluation of the command versus feedback obtained in monotonic loading/unloading tests at constant strain rate and in strain rate jump tests revealed an excellent agreement between the two signals.

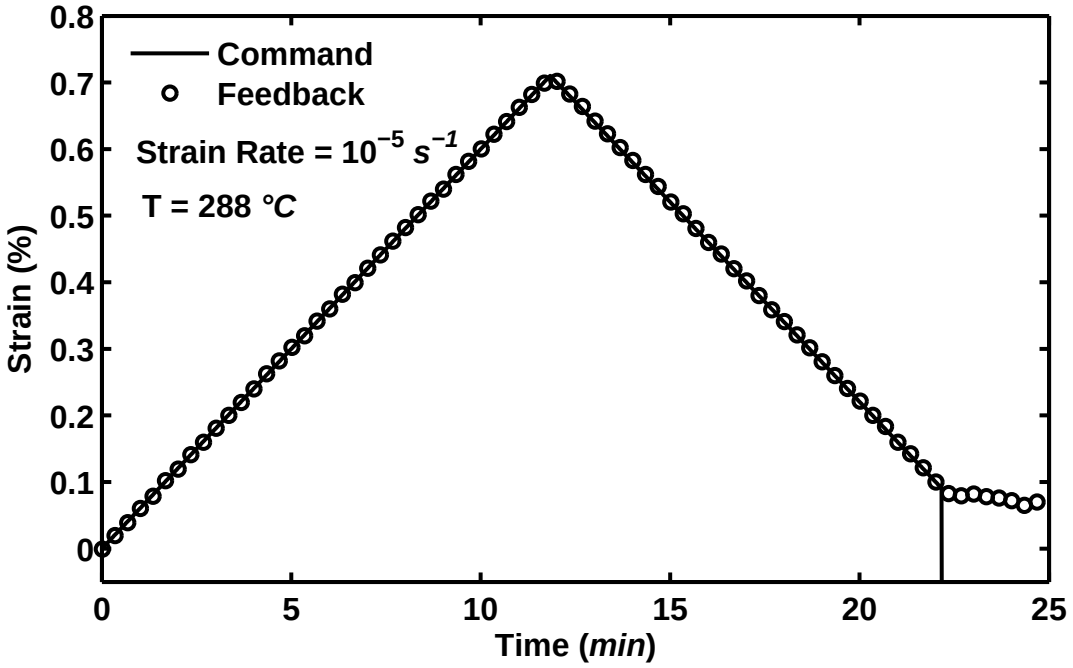

Figure 4.9: Strain Control Tuning with PMR-15 and Low Contact Force Extensometer: Loading and Unloading in Strain Control at 288 $^{\circ}C$. Strain Rate is 10^{-5} s^{-1}.

Finally, the strain-controlled validation tests were carried out at at 288 $^{\circ}C$ (test temperature for the present research). The determined gain settings proved to be successful in the elevated temperature tests as well. Excellent agreement between the command and the feedback signal was achieved under cyclic loading with the sinusoidal waveform, in loading an unloading at constant strain rate magnitudes (Figures 4.9 and 4.10), in the constant strain rate test with intermittent periods of relaxation (Figure 4.11), and in the strain rate jump test (Figure 4.12).

It should be noted that the PMR-15 specimen used in the tuning effort was not kept in a controlled environment (therefore its moisture content is unknown) and was furthermore subjected to prior loading history. This specimen was suitable for the

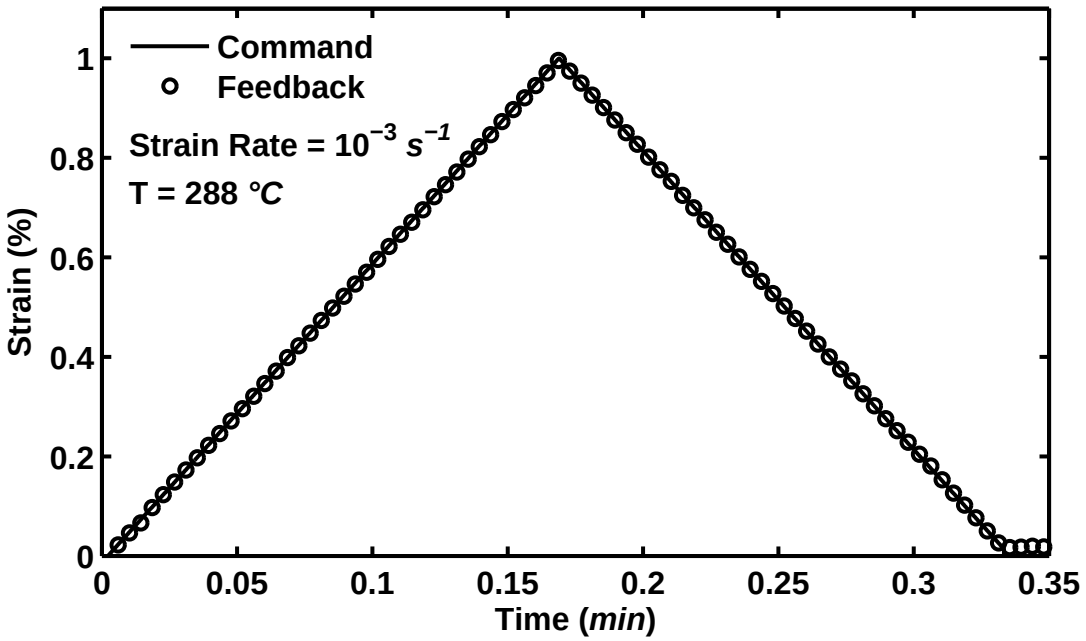

Figure 4.10: Strain Control Tuning with PMR-15 and Low Contact Force Extensometer: Loading and Unloading in Strain Control at 288 $^{\circ}C$. Strain Rate is 10^{-3} s^{-1}.

tuning of the testing system and the results of the several tests thoroughly validate the gain settings. However, because of the unknown prior loading history and moisture content, these results cannot be used in assessing the deformation behavior of the PMR-15 polymer.

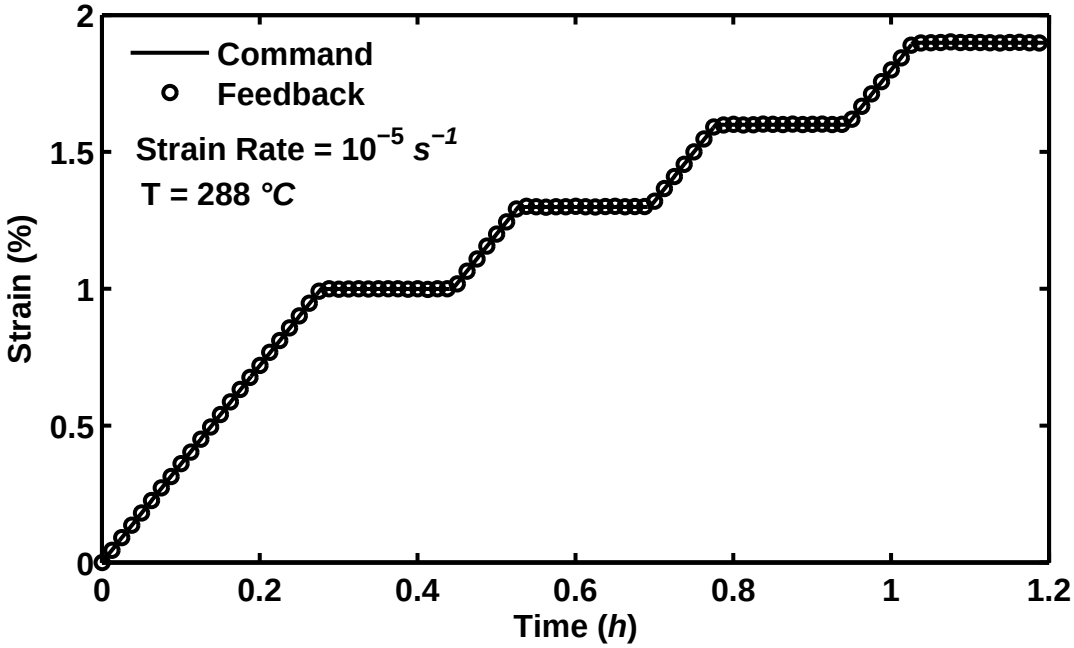

Figure 4.11: Strain Control Tuning with PMR-15 and Low Contact Force Extensometer: Constant Strain Rate with Intermittent Periods of Relaxation at 288 $^{\circ}C$.

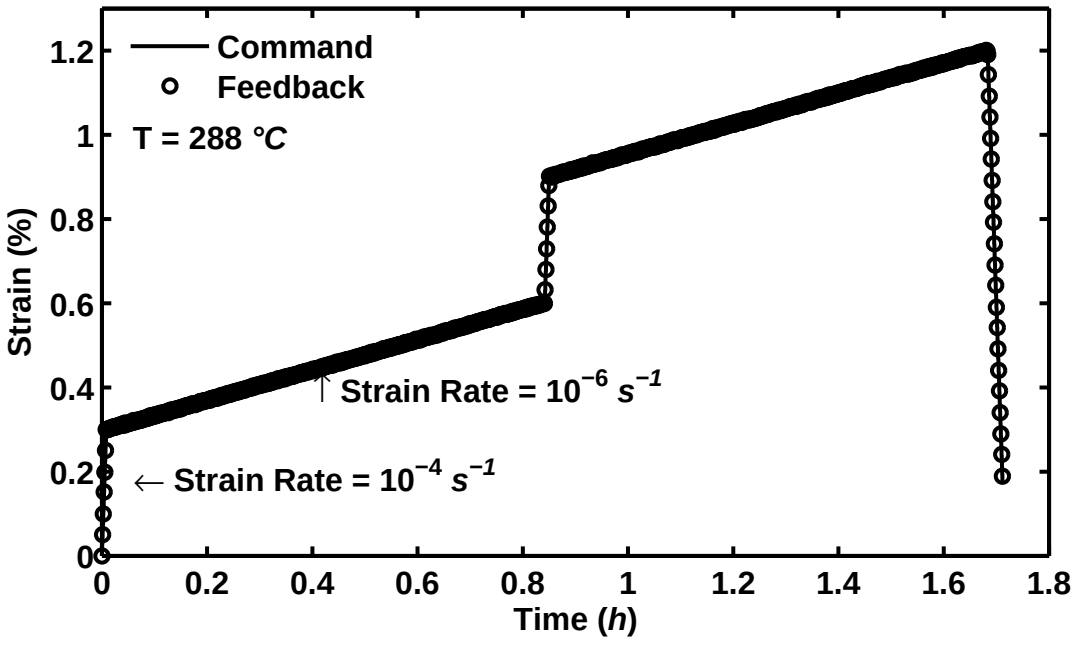

Figure 4.12: Strain Control Tuning with PMR-15 and Low Contact Force: Strain Rate Jump Test at 288 $^{\circ}C$.

V. Unaged PMR-15 Neat Resin: Experimental Observations

This chapter discusses the results of the mechanical tests for the unaged PMR-15.

5.1 Assessment of Specimen-to-Specimen Variability

Room temperature elastic modulus measurements were carried out for each specimen in order to determine the sample-to-sample variability within the material.

The experiment for this measurement was carried out in stress control mode. Each specimen was loaded at 1 MPa/s up to 3 MPa stress, then unloaded at 1 MPa/s to zero stress.

The mathematical tool utilized to calculate the elastic modulus from the experimental results was the 'polyfit' command in MATLAB. When executing the command 'polyfit(x,y,n)', MATLAB finds the coefficients of a polynomial $p(x)$ of degree n that fits the data y best in a least-squares sense. The polynomial is of the form

$$p(x) = p_1 x^n + p_2 x^{n-1} + ... + p_{n-1} x + p_{n+1}. \tag{5.1}$$

For the elastic modulus calculations, the degree $n = 1$; the polynomial reduced to the linear form

$$p(x) = p_1 x + p_2, \tag{5.2}$$

where x = strain data and y = stress data. The MATLAB function output provides the best fit values of p_1 and p_2, where p_1 = elastic modulus.

The mean room temperature elastic modulus is 4.2 GPa. Some scatter was observed (the associated standard deviation is 0.21 GPa). However, it was decided that no single sample should be eliminated based solely on the room temperature elastic modulus measurement.

5.2 Deformation Behavior at 288 $^{\circ}C$

The experimental investigations described in Section 4.2 were carried out on PMR-15 neat resin with no prior thermal aging. This research aims to investigate the strain rate (time)-dependent deformation behavior of the PMR-15 polymer at 288 $^{\circ}C$. The experimental program includes strain-controlled tests of monotonic loading and unloading with periods of relaxation as well as changes in strain rate. Effects of prior strain rate on creep behavior as well as on the recovery of strain at zero stress are also explored.

5.2.1 Monotonic Tension to Failure. Effect of strain rate was explored in tensile tests to failure conducted at constant strain rates of 10^{-6}, 10^{-5}, 10^{-4}, and 10^{-3} s^{-1}. The results are shown in Figure 5.1. It is seen that the stress-strain curves do not exhibit a distinct linear range; the slope continues to decrease slowly with increasing stress. The stress-strain curves obtained at different constant strain rates show little dependence on rate initially, producing the same quasi-elastic slope of approximately 2.1 GPa upon leaving the origin. After the transition to the inelastic regime, the material exhibits positive, nonlinear strain rate sensitivity. The flow stress level increases with increasing strain rate. Furthermore, the shape of the stress-strain

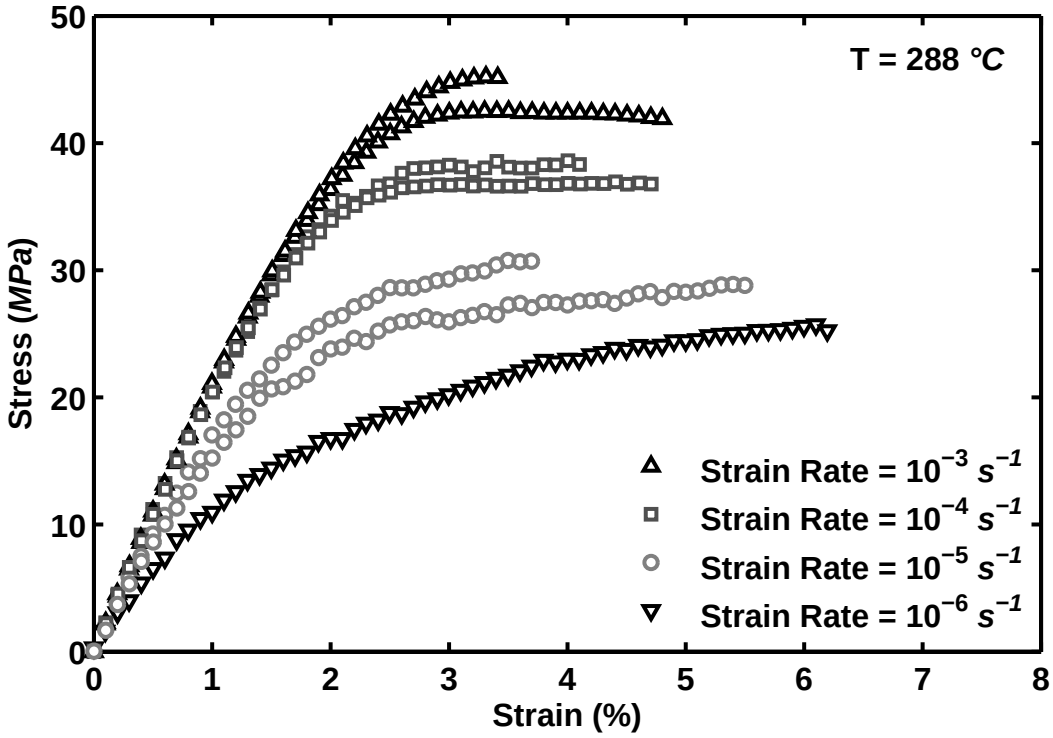

Figure 5.1: Stress-Strain Curves Obtained for PMR-15 in Tensile Test to Failure Conducted at Constant Strain Rates of 10^{-3}, 10^{-4}, 10^{-5}, and 10^{-6} s^{-1} at 288 $^{\circ}C$. The Dependence of the Stress-Strain Behavior on the Strain Rate is Evident.

curve undergoes a gradual change as the strain rate increases. The stress-strain curves obtained at slower strain rates depart from near-linear behavior at much lower stress levels than those obtained at faster strain rates. In addition, the "knee" of the stress-strain curve, where the quasi-linear elastic behavior transitions to inelastic flow becomes considerably more pronounced with increasing strain rate.

In order to establish repeatability, these tests were repeated for the three fastest strain rates. The results of the repeated tests were consistent in all cases as can be seen in Figure 5.1.

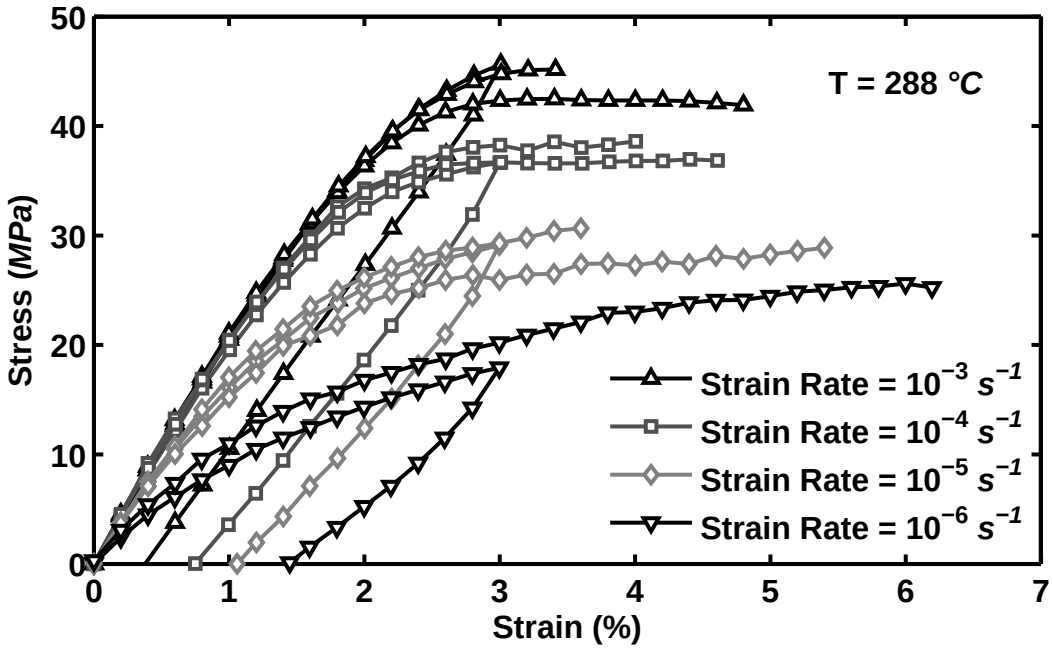

Figure 5.2: Stress-Strain Curves Obtained for PMR-15 in Loading/Unloading Tests Conducted at Constant Strain Rates of 10^{-3}, 10^{-4}, 10^{-5}, and 10^{-6} s^{-1} at 288 $^{\circ}C$ Compared to Tension to Failure Results. The Dependence of the Unloading Behavior on the Strain Rate is Evident.

5.2.2 Loading and Unloading. To assess the effect of strain rate on the unloading stress-strain behavior, strain-controlled tests consisting of loading to a fixed strain of 3% and unloading to zero stress at constant strain rate magnitude were carried out. Strain rate magnitudes ranging from 10^{-6} to 10^{-3} s^{-1} were employed. A maximum mechanical strain of 3% was selected based on tension to failure results so that the material could withstand the maximum strain at all four strain rates. As seen in Figure 5.2, the unloading stress-strain behavior is "curved" and strongly influenced by strain rate. The curved unloading behavior becomes increasingly more pronounced as the strain rate magnitude decreases. The inelastic strain measured immediately after reaching zero stress increases with decreasing strain rate magnitude.

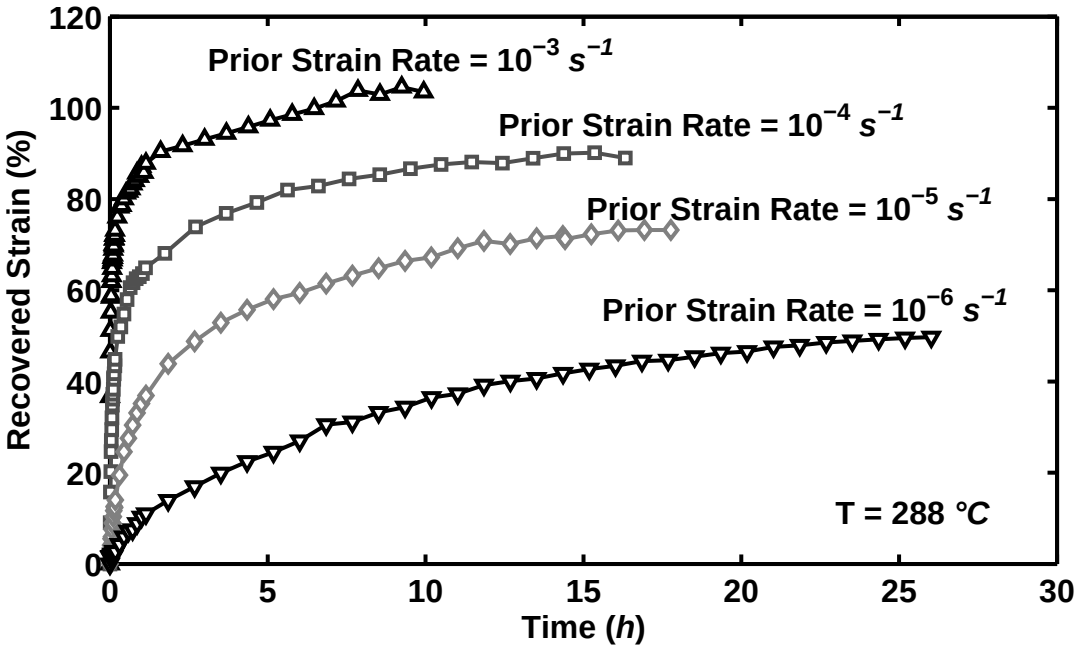

Figure 5.3: Recovery at Zero Stress at 288 $^{\circ}C$ (Following Loading and Unloading in Strain Control). Recovered Strain is Shown as a Percentage of the Initial Value (Inelastic Strain Value Measured Immediately After Reaching Zero Stress). The Effect of The Prior Strain Rate on the Recovered Strain is Apparent.

5.2.3 Recovery of Strain at Zero Stress. Following loading and unloading to zero stress at constant strain rate magnitude, the control mode was switched from strain to load, and the load was controlled to stay at zero for at least 10 h to observe the subsequent strain recovery. Results of the recovery tests are given in Figure 5.3, where the recovered strain is shown as a percentage of the inelastic strain value measured immediately after reaching zero stress. A profound influence of the prior strain rate on the recovery of strain is evident. Figure 5.3 reveals that a larger percentage of inelastic strain is recovered in tests conducted with higher prior strain rate magnitude. The strain rate during the recovery period decreases rapidly and most of the strain is recovered after approximately 8 h for all but the slowest prior

strain rate. In the test conducted with the strain rate magnitude of 10^{-3} s^{-1}, the inelastic strain measured upon unloading is fully recovered after 8 h. Conversely, in the tests conducted with slower strain rates, the inelastic strain was only partially recovered. In tests conducted with strain rate magnitudes of 10^{-4} and 10^{-5} s^{-1}, the recovery rate dropped to near zero after 15 h. Nearly 90% of the inelastic strain measured upon unloading was recovered in the 10^{-4} s^{-1} test and approximately 70% of the inelastic strain was recovered in the 10^{-5} s^{-1} test. Considering the near zero recovery rate, the full recovery of strain is unlikely in these tests. In the 10^{-6} s^{-1} test, only about one half of the inelastic strain measured upon unloading was recovered after 26 h. Given the slow rate of recovery and the strain of 0.73% remaining at the end of the 26-h recovery period, full recovery is improbable even after a long time. A permanent strain can be reasonably assumed.

5.2.4 Constant Strain Rate Loading with Periods of Relaxation.

5.2.4.1 Exploratory Tests. The first three experiments of this type were exploratory tests into the behavior of PMR-15. Since relaxation data was not available for this material, exploratory testing was needed to determine proper strain intervals for the relaxation periods as well as to determine adequate durations of relaxation periods to allow for saturation. (Saturation refers to the state where the relaxation rate approaches zero.) The strain intervals in this type of test need to be high enough to allow the material (following a period of relaxation) to reach the flow stress levels attained in monotonic loading. This allows for full comparison of the

subsequent relaxation periods while avoiding erroneous conclusions about the effect of the loading history. (For more details on these possible erroneous conclusions, see Bordonaro and Krempl [4].) In addition, if the material is allowed to reach the flow stress levels following a relaxation period, the results can be used to confirm the value of the tangent modulus. The exploratory tests were conducted at strain rates of 10^{-3} and 10^{-5} s^{-1}.

The first exploratory test was conducted at the rate of 10^{-3} s^{-1}. The first relaxation period was introduced at the strain of 1%. In order to ensure that near zero relaxation rate can be achieved, the initial tests were programmed such that the relaxation period could be monitored and the length increased as needed (or decreased if appropriate) during the individual relaxation periods. The individual relaxation durations were varied from just over 1.5 h to just under 12 h. Due to the limited ductility observed in the tension to failure tests (max strain of 5% at the rate of 10^{-3} s^{-1}) it was desirable to find a small strain interval so that multiple relaxation periods could be carried out within a single test. The interval of strain between the relaxation periods was initially set to 0.5%. The stress-strain results from this test are shown in Figure 5.4.

The graph in Figure 5.4 shows that at this high strain rate, the location of the initial relaxation period, coupled with the small interval of strain between relaxation periods caused a scenario where the material could not reach the levels of flow stress that were found during tension to failure tests. Therefore, the strain interval was increased to 1.0% and then again to 1.5%. It was determined that the strain interval of

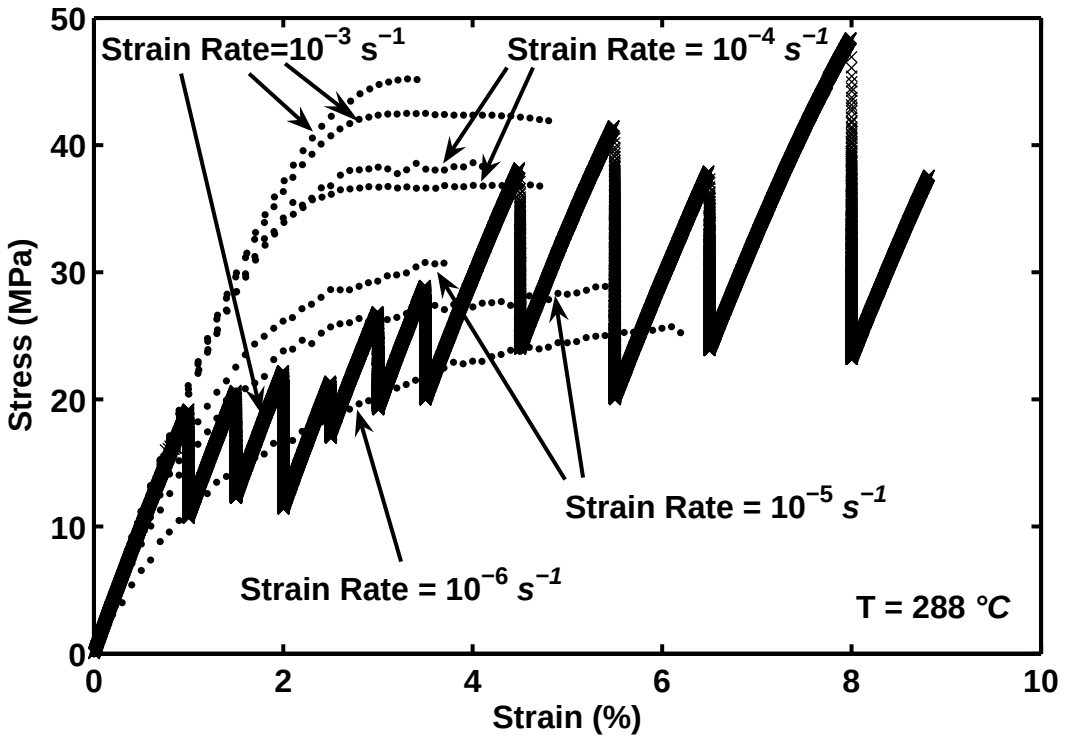

Figure 5.4: Exploratory Constant Strain Rate Loading ($10^{-3}\ s^{-1}$) with Intermittent Periods of Relaxation. Results Show the Need for Strain Intervals > 1.5% Between Relaxation Periods and for Relaxation Durations of 12 h or More.

1.5% was sufficient to allow the material to reach the plastic flow curve during loading. A quasi-linear behavior is observed in each portion of strain-controlled loading. It is postulated that the material would diverge from this linear behavior and begin to follow the tensile stress-strain curve for a given strain rate provided the strain intervals were large enough. This test revealed a surprising result: the material reached strains in excess of 8%, a strain level not approached at any strain rate in the tension to failure tests.

The stress vs time curves produced during the relaxation periods included in this test are shown in Figures 5.5 to 5.7. The results show that for relaxation periods

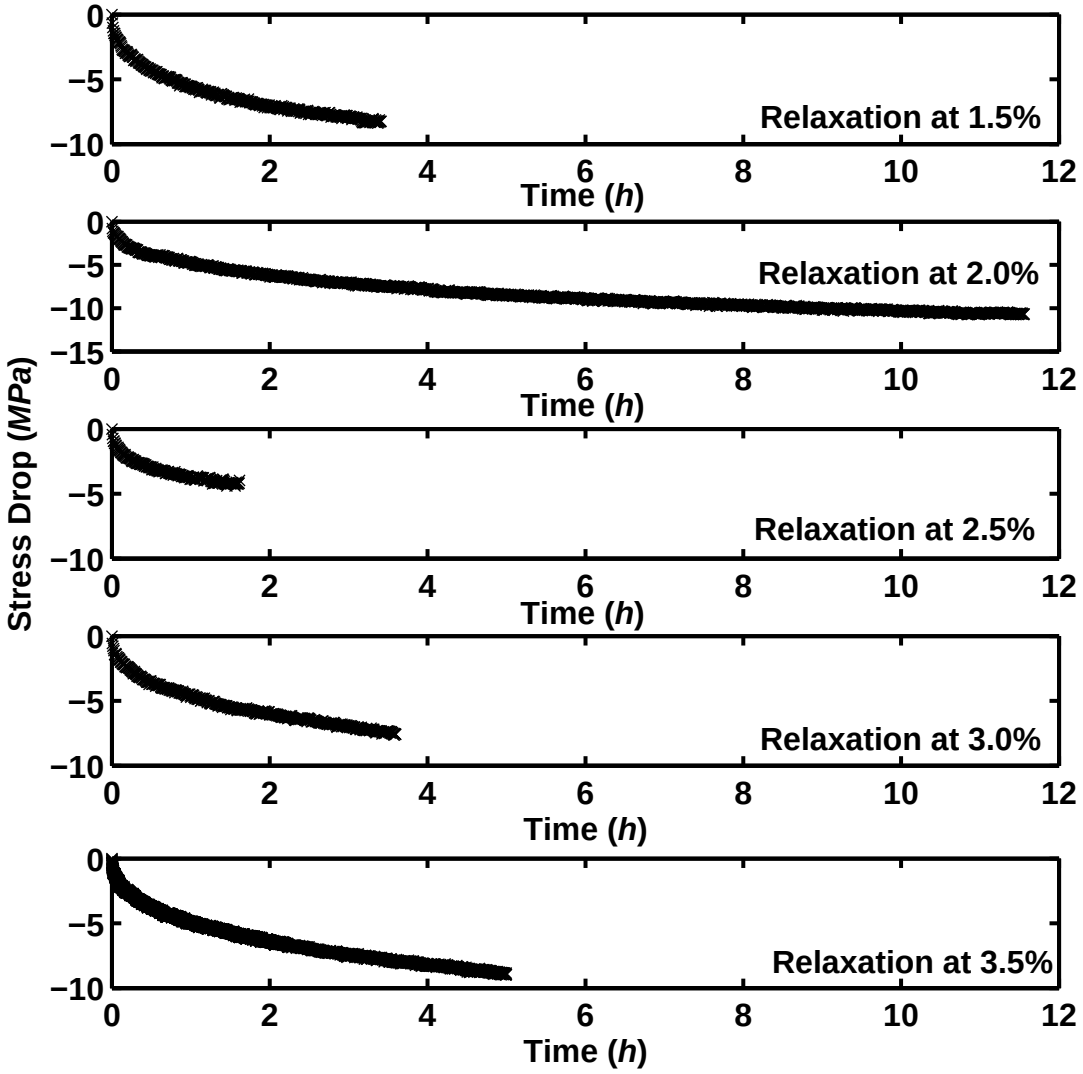

Figure 5.5: Stress Drop During Relaxation vs Time Curves Obtained in Exploratory Constant Strain Rate (10^{-3} s^{-1}) Test with Intermittent Periods of Relaxation. Strain Interval Between Relaxation Tests is 0.5%.

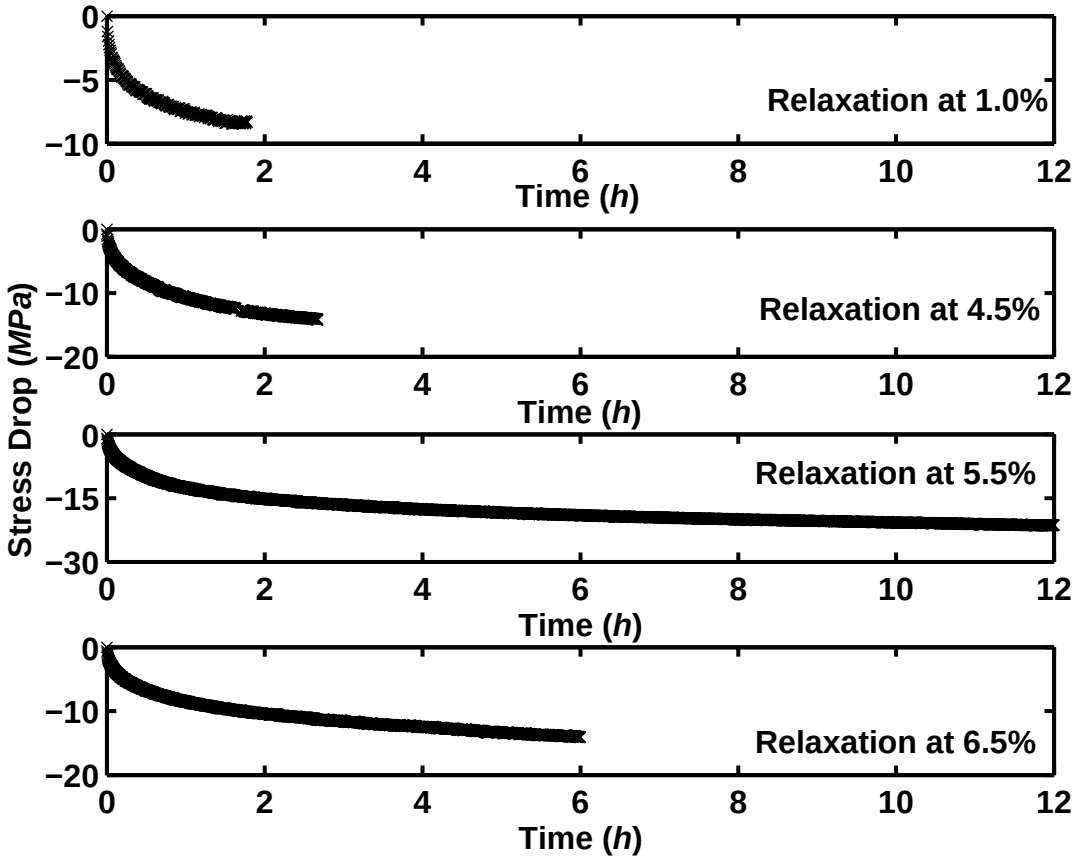

Figure 5.6: Stress Drop During Relaxation vs Time Curves Obtained in Exploratory Constant Strain Rate (10^{-3} s^{-1}) Test with Intermittent Periods of Relaxation. Strain Interval Between Relaxation Tests is 1.0%.

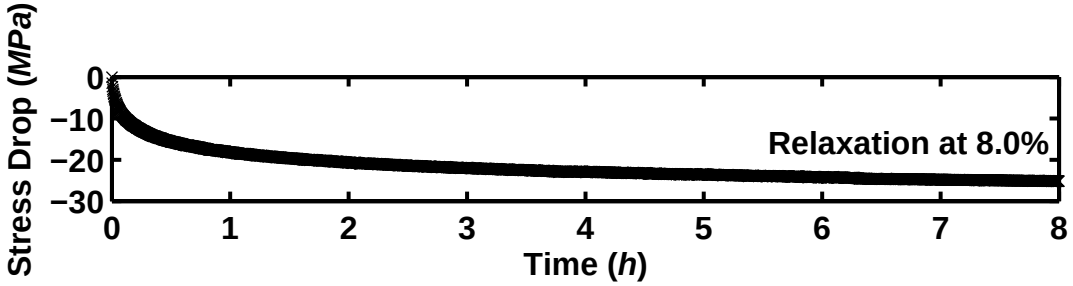

Figure 5.7: Stress Drop During Relaxation vs Time Curves Obtained in Exploratory Constant Strain Rate (10^{-3} s^{-1}) Test with Intermittent Periods of Relaxation. Strain Interval Between Relaxation Tests is 1.5%.

starting at higher stress levels, the stress relaxation takes longer to saturate. The results also show that in most relaxation tests, the stress relaxation rate had still not reached zero after 12 h. However, it does appear that the stress values at the end of the relaxation periods are tending to stationary points which form a curve just below the stress-strain curve obtained at a strain rate of $10^{-6}\ s^{-1}$. This behavior suggests the existence of an equilibrium stress curve with the shape similar to that of the stress-strain curve obtained at $10^{-6}\ s^{-1}$. In tests conducted with this slow strain rate, the relaxation test that last for 12 h still produce some stress drop at the end of the 12 h period. However, the change in stress during the last hour constitutes $< 3\%$ of the total stress drop. Furthermore, the drop in the last six hours of relaxation is $< 20\%$ of the total stress drop. Therefore it is reasonable to assume that saturation of the relaxation is imminent. Hence, the relaxation duration was set to 12 h for the remaining tests.

The second exploratory test was carried out at $10^{-5}\ s^{-1}$. The results are shown in Figure 5.8. The first relaxation period was introduced at 2%. The strain intervals between relaxation periods were 1% and 1.5%. These strain intervals were large enough for the stress to reach the flow stress values expected for the $10^{-5}\ s^{-1}$ rate based on the tensile tests conducted at $10^{-5}\ s^{-1}$ results and based on the results of the exploratory test with periods of relaxation conducted at $10^{-3}\ s^{-1}$. A stress overshoot was seen during loading following a relaxation test at $\epsilon = 1.5\%$. Based on the results of Bordonaro and Krempl [4, 5] and Khan [25, 26] it was postulated that if the material was given an even larger strain interval between relaxation periods,

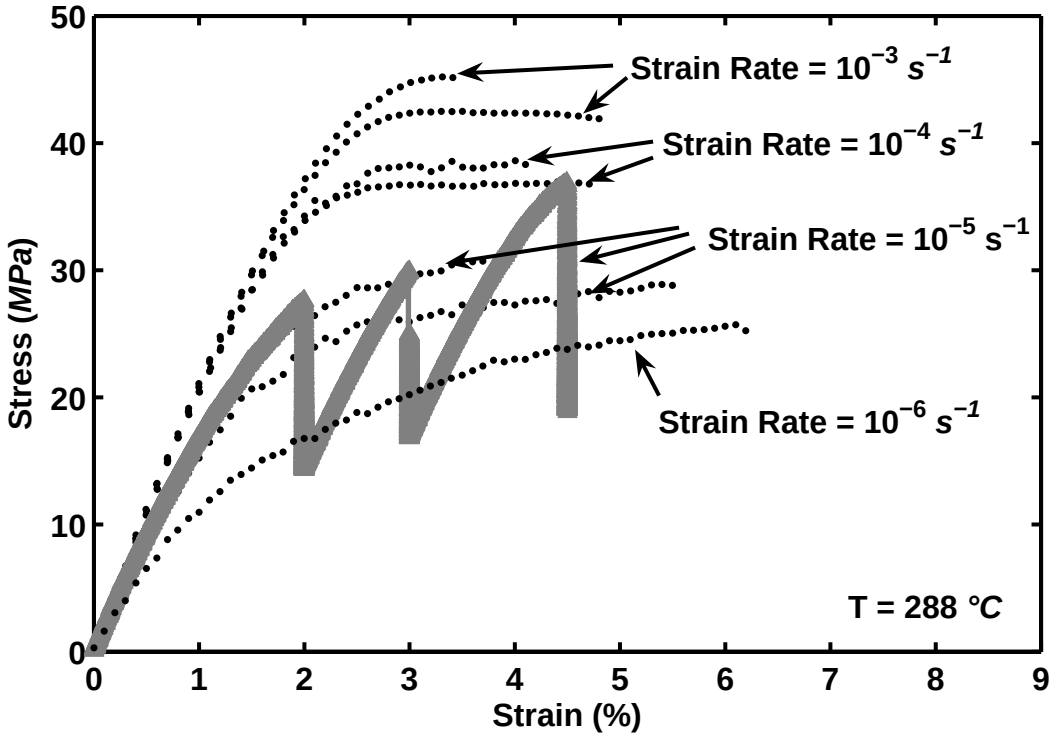

Figure 5.8: Exploratory Constant Strain Rate Loading (10^{-5} s^{-1}) with Intermittent Periods of Relaxation. Shows the Need for Wide Strain Intervals Between Relaxation ($> 1.5\%$) and for Relaxation Durations of 12 h. Also Shows a Material Overshoot Once Loading is Resumed After a Relaxation Period.

the stress would settle back to the characteristic stress-strain curve obtained in the tension to failure test. The stress drop during the relaxation for each of these periods is shown in Figure 5.9.

This conclusion was confirmed in a test conducted at the strain rate of 10^{-5} s^{-1} with a single relaxation period introduced at the strain of 3%. After the relaxation, the loading was resumed at the rate of 10^{-5} s^{-1} and continued until failure. The stress-strain curve and the relaxation curve obtained in this test are shown in Figures 5.10 and 5.11, respectively. Results in Figure 5.10 demonstrate that when the strain-

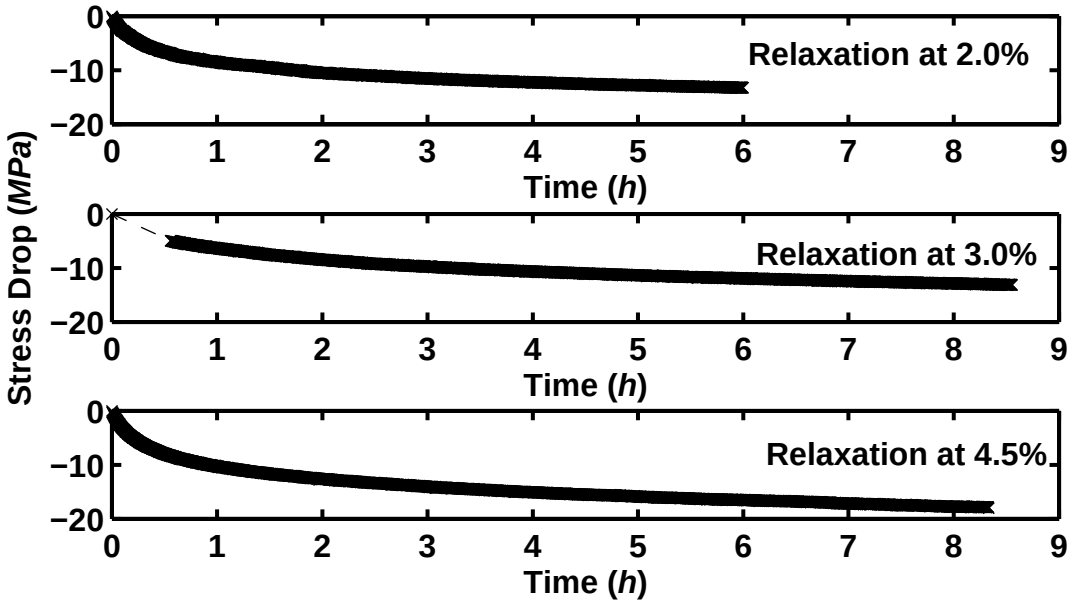

Figure 5.9: Stress Drop During Relaxation vs Time Curves Obtained in Exploratory Constant Strain Rate (10^{-5} s^{-1}) Test with Intermittent Periods of Relaxation. Strain Interval Between Relaxation Tests is Varied.

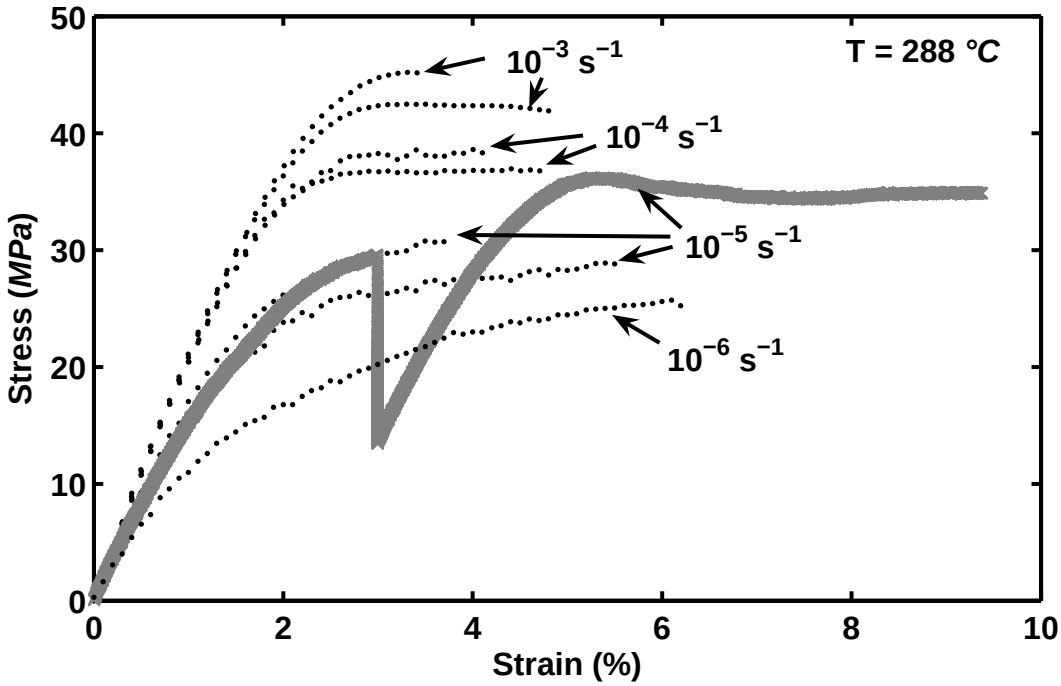

Figure 5.10: Constant Strain Rate Loading (10^{-5} s^{-1}) with a Single Period of Relaxation. Once Loading is Resumed After Relaxation, the Material First "Overshoots" and then Returns to the Stress-Strain Curve Characteristic for a Given Strain Rate.

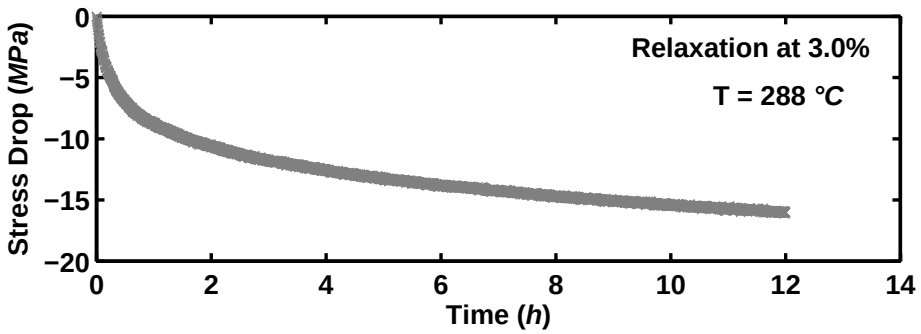

Figure 5.11: Stress Drop During Relaxation vs Time Curves Obtained in Exploratory Constant Strain Rate (10^{-5} s^{-1}) Test with One Period of Relaxation.

controlled loading is resumed after relaxation, the material initially "overshoots" but then returns to the stress-strain curve characteristic for a given strain rate. This test was repeated with an attempt at an additional relaxation period once the transients had died out. The results in Figures 5.12 and 5.13 show that the specimen failed before the transients had died out.

The results of these exploratory tests were evaluated in order to determine suitable test parameters for the constant strain rate tests with intermittent periods of relaxation. These exploratory results reveal that only one relaxation period can be achieved within a single test due to the large interval of strain needed between relaxation periods and the low ductility of the material. The results also show that a relaxation period of at least 12-h duration is needed for relaxation to approach saturation.

5.2.4.2 Monotonic Tests with a Single Period of Relaxation. Because only one relaxation period can be achieved within a single test, two tests of this type

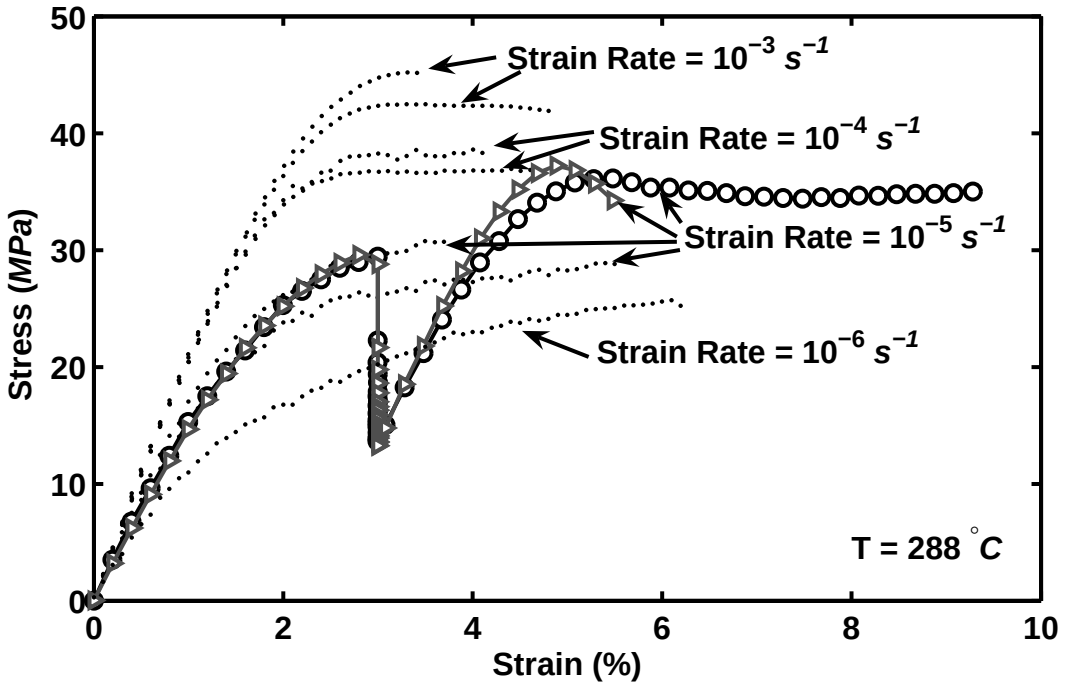

Figure 5.12: Constant Strain Rate Loading (10^{-5} s^{-1}) with a Single Period of Relaxation. Showing Repeatability of "Overshoot" Once Loading is Resumed.

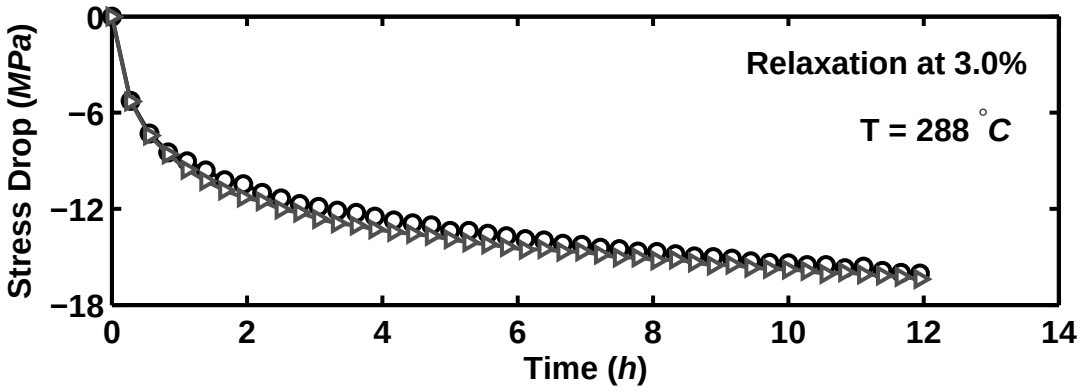

Figure 5.13: Stress Drop During Relaxation vs Time Curves Obtained in Exploratory Constant Strain Rate (10^{-5} s^{-1}) Test with One Period of Relaxation. Illustrating Repeatability of Relaxation Response.

per strain rate of interest are needed in order to evaluate the effect of the stress and strain at the beginning of relaxation on the relaxation behavior. In these tests, a specimen is subjected to uninterrupted loading at a constant strain rate to a target strain in the region of fully established inelastic flow, where a 12-h relaxation period is introduced. After the end of the relaxation period, straining resumes at the given strain rate and continues to specimen failure. The tests were conducted under strain control using strain rates of 10^{-6}, 10^{-5}, 10^{-4}, and 10^{-3} s^{-1} during loading and, naturally, $\dot{\epsilon} = 0$ s^{-1} during relaxation. Two tests were conducted at each strain rate incorporating a relaxation period at (1) the strain of 3% and (2) the strain of 4.5%. Results are presented in Figures 5.14 and 5.15. The stress-strain curves in Figure 5.14 reveal that, once the monotonic loading is resumed after the relaxation, the stress-strain curve first "overshoots", then quickly returns to the stress level characteristic for a given strain rate (compare with uninterrupted stress-strain curves in Figure 5.1). The "overshoot" is most pronounced at the fast strain rate of 10^{-3} s^{-1} and hardly noticeable at the slow strain rate of 10^{-6} s^{-1}. A similar "overshoot" or transient region is observed in the results of Bordonaro and Krempl [4, 5] and Khan [25, 26].

Relaxation curves showing the stress drop vs time (see Figure 5.15) demonstrate that the decrease in stress during relaxation is profoundly influenced by the prior strain rate. A much larger decrease in stress is observed in relaxation following loading at 10^{-3} s^{-1} than in relaxation following loading at 10^{-6} s^{-1}. The total stress drops in the 12-h relaxation tests are increasing with increasing prior strain rate. (Note that viscoelastic models such as Schapery's do not address this effect.) Furthermore,

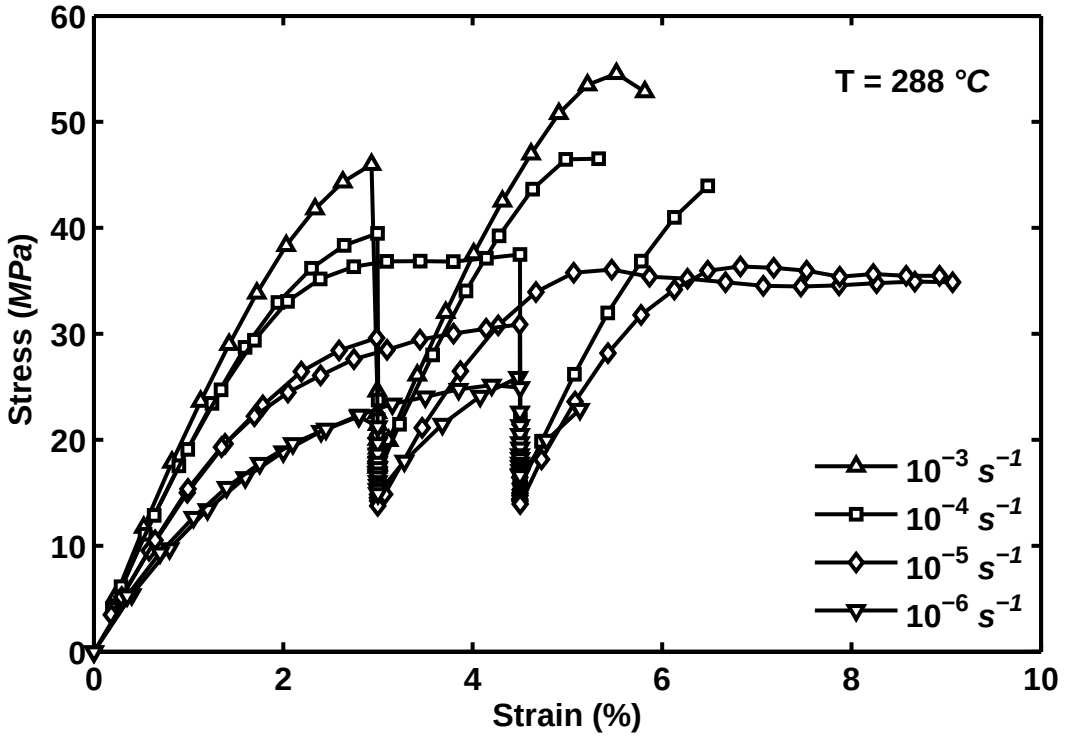

Figure 5.14: Stress-Strain Curves Obtained for PMR-15 Polymer in Constant Strain Rate Tests with Intermittent Periods of Relaxation at 288 $°C$. When Loading at a Constant Strain Rate is Resumed After the Relaxation Period, the Material Reaches the Flow Stress Characteristic for that Particular Strain Rate.

within each strain rate the relaxation stress drops are essentially independent of the stress and strain at the beginning of the relaxation period. For each of the prior strain rates of 10^{-6}, 10^{-5}, and 10^{-4} s^{-1}, the relaxation curves measured at $\epsilon = 3\%$ and those measured at $\epsilon = 4.5\%$ are nearly identical. Note that the relaxation rate was not zero when relaxation tests shown in Figures 5.14 and 5.15 were stopped. Upon continuation of the relaxation tests, the stress would have dropped further at an ever-decreasing rate, finally coming to rest at a nonzero level. However, the change in stress during the last hour in all tests constitutes $< 6\%$ of the total stress

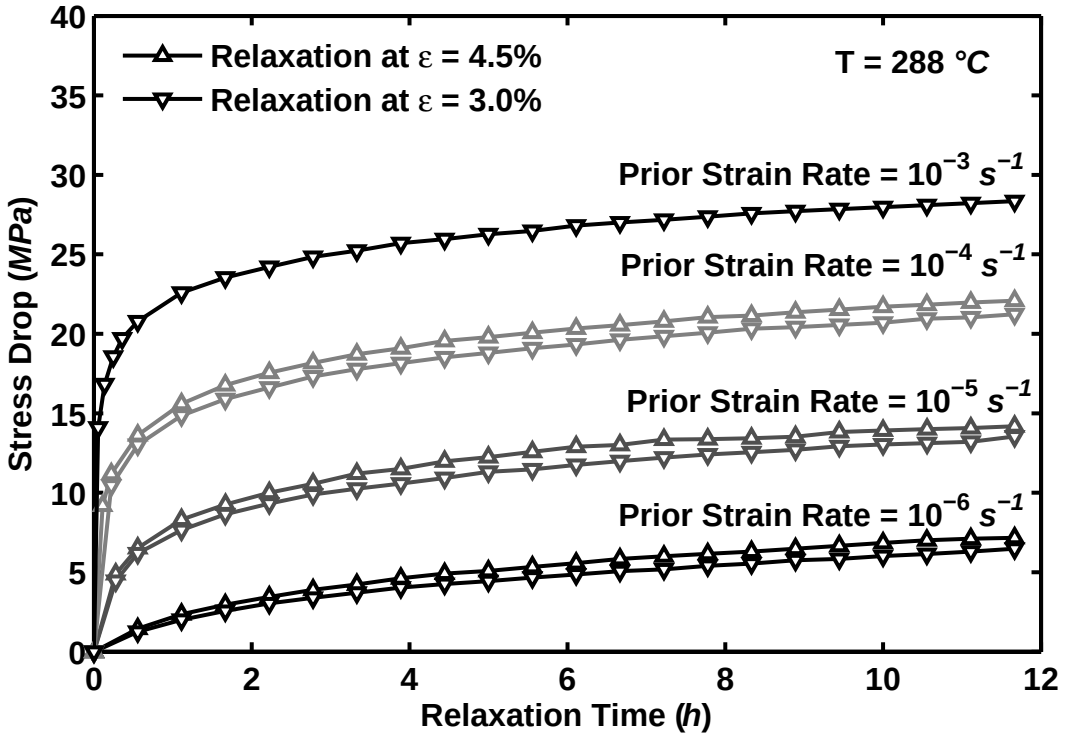

Figure 5.15: Stress Decrease vs Relaxation Time for the PMR-15 Polymer at 288 $^{\circ}C$. Influence of Prior Strain Rate on the Stress Drop During Relaxation is Evident. Stress Drop During Relaxation of a Fixed Duration is Independent of the Stress and Strain at the Beginning of Relaxation.

drop. Furthermore, the stress rate at the end of the aforementioned relaxation tests was between 0.000004 and 0.00009 MPa/s. Therefore, it is reasonable to assume that saturation of the relaxation stress was imminent after 12 h of relaxation. It is recognized that extending the relaxation periods to achieve zero relaxation rate may be impractical. Hence the relaxation rate of $\leq 0.00009\ MPa/s$ is adopted as a practical definition of "nearly-saturated" relaxation. Results in Figure 5.14 suggest that the stress-strain points at the end of the relaxation tests form a curve that has a shape of a stress-strain diagram. Hence, it may be expedient to postulate that

the relaxation comes to rest at nonzero stresses that form the equilibrium boundary, which may be interpreted as the stress-strain curve for vanishing strain rate. It is recognized that in practice the equilibrium boundary cannot be determined exactly, it can only be inferred. In practice it would be impossible to obtain the stress-strain curve for strain rates $\leq 10^{-12}\ s^{-1}$. A tensile test conducted at $10^{-12}\ s^{-1}$ would take over 475 years to reach a strain of 1.5%.

5.2.4.3 Relaxation Upon Unloading Stress-Strain Path. As seen in Figures 5.14 and 5.15, when relaxation tests are performed on the loading segment of a stress-strain curve, the drop in stress occurs in a monotonic fashion. However, in the instance of relaxation tests conducted on the unloading segment of the stress-strain curve, different material behavior is observed. Figure 5.16 depicts stress-strain curves obtained in three tests, which consist of loading a specimen to a strain of 4%, unloading at the same strain rate magnitude to a fixed strain where a relaxation test is performed and, finally, unloading to zero stress with the same strain rate magnitude. The loading/unloading is carried out at a constant strain rate magnitude of $10^{-4}\ s^{-1}$, while the 12-h relaxation test is performed at (1) $\epsilon = 3.5\%$, (2) $\epsilon = 2.5\%$, and (3) $\epsilon = 1.5\%$. The relaxation curves presented in Figure 5.17 reveal that the relaxation behavior during unloading is greatly influenced by the strain point at which the relaxation period is introduced. At $\epsilon = 3.5\%$, a strain close to the point where unloading begins, a monotonic decrease in stress is recorded. Conversely, in relaxation tests performed further along the unloading stress-strain curve (a smaller

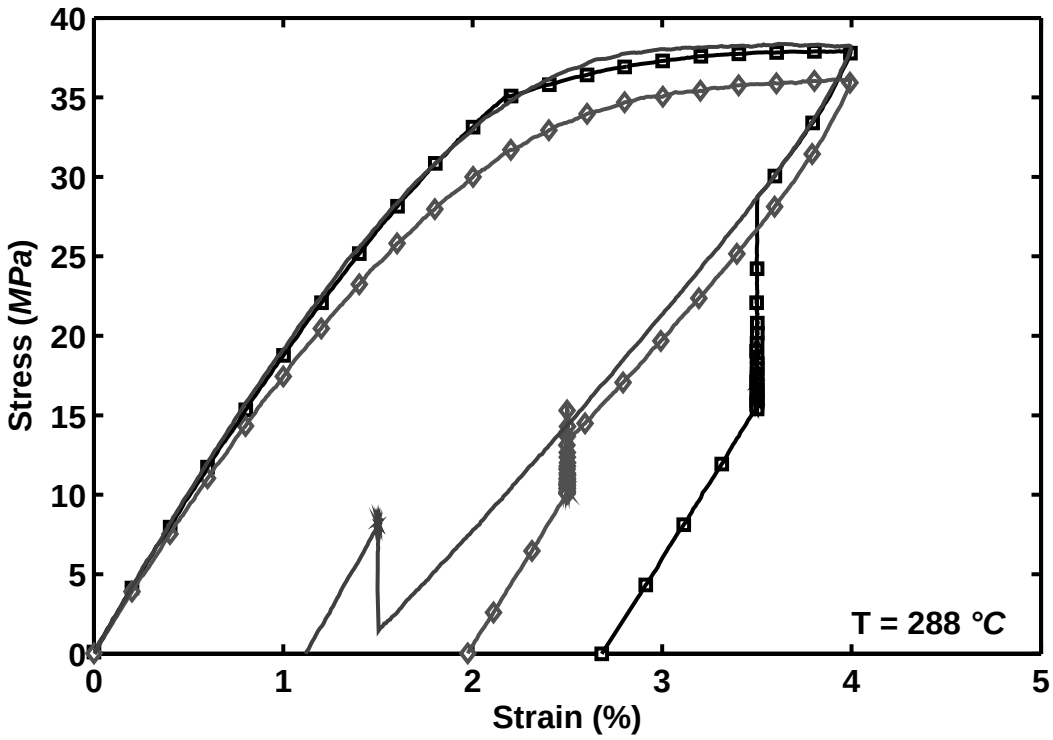

Figure 5.16: Stress-Strain Curves Obtained in Constant Strain Rate Tests Conducted at 10^{-4} s^{-1} with 12-h Relaxation Tests at 3.5%, 2.5% and 1.5% Strain During Unloading. Monotonic Decrease in Stress is Observed in Relaxation Test at 3.5%. Initial Stress Increase Followed by Stress Decrease is Observed in Relaxation Test at 2.5%. Stress Increase is Observed in Relaxation Tests at 1.5%.

strain of 1.5%), the stress during relaxation increases. Of particular interest is the relaxation test performed during unloading at an intermediate strain of 2.5%. In this case, a non-monotonic change in stress is observed; the stress first increases and then begins to decrease. The corresponding rate of change of stress is first positive and then becomes negative. The reversal of stress rate in relaxation tests conducted during unloading was also reported for several amorphous and semicrystalline polymers at room temperature [4, 27, 28]. It is noteworthy that creep tests performed during unloading exhibit a similar tendency to undergo a change in the sign of the rate of

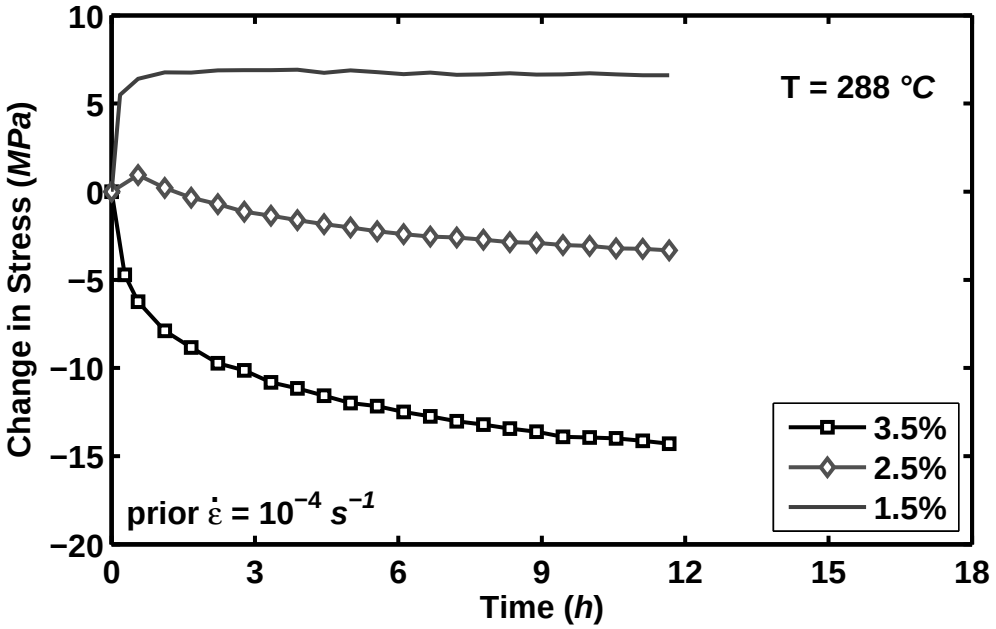

Figure 5.17: Change in Stress vs Time for the Relaxation Tests Shown in Figure 5.16. Prior Strain Rate Magnitude is 10^{-4} s^{-1}. The Sign of the Change in Stress is Strongly Influenced by the Strain Point at which the Relaxation Period is Introduced on the Unloading Stress-Strain Path.

change of strain (strain rate reversal), as shown by Falcone and Ruggles-Wrenn [15] for PMR-15 at 288 $°C$.

Similar trends in relaxation behavior during unloading are observed in tests conducted with a loading/unloading strain rate magnitude of 10^{-6} s^{-1} (see stress-strain curves in Figures 5.18 and relaxation curves in Figure 5.19). In this case, stress rate reversal (a very slight stress increase followed by a stress decrease) is seen during relaxation at 3.5% strain. Monotonic increase in stress is observed during relaxation at 2.5% strain. In addition, results in Figures 5.16–5.19 demonstrate that the magnitude of stress change during relaxation is larger for tests conducted with

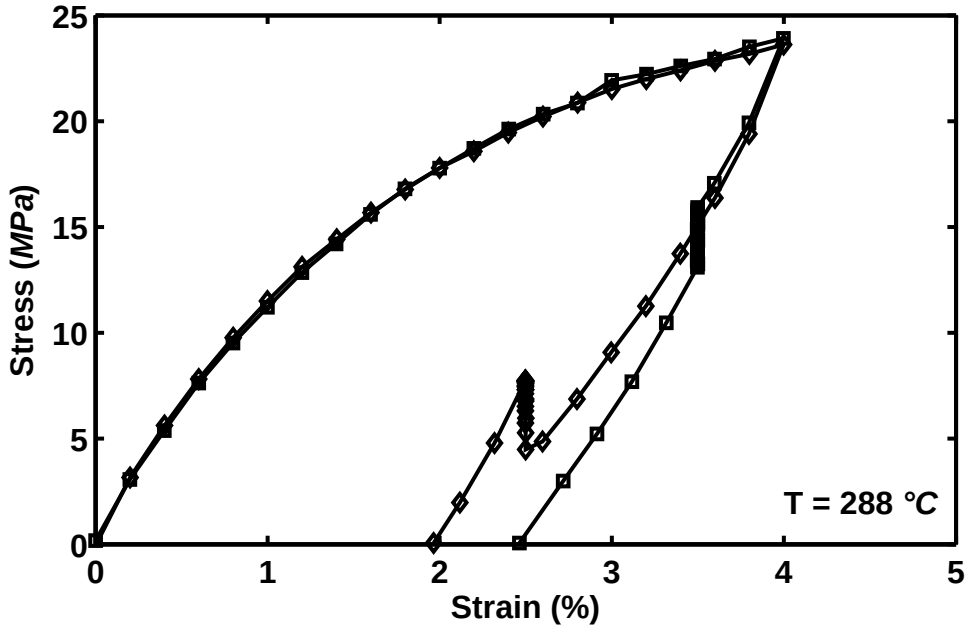

Figure 5.18: Stress-Strain Curves Obtained in Constant Strain Rate Tests Conducted at 10^{-6} s^{-1} with 12-h Periods of Relaxation at 3.5% and 2.5% Strain During Unloading. Monotonic Decrease in Stress is Observed in Relaxation Test at 3.5%, and Monotonic Increase in Stress, in Relaxation Test at 2.5%.

higher prior strain rate magnitude. Note that following the relaxation period, regular unloading behavior is resumed (compare with the stress-strain curves in Figure 5.2).

5.2.5 Strain Rate Jump Test. The Strain Rate Jump Test (SRJT) [59, 61] consisting of segments of monotonic loading at two different strain rates was performed to assess whether the PMR-15 polymer exhibits the strain rate history effect at 288 $°C$. The terminology "strain rate history effect" is used here as defined by Krempl and co-workers [5,25,61]. A material exhibits a lack of a strain rate history effect when it has a rapidly fading "memory" for the prior imposed strain rate, with the currently imposed strain rate having the most influence on the response. This term

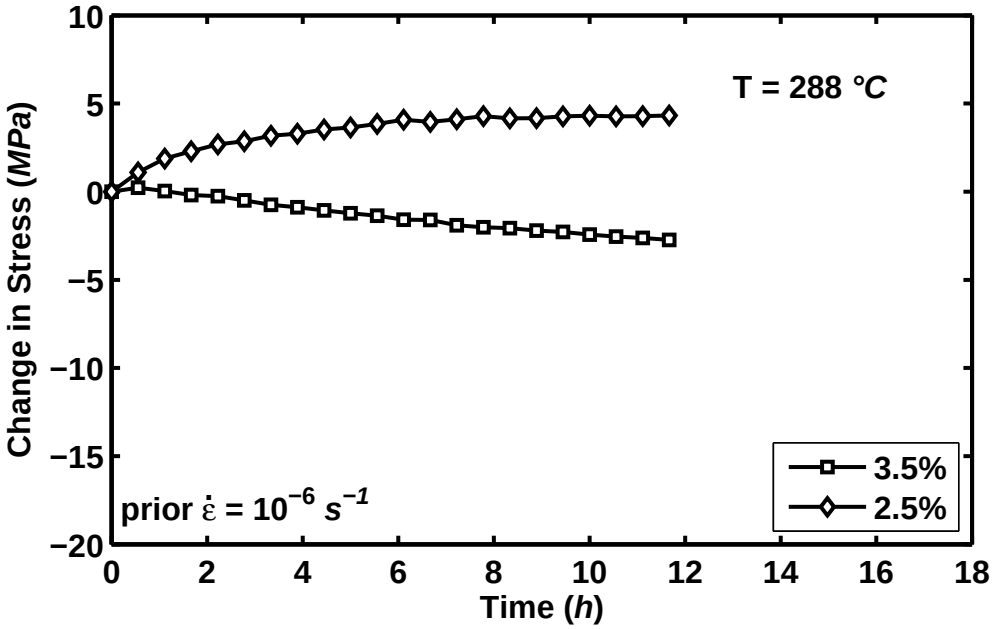

Figure 5.19: Change in Stress vs Time for the Relaxation Tests Shown in Figure 5.18. Prior Strain Rate Magnitude is 10^{-6} s^{-1}. The Sign of the Change in Stress is Strongly Influenced by the Strain Point at which the Relaxation Period is Introduced on the Unloading Stress-Strain Path. The Magnitude of the Change in Stress Depends on the Strain Rate Preceding the Relaxation Test.

is used in the discussion of the SRJT and not in the discussion of other experimental results.

In the current test, the strain rates were 10^{-3} and 10^{-5} s^{-1}. The stress-strain curves produced in two SRJTs are shown in Figure 5.20 together with the stress-strain curves obtained in constant strain rate tests conducted at 10^{-3} and 10^{-5} s^{-1}. It is seen that a reduction in strain rate by two orders of magnitude causes a sharp decrease in stress, with the flow stress reaching a level characteristic of a lower strain rate. The portions of the stress-strain curves obtained at 10^{-5} s^{-1} in the SRJT fall essentially on top of the stress-strain curves produced in constant strain rate tests

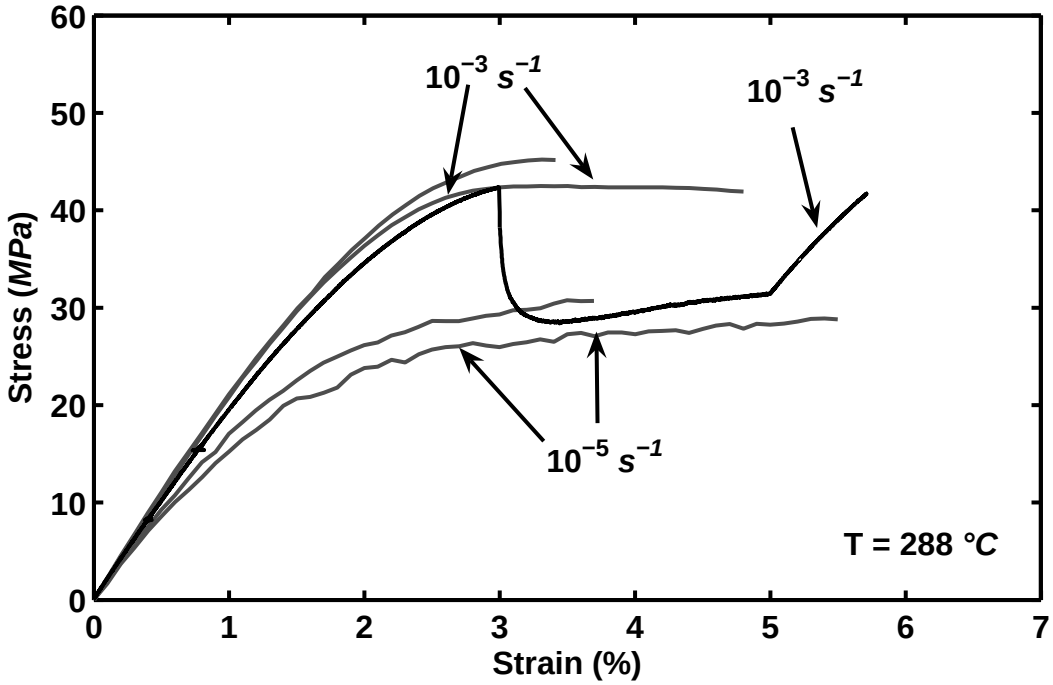

Figure 5.20: Stress-Strain Curves Obtained for PMR-15 Polymer in Strain Rate Jump Tests and in Constant Strain Rate Tests at 288 $°C$. Upon a Change of the Strain Rate, the Material "Returns" to the Stress-Strain Curve Characteristic for that Particular Strain Rate.

conducted at that strain rate. Once the strain rate in the SRJT is increased from 10^{-5} to 10^{-3} s^{-1} the stress increases until the flow stress level characteristic of the strain rate of 10^{-3} s^{-1} is reached. These results suggest that once the inelastic flow is fully established, a unique stress-strain curve is obtained for a given strain rate. This behavior has been termed as an absence of a strain rate history effect by Ruggles and Krempl [61]. Therefore, it can be state that at 288 $°C$, the PMR-15 polymer does not exhibit the strain rate history effect, i. e. the material rapidly "forgets" prior history of straining at different rates and "returns" to the stress-strain curve characteristic of a given strain rate.

The lack of a strain rate history effect in PMR-15 supports the selection of VBO as a constitutive equation. Once plastic flow is fully established, a unique stress-strain curve is obtained for a given strain rate. The flow stresses do return to the stress-strain curve characteristic for a particular strain rate after initial transients have died out.

5.2.6 Creep. The influence of prior strain rate on creep behavior was explored in creep tests of 6-h duration preceded by uninterrupted loading to a target creep stress of 21 MPa at constant strain rates of 10^{-6} and 10^{-4} s^{-1}. The capability of the testing system to instantaneously switch control mode made it possible to load a specimen to a target stress of 21 MPa at a constant strain rate under strain control, then switch mode to load control to perform a creep test. The creep strain vs time curves are presented in Figure 5.21. Primary and secondary creep was observed in the test preceded by loading at 10^{-4} s^{-1}, while only primary creep was observed in the test with prior strain rate of 10^{-6} s^{-1}. Results in Figure 5.21 demonstrate that creep behavior is strongly influenced by prior strain rate. For a given stress level, creep strain accumulation increases nonlinearly with increasing prior strain rate. An increase of two orders of magnitude in prior strain rate results in a less than twofold increase in creep strain. Creep behavior of PMR-15 polymer at 288 $^{\circ}C$ has been studied in fully load-controlled tests as well [15]. It was found that the creep strain increased nonlinearly with prior stress rate (see Figure 5 of Reference [15]). The amount of creep strain accumulated during a given hold time does not depend on

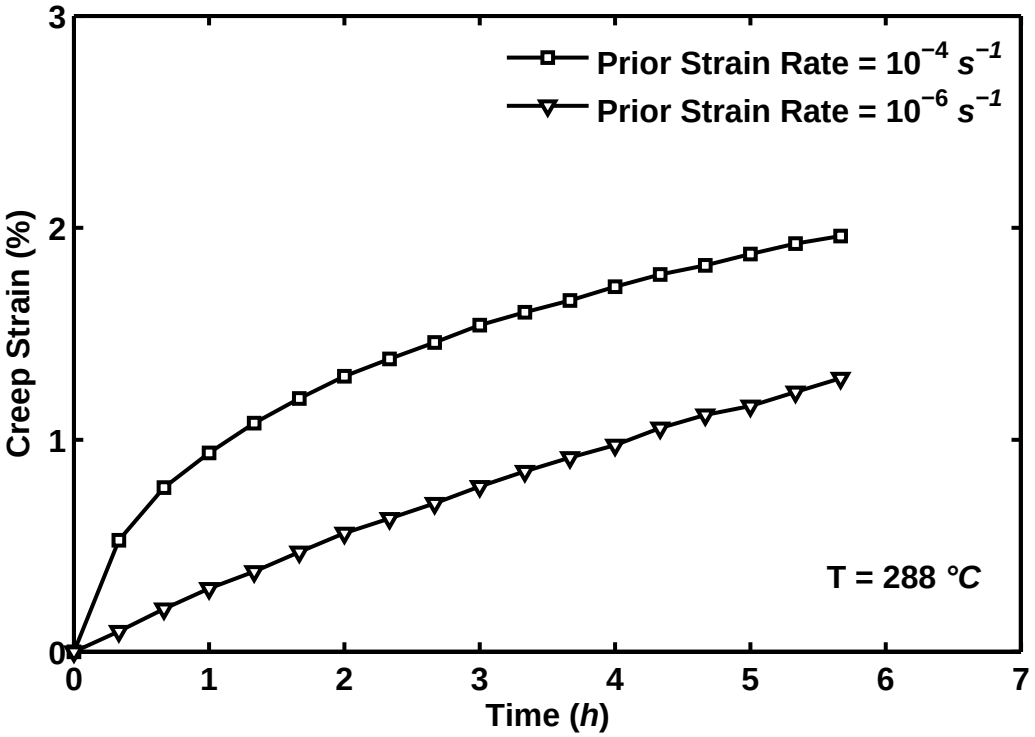

Figure 5.21: Creep Strain vs Time at 21 MPa and 288 $°C$. Effect of Prior Strain Rate on Creep is Apparent. Creep Strain Increases Nonlinearly with Prior Strain Rate.

the stress alone. Therefore, it is not sufficient to merely state a stress level when presenting creep results, prior loading rate must be accounted for as well.

VI. Implications For Modeling

The experimental results reported here and previously by Falcone and Ruggles-Wrenn [15] reveal several key features of the deformation behavior of the unaged PMR-15 neat resin at 288 $^{\circ}C$:

(i) Linear, quasi-elastic behavior observed upon initial loading transitions into the region of inelastic deformation (or flow stress region), which is characterized by a low tangent modulus (slope of the stress-strain curve).

(ii) The unaged PMR-15 neat resin exhibits significant nonlinear strain rate sensitivity in monotonic loading. The flow stress increases nonlinearly with increase in the loading rate. A ten-fold increase in strain rate does not cause a ten-fold increase in the flow stress level.

(iii) A unique stress-strain curve is obtained for a given strain rate. There the lack of a strain rate history effect in the response to the strain rate jump test.

(iv) Recovery of strain is strongly influenced by prior strain rate. The recovery rate increases with prior strain rate.

(v) Creep rate at a given stress increases with prior strain rate. For a given creep stress and time, creep response is different in magnitude and in form when a creep test is conducted during loading and unloading. Creep strain rate reversal (i. e. the change in strain is initially negative then becomes positive) is observed in creep test introduced on the unloading stress-strain curve.

(vi) Relaxation behavior is influenced by prior strain rate. Stress drop in relaxation depends only on time and prior strain rate and is independent of stress and strain at the beginning of relaxation. It appears that relaxation comes to rest at the equilibrium boundary, which has the form of a stress-strain diagram and is positioned below the stress-strain curves obtained at finite strain rates. Relaxation tests on the unloading stress-strain path can cause a decrease in stress, an increase in stress, or an initial increase followed by a decrease in stress.

It is noteworthy that these features of the inelastic deformation behavior of the PMR-15 polymer at 288 $^{\circ}C$ are qualitatively similar to those exhibited by metals [35, 45, 46, 59] as well as by several polymers at room temperature [8, 26–28]. The experimental observations of inelastic behavior of metals and alloys presented in [35, 46] served as the basis for developing the VBO, a constitutive, state variable model where the inelastic strain rate depends on the overstress [40, 44]. The VBOP was successfully applied to modeling the inelastic behavior of Nylon-66 at room temperature [43]. The versatility of the VBOP in reproducing the room-temperature rate-dependent inelastic behavior of several semicrystalline and amorphous polymers was demonstrated by Krempl and Khan [45], Khan and Krempl [27,28], and Khan [26].

In the previous effort Falcone and Ruggles-Wrenn [15] demonstrated that nonlinear viscoelastic model was not capable of accounting for the effects of prior loading rate on creep behavior of PMR-15 neat resin at 288 $^{\circ}C$ or on the recovery at zero stress. Additionally, the experimental results presented here strongly suggest the use-

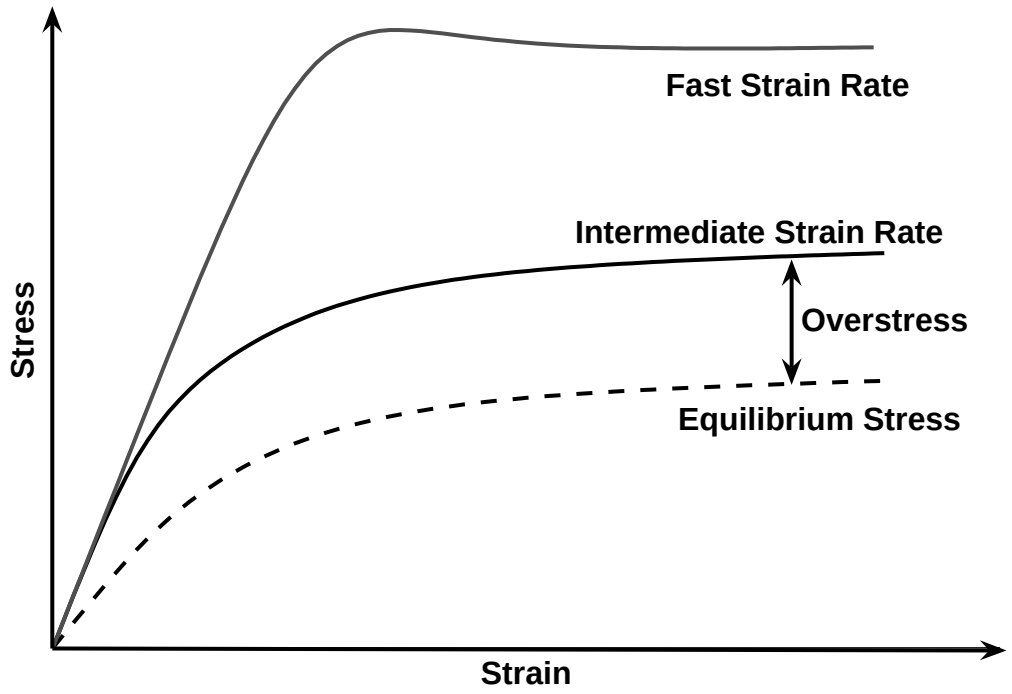

Figure 6.1: Simulation of a Stress-Strain Curve During Loading at Two Different Constant Strain Rates. The Equilibrium Stress and the Overstress are Also Shown. The Nonlinear Strain Rate Sensitivity is Evident.

fulness of the overstress concept in the modeling inelastic deformation of the PMR-15 neat resin at 288 $^{\circ}C$. To assess the ability of the VBOP to reproduce the essential qualitative features of the PMR-15 inelastic behavior, several preliminary VBOP simulations were carried out. The simulation of stress-strain behavior during loading at two different constant strain rates is shown in Figure 6.1. Solid lines depict the evolution of stress and the dashed line represents the evolution of the equilibrium stress. The VBOP simulations are consistent with the qualitative features of the inelastic behavior exhibited by the PMR-15 at 288 $^{\circ}C$. The initial quasi-linear behavior is reproduced. The positive, nonlinear rate sensitivity is also evident in monotonic

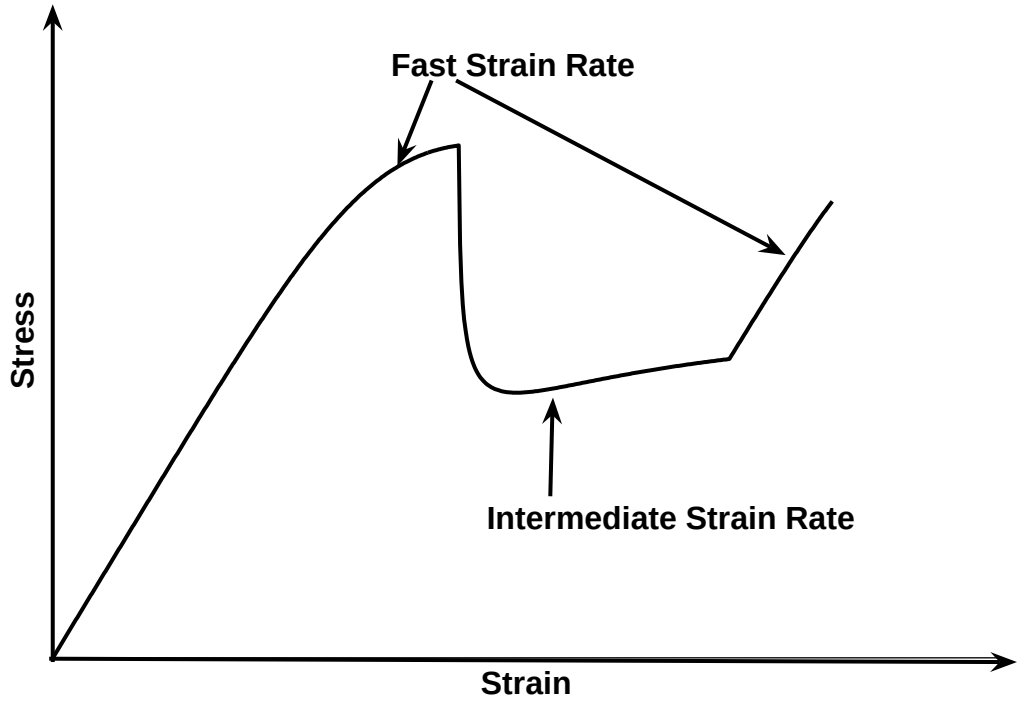

Figure 6.2: Simulation of a Stress-Strain Curve in a Strain Rate Jump Test. Upon a Change in Strain Rate, the Predicted Stress "Returns" to the Stress-Strain Curve Characteristic for that Strain Rate.

loading. The simulation of the stress-strain behavior in the SRJT is presented in Figure 6.2, where the absence of the strain rate history effect is clearly demonstrated in the VBOP simulations. (Note: the terminology lack of a "strain rate history effect" is described in detail in section 5.2.5.) The VBOP has no difficulty reproducing "the rapid forgetting" of the prior history that was observed in experiments. In the simulation, upon a change in strain rate, the stress rapidly "returns" to the stress-strain curve characteristic for that strain rate.

The simulation of stress-strain behavior during loading and unloading at a finite constant strain rate is presented in Figure 6.3, where the evolution of the equilibrium

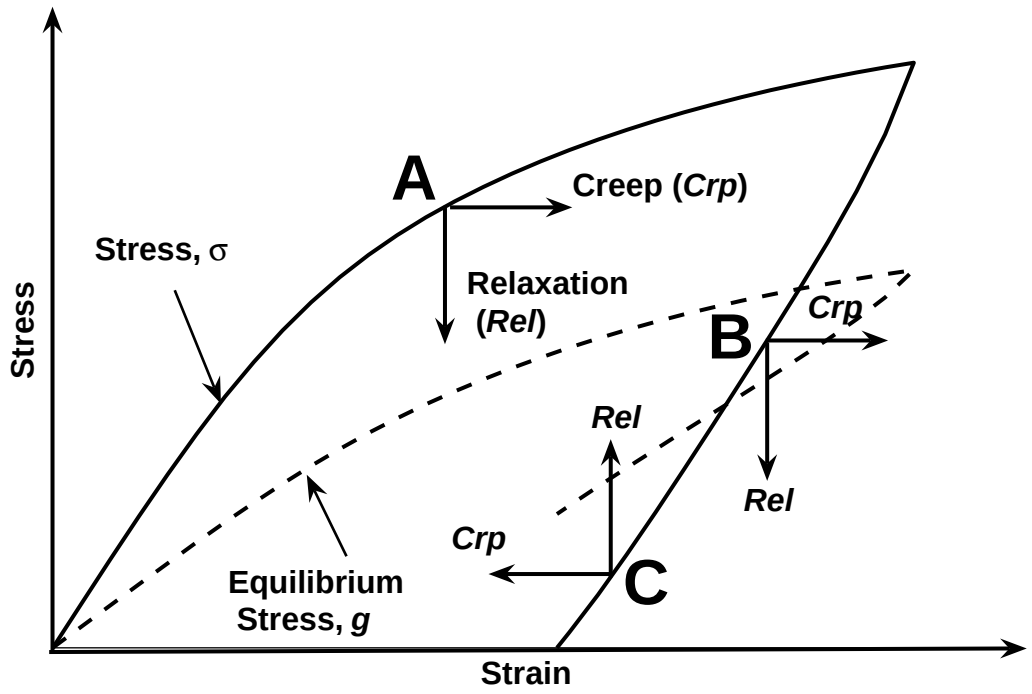

Figure 6.3: Simulation of a Stress-Strain Curve During Loading and Unloading at a Finite Strain Rate. The Equilibrium Stress Curve is Also Shown.

stress is also shown. The equilibrium stress curve is of particular interest because its position relative to the $\sigma - \epsilon$ curve governs the sign of change in stress (strain) during relaxation (creep). Within the VBOP, the stress rate during relaxation as well as the strain during creep are governed by the overstress. During relaxation $\dot{\epsilon} = 0\ s^{-1}$, consequently from Eq. (3.6), $\dot{\sigma} = -(\sigma - g)/k$. Thus at point A in Figure 6.3, the overstress $(\sigma - g)$ is positive and relaxation occurs downwards (decrease in stress). Similarly, at point B a positive overstress results in a negative relaxation rate (decrease in stress). In contrast, at point C the model predicts negative overstress and positive relaxation rate yielding upwards relaxation (increase in stress). In the case of creep $\sigma = \sigma_o = const$, therefore from Eq. (3.6), $\dot{\epsilon} = \dot{\epsilon}^{creep} = (\sigma_o - g)/Ek$. At points

A and B the VBOP predicts positive overstress and increasing strain during creep. Conversely, at point C a negative overstress yields decreasing strain during creep.

In addition, the VBOP is capable of reproducing the effect of prior loading rate on relaxation and creep behaviors. As seen from the differential equations to be solved for stress in relaxation (strain in creep), in relaxation (creep) the VBOP flow law depends only on the overstress. With the increase in prior strain rate the overstress increases; higher overstress results in higher relaxation (creep) rate. Furthermore, the VBOP would have no difficulty reproducing influence of prior strain rate on recovery at zero stress. In the case of recovery $\sigma = 0 = const$, then from Eq. (3.6), $\dot{\epsilon} = \dot{\epsilon}^{recovery} = -g/Ek$. The recovery rate is determined by the equilibrium stress. Simulations of stress-strain behavior during loading and unloading at two different strain rates carried out for Nylon-66 by Krempl and Ho [43] revealed the hysteretic and rate-dependent behavior of the equilibrium stress upon unloading. Krempl and Ho [43] also demonstrated that within the VBOP the equilibrium stress associated with the high strain rate always exceeds that associated with the low strain rate. Larger overstress results in higher recovery rate. The preliminary simulations obtained with the VBOP are qualitatively consistent with the experimental observations presented above, once more pointing to the VBOP as a suitable choice of constitutive framework for modeling the inelastic behavior of the PMR-15 neat resin at 288 $^{\circ}C$.

VII. Unaged PMR-15 Neat Resin: Constitutive Modeling and Characterization of Model Parameters

This chapter explores the capability of Viscoplasticity Based on Overstress for Polymers (VBOP) to represent the mechanical behaviors of the PMR-15 at 288 $^{\circ}C$ which were discussed in the previous chapter. This chapter first discusses the systematic characterization procedure developed within this research for establishing the functions of the VBOP from experimental results. The experimental results obtained for the unaged PMR-15 at 288 $^{\circ}C$ are used to illustrate the procedure. Then predictions of the deformation behavior of the unaged PMR-15 at 288 $^{\circ}C$ are presented.

7.1 Brief Review of Chosen Formulation

The chosen VBOP formulation for the PMR-15 at 288 $^{\circ}C$ is summarized as follows. The uniaxial flow law retains the form

$$\dot{\epsilon} = \dot{\epsilon}^{el} + \dot{\epsilon}^{in} = \frac{\dot{\sigma}}{E} + \frac{\sigma - g}{Ek}. \tag{7.1}$$

The growth (or evolution) of the equilibrium stress is given by

$$\dot{g} = \Psi \frac{\dot{\sigma}}{E} + \Psi \left[\frac{(\sigma - g)}{Ek} - \frac{(g - f)}{A} \left| \frac{(\sigma - g)}{Ek} \right| \right] + \left[1 - \frac{\Psi}{E} \right] \dot{f}. \tag{7.2}$$

The evolution of the kinematic stress retains the form

$$\dot{f} = \left[\frac{|\sigma|}{\Gamma + |g|}\right] E_t \frac{(\sigma - g)}{Ek}, \tag{7.3}$$

where Γ is the overstress invariant

$$\Gamma = |\sigma - g|. \tag{7.4}$$

The isotropic stress evolution for polymers remains the same as that in the standard VBO

$$\dot{A} = A_c[A_f - A] \left|\frac{\sigma - g}{Ek}\right|. \tag{7.5}$$

In the case of the PMR-15 at 288 $^{\circ}C$, this is simplified by setting $A_c = 0$ and making A a constant.

The shape function retains the form

$$\Psi = C_1 + (C_2 - C_1)e^{-C_3|\epsilon^{in}|} \tag{7.6}$$

The viscosity function for polymers [20, 43] reduces in the case where A is constant to the form

$$k = k_1 \left[1 + \frac{\Gamma}{k_2}\right]^{-k_3}, \tag{7.7}$$

where k_1, k_2, and k_3 are material constants.

The specific form of each equation was chosen based on the mechanical behavior observed in the experiments of the PMR-15 at 288 $^{\circ}C$ described in Chapter V.

7.2 Systematic Model Characterization Procedure

A well-defined procedure for the estimation of the nine constants in VBOP from experimental data is the key to enabling the wide use of this constitutive framework. The elastic modulus and the tangent modulus are readily determined as the slopes (measured in the appropriate regions) of the tensile stress-strain curves. The isotropic stress can be readily determined once the equilibrium stress is known. However, the remaining constants and functions are left to a "guess-and-check" method of matching simulations to experimental data. This procedure can become cumbersome and time-consuming, thereby inhibiting the wide use of this powerful constitutive framework.

One of the objectives of the current effort is to develop a systematic characterization scheme for VBOP. The following discussion describes the steps of the systematic process, which has been validated using the experimental results obtained for the PMR-15 neat resin. The model parameters obtained with the developed characterization procedure for the PMR-15 polymer are summarized in Table 7.1.

7.2.1 Elastic Modulus and Tangent Modulus. The elastic modulus is obtained from the initial quasi-linear region of the tensile stress-strain curve. The tangent modulus, defined as the slope of the stress-strain curve at the highest strain of interest, is obtained from the region considerably past the "knee" of the stress-strain

Table 7.1: Material Parameters Used in the VBOP Predictions of the Deformation Behavior of the Unaged PMR-15 Neat Resin at 288 $^{\circ}C$.

Moduli	$E = 2080\ MPa$, $E_t = 18\ MPa$
Isotropic Stress	$A = 20\ MPa$
Viscosity Function	$k_1 = 1.0e4\ s$, $k_2 = 35\ MPa$, $k_3 = 12$
Shape Function	$C_1 = 100\ MPa$, $C_2 = 1.0e3\ MPa$, $C_3 = 10$

diagram. The average elastic modulus was E =2.08 GPa. The largest strains were achieved during the constant strain rate test conducted at $10^{-5}\ s^{-1}$ with intermittent periods of relaxation (see Figure 5.14). Therefore the data at the highest strain values obtained during that test were used in determining the tangent modulus. The tangent modulus was E_t =18 MPa.

7.2.2 Equilibrium Stress and Isotropic Stress. Results of the constant strain rate tests with intermittent periods of relaxation reveal that the stress-strain points obtained at the end of the relaxation periods form a curve. Within the framework of the VBOP, the measured stress is at the equilibrium stress when the Cauchy (applied) stress becomes stationary. Results of the constant strain rate tests with periods of relaxation at the strain of 4.5% were used to determine the equilibrium stress (see Figure 5.14). The experimental results give an estimate of the equilibrium stress for the slowest prior loading rate as 20.9 MPa.

This value of the equilibrium stress at the strain of 4.5% was used to determine the isotropic stress from

$$A = \{g - E_t\epsilon\}, \tag{7.8}$$

where the brackets $\{n\}$ designate the asymptotic limit of n. For PMR-15 the isotropic stress $A = 20\ MPa$ was established.

It is important to note that the isotropic stress may evolve with time. Fully reversed tension-compression cyclic tests are required to assess the evolution of the isotropic stress. As the PMR-15 could be obtained only in the form of flat panels, only flat tensile specimens were available, which cannot be loaded in compression without buckling. Hence the isotropic stress was approximated by a constant. A stout specimen with a round cross-section is better suited for fully reversed cyclic loading. If such specimens are available, fully reversed cyclic tests should be carried out to determine whether the material exhibits cyclically neutral or cyclically hardening (softening) behavior. Isotropic stress A is a constant in the case of the cyclically neutral material. In the case of the cyclically hardening (softening) material, the evolution of the isotropic stress with time could be measured and assessed according to Eq. (3.16).

7.2.3 Viscosity Function. The viscosity function controls the rate-dependent aspects of the material response. The parameters k_1, k_2, and k_3 of the viscosity function are obtained from the results of the relaxation tests conducted with various prior strain rates. Thus the effect of prior strain rate on the material behavior can be captured. During the relaxation the total strain rate is zero. Therefore Eq. (3.12)

can be simplified and rearranged to the form

$$\sigma - g = -k\dot{\sigma}. \tag{7.9}$$

Since the equilibrium stress has been determined and the stress and the stress rate can be calculated from experimental data, k can now be determined from the stress levels during the relaxation periods. Note that only the relaxation data obtained at strain levels in the region where the plastic flow is fully established should be used to evaluate the viscosity function k. Relaxation results obtained at strain levels occurring before the "knee" in the stress-strain diagram can be influenced by the transients in the material behavior and therefore would not yield reliable characterization of the viscosity function k.

The value of k_1 also significantly affects the strains at which the predicted stress-strain curve departs from quasi-linear behavior. Therefore it is desirable not only to select the material parameters k_1, k_2, and k_3 to capture relaxation, but also to consider the departure from linearity in determining k_1. Otherwise, a precise match in relaxation behavior may lead to inadequate predictions of the inelastic strain at low stress-strain levels.

For the unaged PMR-15 polymer, the parameters of the viscosity function were established using the least squares optimization routine in MATLAB to fit to the VBOP simulations to the experimental stress values in the last two hours of the relaxation periods. A more detailed description of the optimization is given in Ap-

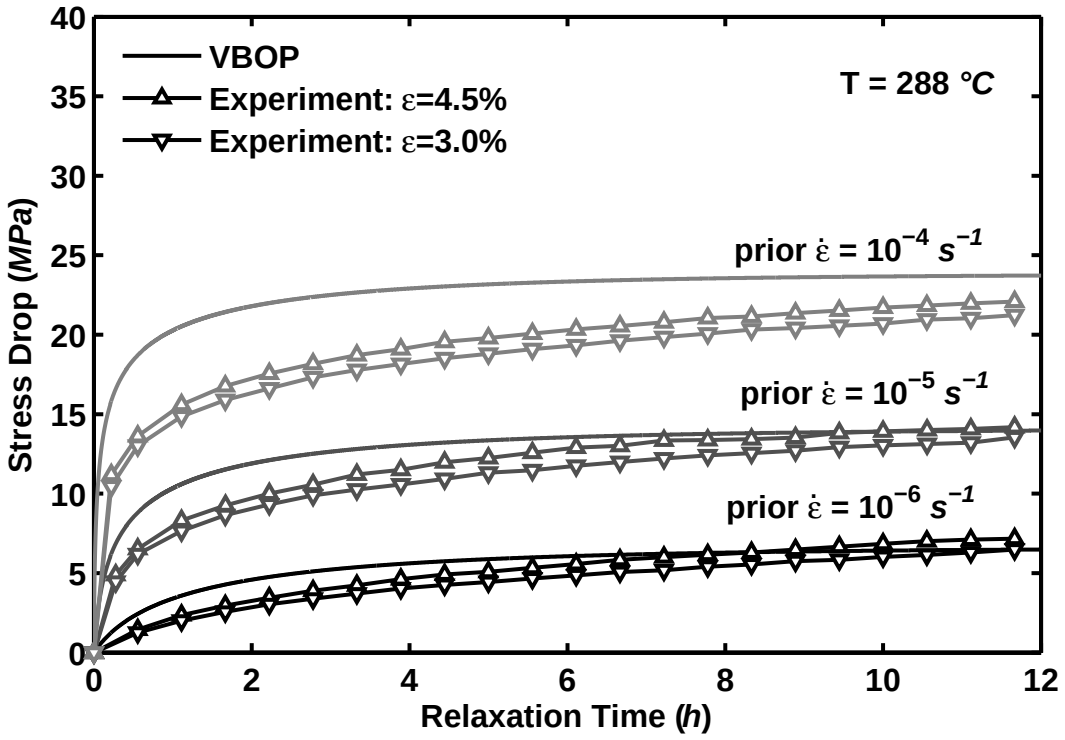

Figure 7.1: A Comparison Between Experimental and Predicted Stress Decrease vs Relaxation Time for the PMR-15 Polymer at 288 $^{\circ}C$. Influence of Prior Strain Rate on the Stress Drop During Relaxation is Evident. The Model Successfully Represents the Stress Drop During Relaxation.

pendix C. The parameters of the viscosity function were found to be $k_1 = 1.0e+04\ s$, $k_2 = 35\ MPa$, and $k_3 = 12$. The numerical simulations of the stress-time behavior during relaxation periods at 4.5% strain with prior loading at 10^{-6}, 10^{-5}, and $10^{-4}\ s^{-1}$ generated using these values of k_1, k_2, and k_3 are shown in Figure 7.1. The numerical results slightly over-predict the stress drop in the early stages of relaxation. However, after approximately 4 h of relaxation time, the predictions and the experimental results begin to merge together. (At approximately 4 h of relaxation time the error between the experimental stress drop and the simulated stress drop is less than 4 MPa and continuously reducing, while the scatter within the experimental data is

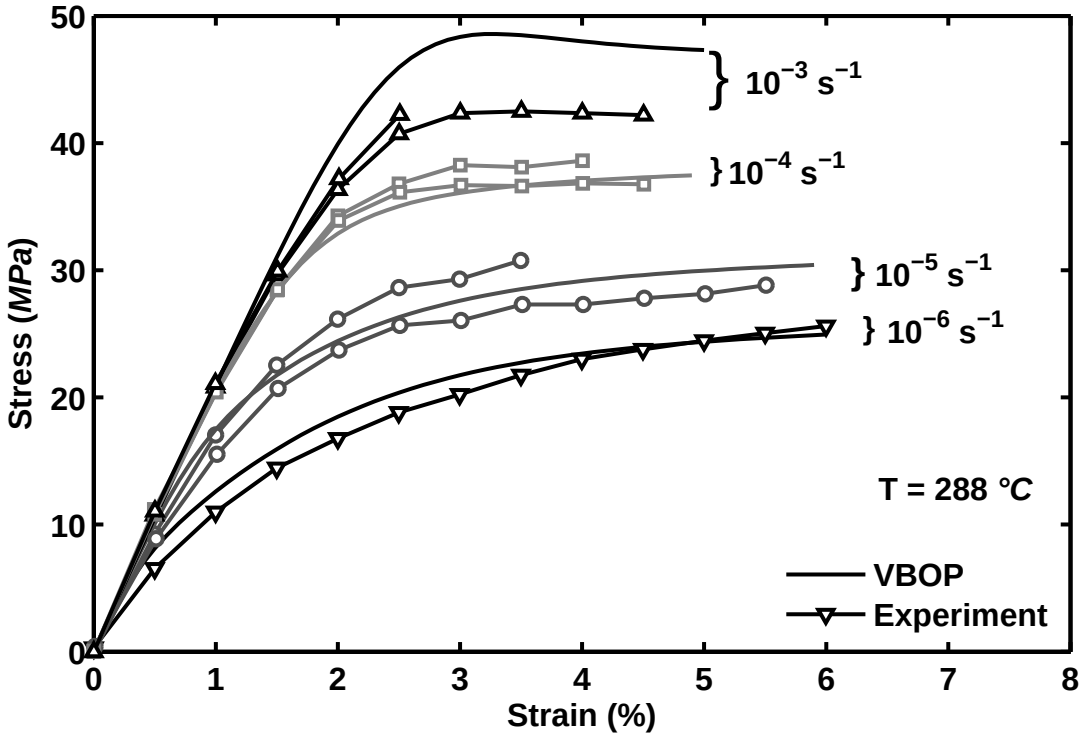

Figure 7.2: A Comparison Between Experimental and Predicted Stress-Strain Curves Obtained for PMR-15 Polymer at Constant Strain Rates of 10^{-6}, 10^{-5}, 10^{-4}, and 10^{-3} s^{-1} at 288 $^{\circ}C$. The Model Successfully Represents the Strain Rate Dependence.

approximately 1 MPa for all three prior strain rate.) Overall, the fit is an appropriate choice within the power law shape of the viscosity formulation. The influence of prior strain rate on stress response in relaxation is captured well in the simulation.

7.2.4 Shape Function. The shape function governs the shape of the "knee" in the stress-strain diagram and the curvature of the unloading stress-strain curve. The experimental stress results representing these regions of the stress-strain behavior were used in a least square optimization in MATLAB to determine the parameters of the shape function.

The predictions of the tension to failure behavior of the PMR-15 at 288 $^{\circ}C$ are shown in Figure 7.2. The resulting model gave a good representation of the experimental data except for a slight overprediction of stress in the "knee" of the stress-strain curve at the strain rate of 10^{-3} s^{-1}. The maximum scatter within the experimental data in tension to failure at this strain rate is 3.5 MPa, while the difference between the simulations and the experimental data is within 5.5 MPa. The shape function parameters obtained for PMR-15 are shown in Table 7.1.

To more thoroughly verify the validity of the characterization scheme, predictions of experiments that were not utilized in the characterization process were carried out. These predictions include the strain rate jump test, loading and unloading in strain control, and periods of creep with varying prior strain rate. These predictions are discussed in Section 7.3.

The proposed model characterization procedure can be summarized as follows:

(1) Determine elastic modulus and tangent modulus from monotonic tensile data.

(2) Determine the equilibrium stress from relaxation data.

(3) Determine the isotropic stress from the equilibrium stress and the tangent modulus.

(4) Assess the viscosity function using results of the relaxation tests conducted with various prior strain rates. Least squares optimization can be used to match experimental data. This optimization does require seed values for the shape function parameters.

(5) Determine the shape function parameters from stress-strain curves obtained in loading tests. Least squares optimization can be used to match experimental data. If the shape function parameters cannot be found to properly predict the knee of the stress-strain curve, then return to step 4 and reassess the regions of experimental data to which the viscosity function parameters are optimized, reassess the optimization weights within the objective function, or reassess the lower and upper bounds on the parameters within the optimization objective function. In particular, if the beginning of the knee is too stiff, return to step 4 and place an upper bound on the value of k_2 in the optimization that is below the value originally found for k_2. Likewise, if the beginning of the knee is too soft, return to step 4 and increase the lower bound on the value of k_2.

(6) If an unacceptable discrepancy exists in the simulations vs the experimental data for the set of loading histories in interest, reassess the particular VBOP formulation chosen to model the material behavior.

The model characterization flowchart in Figure 7.3 depicts the order in which the tests are performed and specifies what model parameters or functions are determined from each test. The chart in Figure 7.3 also shows where other test data (creep and the strain rate jump test are used as the examples in the chart) can be utilized to verify the model characterization. Note that if specimens suitable for cyclic loading are available, then fully reversed cyclic tests should also be used in the determination of the isotropic stress. However, for materials such as the PMR-15 neat resin, where

Figure 7.3: Flowchart Showing the Order of the Systematic Procedure for Characterization of the VBOP Model Parameters.

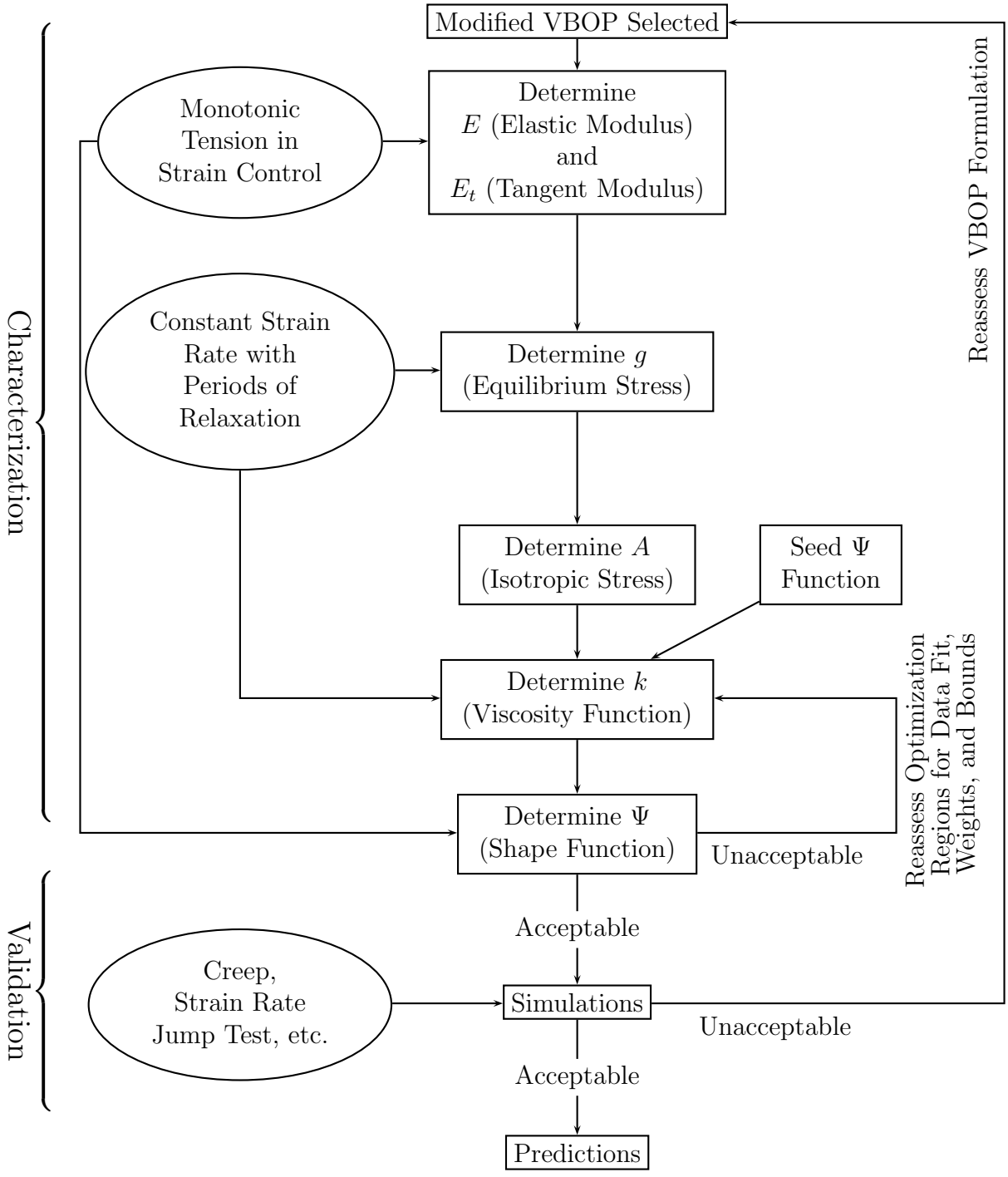

such specimens are not available, the isotropic stress is determined as illustrated in the flowchart.

The resulting set of material parameters for PMR-15 at 288 $^{\circ}C$ obtained with the developed model characterization procedure is shown in Table 7.1. The characterization procedure and the resulting material parameters were validated by comparing model predictions with the experimental results. Note that the experiments used in the characterization process were not used for model validation.

7.3 Model Verification: Predictions of the Inelastic Behavior at 288 $^{\circ}C$*.*

The capabilities of the VBOP and the proposed model characterization procedure were assessed by comparing the predictions with experimental results obtained in tests that differ in kind from those used for model characterization. Numerical simulations of both strain- and stress-controlled test histories were carried out.

Predictions of the strain rate jump test (conducted in strain control with the strain rates of 10^{-3} and 10^{-5} s^{-1}) are shown together with the experimental data in Figure 7.4. While the stress during the initial loading at 10^{-3} s^{-1} is somewhat overpredicted, good agreement with the experimental results is observed during loading at 10^{-5} s^{-1} as well as during the second period of loading at 10^{-3} s^{-1}. The VBOP predictions are within 6 MPa of the experimental data.

The simulations of strain-controlled loading and unloading for strain rates of 10^{-6} and 10^{-3} s^{-1} are shown in Figure 7.5. The model does not reproduce the unloading stress-strain behavior at higher strain rates with the desired accuracy. It does,

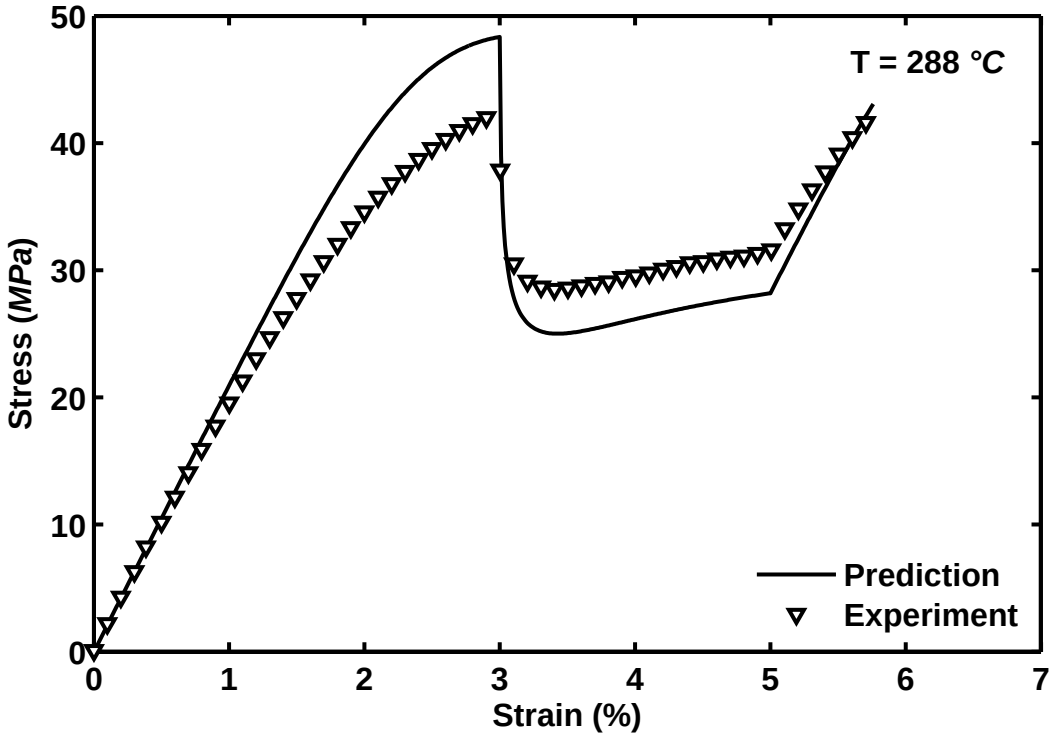

Figure 7.4: A Comparison Between Experimental and Predicted Stress-Strain Curves Obtained for PMR-15 Polymer in the Strain Rate Jump Test at 288 $^{\circ}C$. The Model Successfully Represents the Behavior Upon a Change in Strain Rate.

however, capture the effect of prior strain rate on the unloading stress-strain behavior and the increased curvature of the unloading stress-strain curves observed for the lower strain rate magnitudes. The modeling of the unloading stress-strain behavior is an area that Khan and Krempl [28] also cited as having room for improvement in polymer predictions. Colak [11] also reported curved unloading exhibited by polymers at room temperature and proposed modifications to improve the VBO representation of the unloading behavior. These modifications target the change in elastic stiffness during unloading. Unfortunately, these modifications do not improve the VBOP representation of the unloading behavior of the PMR-15 polymer, which is different from

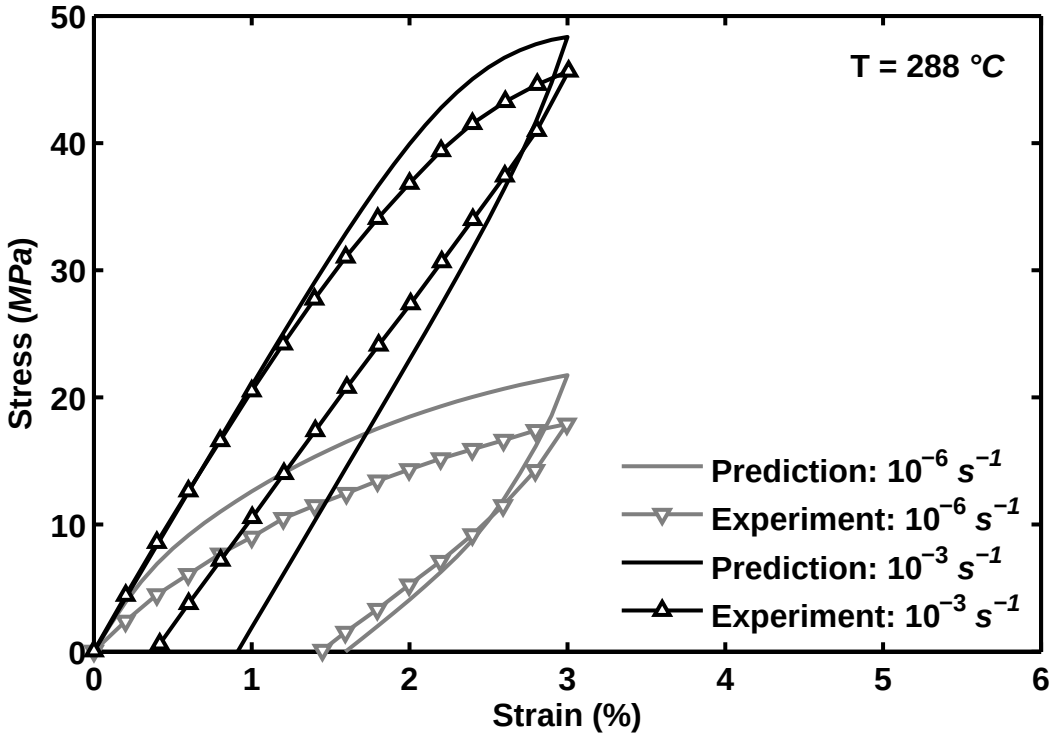

Figure 7.5: A Comparison Between Experimental and Predicted Stress-Strain Curves Obtained for PMR-15 Polymer in Loading and Unloading at Two Constant Strain Rates at 288 $^{\circ}C$. The Model Successfully Represents the Strain Rate Dependence on the Unloading.

the unloading behavior of the polymers studied by Colak. The unloading stress-strain curves obtained at different strain rates in Colak's study either merged or crossed. Modifying the VBO formulation with the purpose of improving predictions of the unloading stress-strain behavior is suggested as an area of future research. The key to improving these predictions will be to increase the value of the equilibrium stress along the unloading path. Such increase would serve to also improve predictions of relaxation upon the unloading stress-strain path. The current predictions show a transition from downward relaxation to upward relaxation at a strain value that is much lower than that exhibited by the PMR-15. Improving predictions of the un-

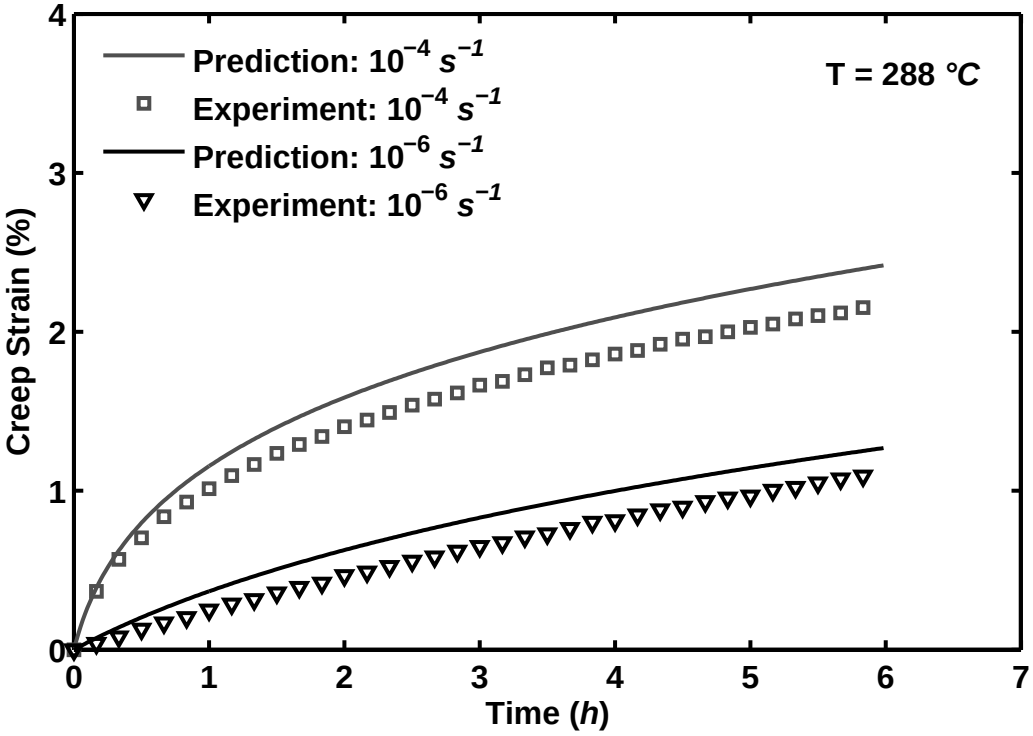

Figure 7.6: Comparison Between the Experimental and Predicted Strain vs Time Curves Obtained for PMR-15 Polymer at 288 $^{\circ}C$ in Creep at 21 MPa. Prior Loading at Strain Rates of 10^{-6} and 10^{-4} s^{-1}.

loading behavior would also potentially improve predictions of any recovery at zero stress as well as predictions of behavior upon re-loading of the material.

Because the model characterization employs tests conducted in strain control, predictions of material response in the stress-controlled tests is a more rigorous examination of the modeling abilities of the VBOP and the model characterization scheme. The effect of the prior strain rate on creep behavior was explored in creep tests of 6 h duration preceded by uninterrupted loading to a target creep stress of 21 MPa at 10^{-6} and 10^{-4} s^{-1}. Results in Figure 7.6 demonstrate that the creep strain increases nonlinearly with prior loading rate. Predictions of the stress-controlled creep

tests are compared with the experimental data in Figure 7.6. The model accurately captures the effects of the prior loading rate on the creep strain within 0.3% of the experimental results.

The experimental results clearly demonstrate that the PMR-15 polymer exhibits rate-dependent behavior at 288 $^{\circ}C$. Of specific interest are the positive strain rate sensitivity during monotonic loading, the dependence of the recovery on prior unloading strain rate, the dependence of relaxation on the prior loading rate, and the lack of strain rate history effect in the strain rate jump test. These results suggest the VBOP as a promising candidate constitutive model to represent the deformation behavior of this high-temperature polymer.

A systematic experimentally based model characterization procedure was developed. The parameters and functions of the VBOP constitutive model have a clear physical meaning, and can therefore be measured experimentally. A limited set of experiments needed to characterize the VBOP parameters was identified in this effort. The developed characterization method relies on experimental data and eliminates the uncertain and time-consuming "guess-and-check" approach to determining model parameters. The model capabilities and the model characterization procedure were evaluated by comparing the model predictions with the experimental results obtained in tests that were not used in model characterization. The prediction of the unloading behavior is seen as an excellent direction for future research. Except for the unloading behavior, the predictions of the material response under both strain-controlled and stress-controlled tests histories were in good agreement with the experimental data.

VIII. Aged PMR-15 Neat Resin: Experimental Observations

The objective of this chapter is to discuss the influence of prior thermal aging at 288 $^{\circ}C$ in argon on the strain rate-dependent mechanical behavior of the PMR-15 neat resin at 288 $^{\circ}C$. The experimental results presented in the current chapter, in Chapter V, and in McClung and Ruggles-Wrenn [54] can be used to extend the capability of the Viscoplasticity Based on Overstress for Polymers (discussed in Chapter VII and in McClung and Ruggles-Wrenn [53]) to capture the effects of the prior thermal aging on the polymer mechanical behavior. Specimens were aged following the methods outlined in Section 4.1.

8.1 Assessment of Specimen-to-Specimen Variability

The room-temperature modulus measurements outlined in Section 5.1 were also carried out for all PMR-15 specimens allocated for aging before any aging was conducted. The room temperature elastic moduli of the specimens allocated for aging were included in the discussion given in Section 5.1.

8.2 Strain-Controlled Monotonic Loading – Influence of Prior Aging

Specimens from each aging group described in section 4.3 were subjected to strain-controlled tension-to-failure tests at constant strain rates of 10^{-6}, 10^{-5}, 10^{-4}, and 10^{-3} s^{-1}. Previous work [54] has shown that the PMR-15 polymer exhibits strain rate dependent behavior during monotonic loading. The results of the strain-controlled tension-to-failure tests for PMR-15 specimens aged in argon for 250 h

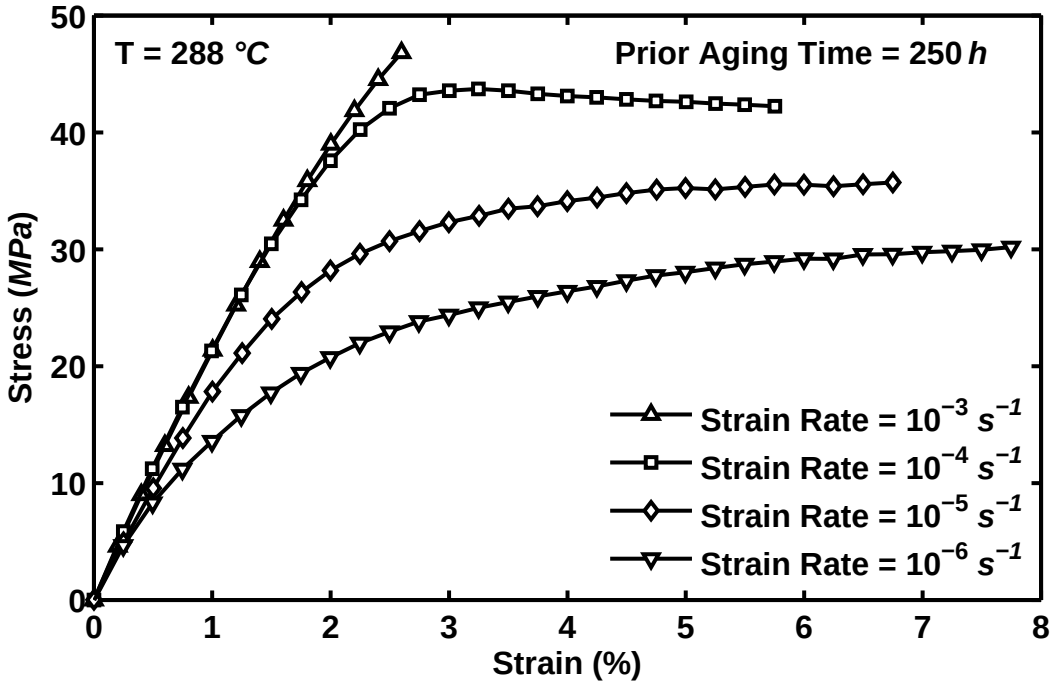

Figure 8.1: Stress-Strain Curves for PMR-15 Specimens Aged for 250 h at 288 $°C$ in Argon Obtained in Tensile Tests to Failure Conducted at Constant Strain Rates of 10^{-6}, 10^{-5}, 10^{-4}, and 10^{-3} s^{-1} at 288 $°C$. The Dependence of the Stress-Strain Behavior on the Strain Rate is Evident.

(Figure 8.1) show that the qualitative influence of the strain rate on the stress-strain behavior is unaffected by prior aging (compare to Figure 5.1). Note that the stress-strain curves in Figure 8.1 do not exhibit a truly linear range upon leaving the origin. The stress-strain curves obtained at different strain rates for the same aging group do however exhibit the same quasi-elastic slope upon leaving the origin. After the transition from the initial quasi-elastic behavior to the inelastic regime, the material exhibits normal positive strain rate sensitivity. The flow stress level increases with increasing strain rate. The shape of the stress-strain curve undergoes a gradual change as the strain rate increases. At the higher strain rates the "knee" of the stress-strain curve is much more pronounced than at the slower rates. Moreover, the stress-strain

curves obtained at slower strain rates depart from linearity at a much lower stress level than those obtained at faster strain rates.

The stress-strain response of specimens aged in argon for durations up to 2000 h obtained during strain-controlled tension to failure tests at the rates of 10^{-6} and 10^{-4} s^{-1} is typified in Figure 8.2. It is seen that prior aging in argon does affect the stress-strain behavior of the material for both strain rates. The elastic modulus increases with prior aging time. The effect of prior aging on the elastic modulus is illustrated in Figure 8.3. The elastic modulus of the material subjected to 100 h of prior aging is $\sim$0.1 GPa higher than that of the unaged material. For aging durations longer than 100 h the increase in elastic modulus progresses slowly. The elastic modulus of the material exposed to 2000 h of prior aging is $\sim$0.2 GPa higher than that of the unaged material.

The shape of the knee of the stress-strain curve also becomes more pronounced with increasing prior aging time. Furthermore, the delay in the departure from the quasi-linear behavior increases with an increase in aging time. This delay was quantified by using the 0.02% offset method to measure the proportional limit in the material behavior. The change in the measured proportional limit with aging time is illustrated in Figure 8.4. The material shows a continuous increase in proportional limit with aging time. The rate of increase lessens after 500 h of prior aging. Note that the proportional limit is not shown for the material subjected to 2000 h of prior aging. The material subjected to prior aging for 2000 h exhibited only quasi-linear

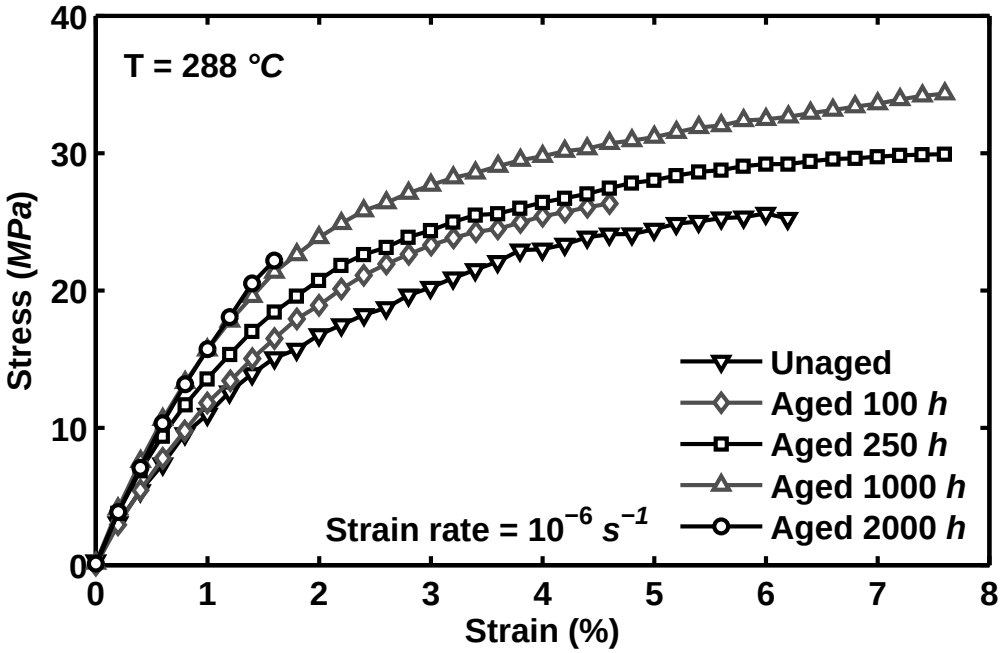

(a) Strain Rate = 10^{-6}

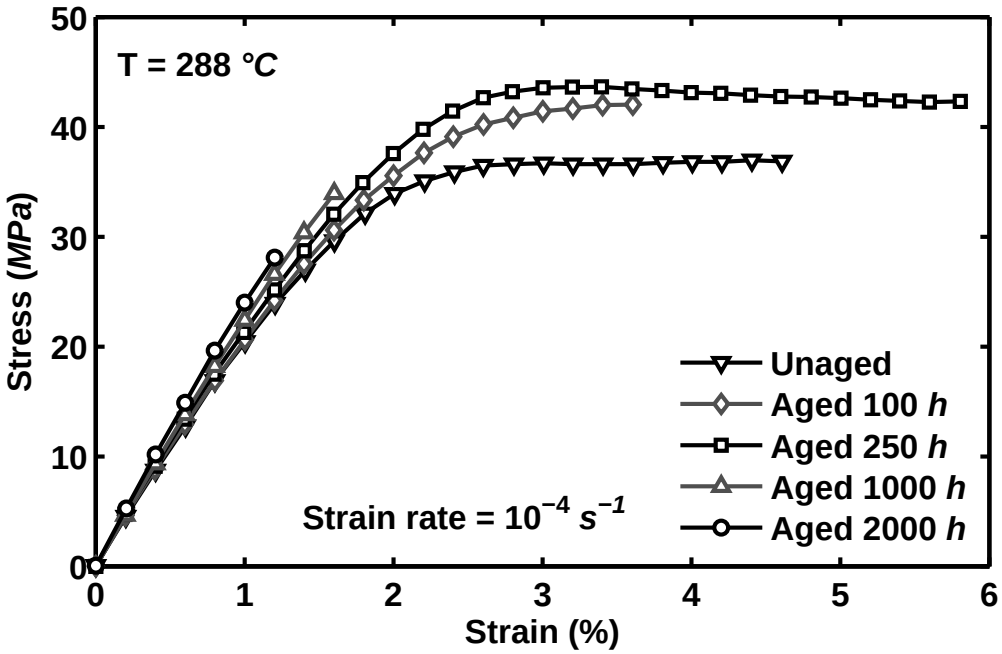

(b) Strain Rate = 10^{-4}

Figure 8.2: Stress-Strain Curves for PMR-15 Specimens Aged at 288 $°C$ in Argon Obtained in Tensile Tests to Failure Conducted at Constant Strain Rates of (a) 10^{-6} s^{-1} and (b) 10^{-4} s^{-1}.

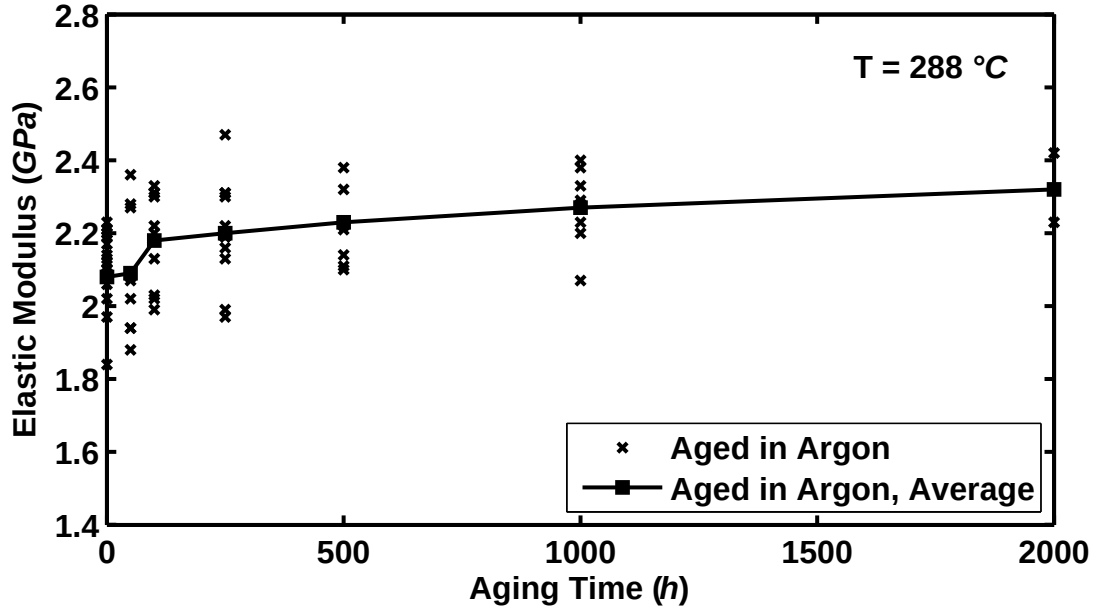

Figure 8.3: Elastic Modulus at 288 $^{\circ}C$ vs Prior Aging Time for the PMR-15 Neat Resin Specimens Aged at 288 $^{\circ}C$ in Argon. Elastic Modulus Increases with Prior Aging Time.

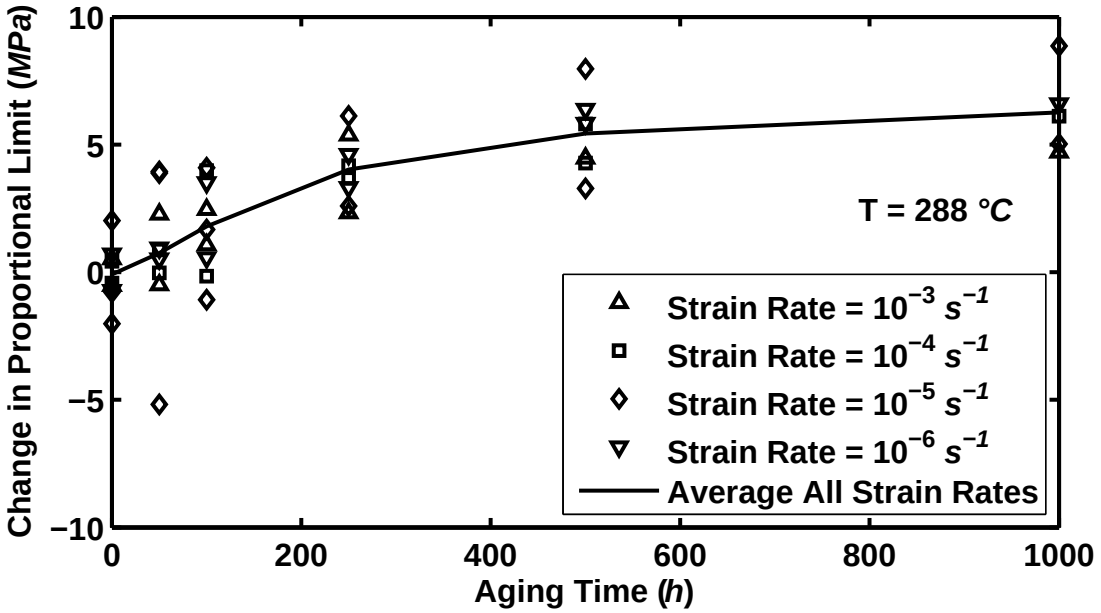

Figure 8.4: Change in Proportional Limit at 288 $^{\circ}C$ vs Prior Aging Time for the PMR-15 Neat Resin Specimens Aged at 288 $^{\circ}C$ in Argon.

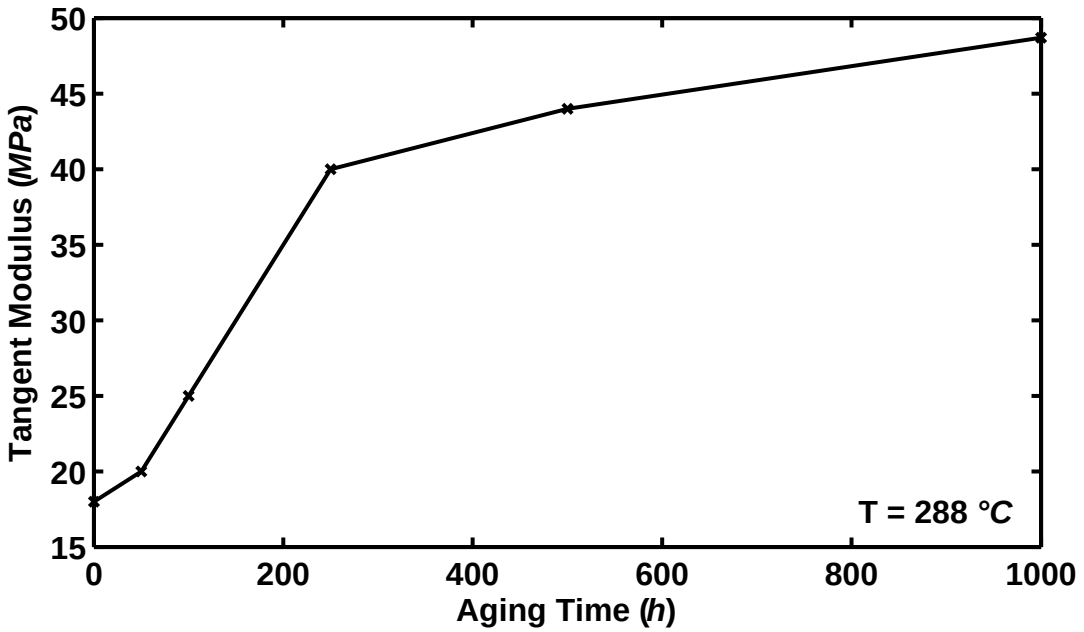

Figure 8.5: Tangent Modulus at 288 $°C$ vs Prior Aging Time for the PMR-15 Neat Resin Specimens Aged at 288 $°C$ in Argon. Tangent Modulus Increases with Prior Aging Time.

behavior until failure. The material subjected to 1000 h of prior aging shows an average proportional limit increase of $\sim$6 MPa.

The stress-strain results obtained at the 10^{-6} and 10^{-4} s^{-1} rate also show an increase in the final slope of the stress strain curve with increasing prior aging time. Similar effects of the prior aging in argon at 288 $°C$ on the stress-strain behavior were seen at 10^{-5} and at 10^{-3} s^{-1} strain rates. The final slope of the stress-strain curve measured sufficiently past the knee of the stress-strain curve is the tangent modulus. The change in tangent modulus vs aging time is shown in Figure 8.5. No data is shown for material subjected to 2000 h of prior aging because the material did not depart from the quasi-linear region of the stress-strain curve.

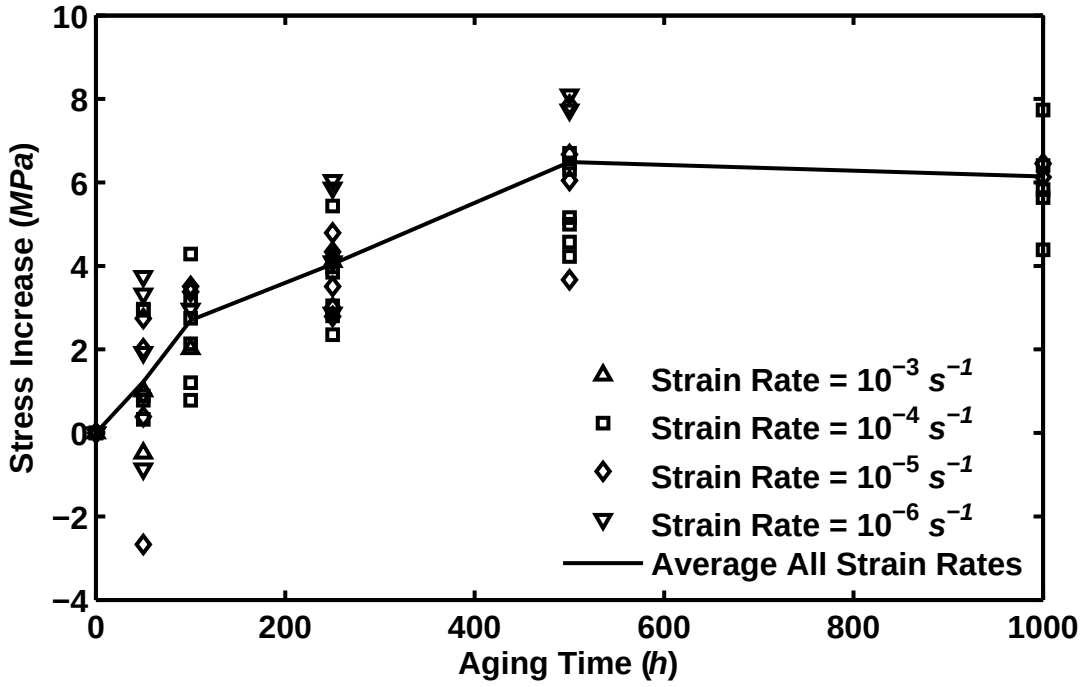

Figure 8.6: Change in Flow Stress at 288 $^{\circ}C$ vs Prior Aging Time for the PMR-15 Neat Resin Specimens Aged at 288 $^{\circ}C$ in Argon. Change in Flow Stress is Measured at 3 and at 4.5% Strain.

The prior aging in argon also leads to an increase in the flow stress. This effect was quantified by measuring the stress level at the strain of 3 and 4.5%. The increase in the flow stress level with an increase in prior aging time is illustrated in Figure 8.6. The increase in flow stress appears to be independent of the strain rate at which the test is conducted. The material aged for 1000 h shows an increase in flow stress of approximately 6 MPa.

Finally, for aging durations above 250 h, the material shows a decreasing capacity for inelastic straining with increasing prior aging time. This observation is made at all strain rates in the 10^{-6} to 10^{-3} s^{-1} range. The specimens aged for 2000 h show an inability to strain past the region of quasi-elastic behavior at strain rates of

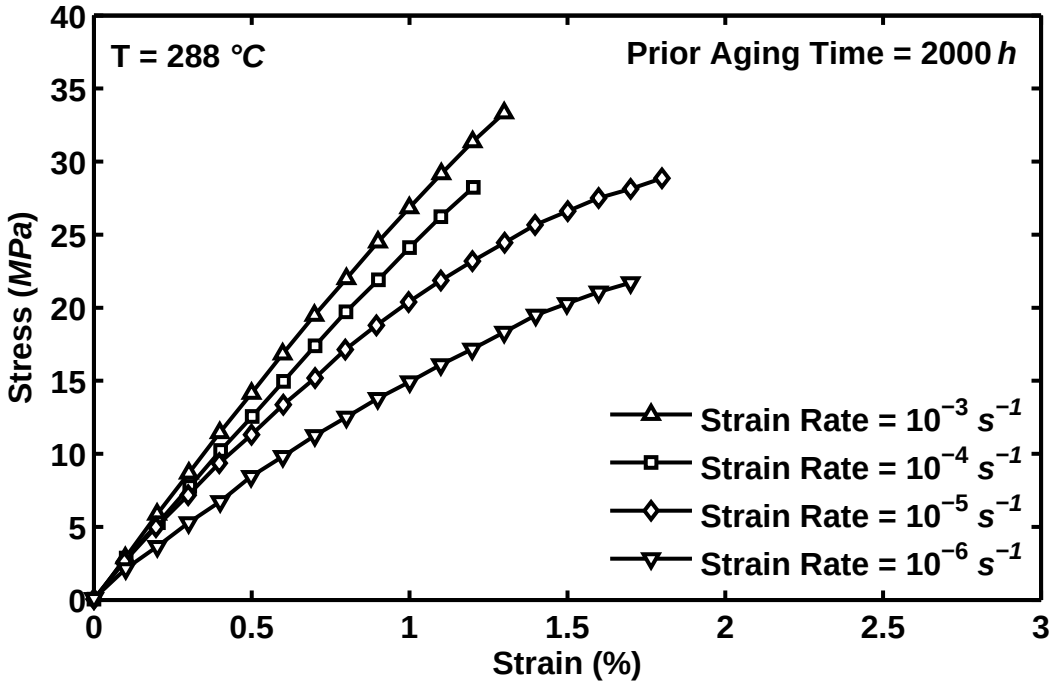

Figure 8.7: Stress-Strain Curves for PMR-15 Specimens Aged for 2000 h at 288 $°C$ in Argon Obtained in Tensile Tests to Failure Conducted at Constant Strain Rates of 10^{-6}, 10^{-5}, 10^{-4}, and 10^{-3} s^{-1} at 288 $°C$. The Limited Capacity for Inelastic Straining is Evident.

10^{-6}, 10^{-5}, 10^{-4}, and 10^{-3} s^{-1}, as shown in Figure 8.7. In addition to the reduced capacity for inelastic straining, the material shows a reduction in strength for aging durations above 1000 h. The material exhibits ultimate tensile strengths (UTS) of 42 to 46 MPa when subjected to prior aging up to 500 h. However, the material aged for 1000 h shows an UTS of 34 MPa and the material aged for 2000 h shows an UTS of 28 MPa.

8.3 Relaxation Behavior – Influence of Prior Aging

Monotonic tests with intermittent periods of relaxation of fixed duration were conducted at the strain rates in the 10^{-6} to 10^{-3} s^{-1} range on specimens subjected

to prior aging up to 2000 h. In all tests, duration of the relaxation period was 12 h. In order to evaluate the effects of stress and strain at the beginning of the relaxation on the stress drop during relaxation, two tests were conduced at each strain rate incorporating a relaxation period at (1) the strain of 3% and (2) the strain of 4.5%. Previous work [54] has shown that for unaged PMR-15 at 288 $°C$ the decrease in stress during relaxation is profoundly influenced by the prior strain rate. Furthermore, within each strain rate the relaxation stress drops are essentially independent of the stress and strain at the beginning of the relaxation period. The stress drop during relaxation following strain loading rates of 10^{-6} and 10^{-5} s^{-1} of specimens aged in argon is typified in Figure 8.8. The stress drop vs prior aging time curves in Figure 8.8 reveal that prior aging has little influence on the stress drop in relaxation.

8.4 Summary of the Key Effects of Prior Aging on Deformation Behavior

It has been demonstrated in this chapter that the prior thermal aging in argon does influence the mechanical behavior of the PMR-15 at 288 $°C$. The key features of material behavior that depend on prior aging time include:

- Initial slope of the stress-strain curve (elastic modulus) increases with increasing aging time.
- Final slope of the stress-strain curve (tangent modulus) increases with increasing aging time.

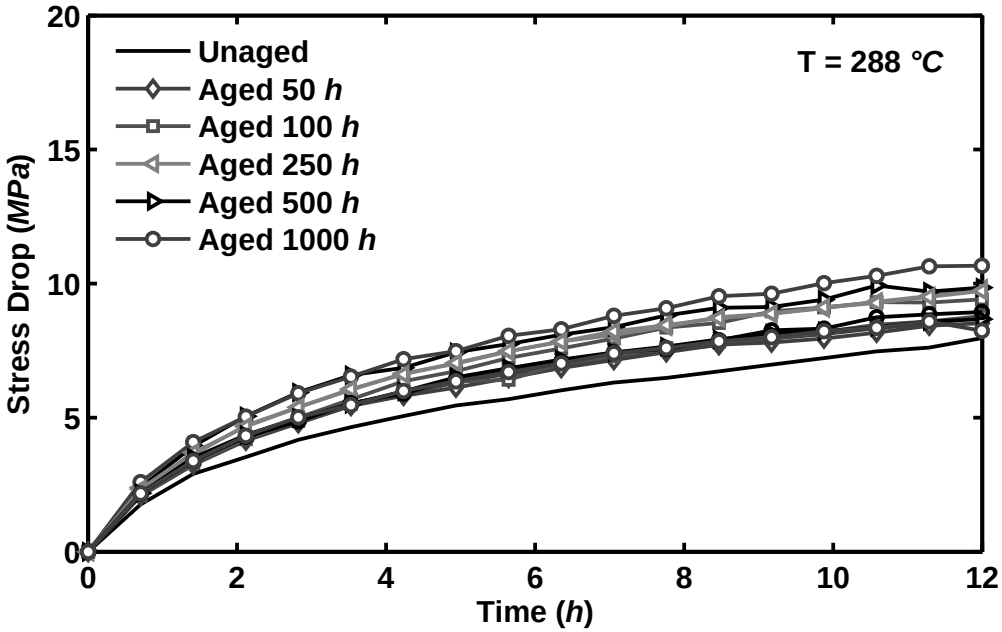

(a) Prior Strain Rate = 10^{-6} s^{-1}

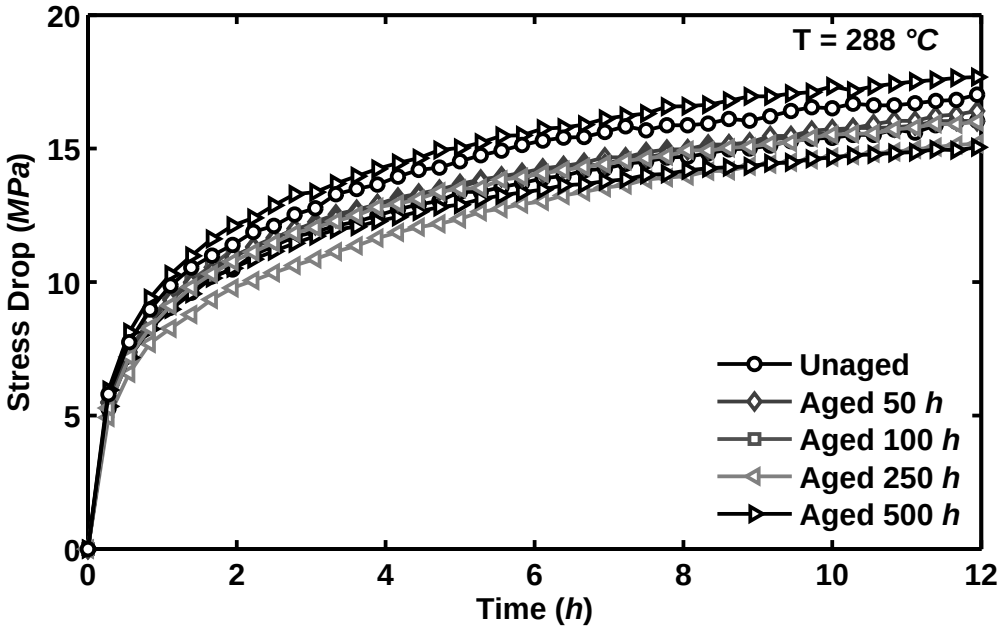

(b) Prior Strain Rate = 10^{-5} s^{-1}

Figure 8.8: Stress Drop During Relaxation for PMR-15 Specimens Aged at 288 °C in Argon Obtained at Constant Prior Strain Rates: (a) $\dot{\epsilon} = 10^{-6}$ s^{-1} and (b) $\dot{\epsilon} = 10^{-5}$ s^{-1}. The Stress Drop is Not Dependent Upon the Prior Aging.

- Flow stress increases with increasing aging time.
- Departure from quasi-linear behavior is delayed with increasing aging time.

In Chapter IX these changes in material behavior are considered in the context of the VBOP constitutive model. Based on the experimental observations, the VBOP is extended in Chapter X to capture the effects of prior aging on the deformation behavior of the PMR-15 polymer. The predictions obtained with the extended VBOP are compared to experimental results.

IX. Implications for Modeling the Effects of Prior Aging

As was discussed in the previous chapter, there are four features of material behavior that are influenced by prior aging duration. These features can be tied to specific parameters within the VBOP formulation.

9.1 Increase in Initial Slope of the Stress-Strain Curve

Clearly the elastic modulus is the initial slope of the stress-strain behavior. Therefore the increase in initial slope can be accounted for by formulating the elastic modulus as an increasing function of prior aging duration.

9.2 Increase in Final Slope of the Stress-Strain Curve

The tangent modulus in VBOP is the final slope of the stress-strain curve. Therefore, to account for the increase in the final slope of the tensile stress-strain curve with an increase in prior aging time, the tangent modulus will become an increasing function of prior aging duration.

9.3 Increase in Flow Stress in the Region of Plastic Flow

It was shown in Chapter VIII that the flow stress levels increase with an increase in prior aging time. This increase in flow stress is independent of the strain rate of loading. Therefore, the equilibrium stress must also increase with an increase in prior aging time. The isotropic stress establishes the difference between the kinematic stress and the equilibrium stress. Consequently the increase in equilibrium stress with prior

aging time can be accounted for by increasing the isotropic stress A. Note that a slight increase in equilibrium stress is achieved with the increase in the tangent modulus. However, the increase in flow stress obtained by increasing the tangent modulus is much smaller than that observed for the aged material. Therefore, the remainder of the increase is accommodated by increasing the isotropic stress value.

9.4 Delayed Departure from Quasi-linear Behavior

The departure from quasi-linear behavior establishes the beginning of the knee of the stress-strain curve. The shape of the knee in the VBOP model is determined by the shape function. The specific parameter within the shape function which governs the departure from quasi-linear behavior is C_2. Therefore, a delayed departure from quasi-linear behavior is achieved in the VBOP by increasing the value of C_2 as the prior aging time increases.

Based on these considerations, the following changes in the VBO model parameters are proposed to account for the changes in deformation behavior due to prior aging:

- Elastic modulus E increases with increasing prior aging time.
- Tangent modulus E_t increases with increasing prior aging time.
- Isotropic stress A increases with increasing prior aging time.
- Shape Parameter C_2 increases with increasing prior aging time.

X. Aged PMR-15 Neat Resin: Constitutive Modeling

This chapter discusses the constitutive modeling of the PMR-15 subjected to prior isothermal aging in argon. The VBOP formulation is extended to account for the effects of prior aging discussed in Chapter VIII.

10.1 Characterization of Model Parameters for PMR-15 Neat Resin Subjected to Prior Aging

In order to determine the appropriate VBOP parameters, the systematic characterization procedure discussed in Section 7.2 was conducted on the PMR-15 at 288 $^{\circ}C$ subjected to prior aging of 50 to 1000-h duration in argon at 288 $^{\circ}C$. The VBOP model parameters, the resulting VBOP fit to monotonic loading and relaxation data, and VBOP predictions of creep behavior for each prior aging duration are reported in this section. The VBOP parameters for PMR-15 subjected to prior aging of various durations are reported in Tables 10.1 to 10.5. The comparisons of the VBOP predictions with the experimental data are shown in Figures 10.1 to 10.15.

The systematic characterization procedure elucidates parameters for the material aged for 50 h, which are shown in Table 10.1. The elastic modulus, tangent

Table 10.1: VBOP Parameters for PMR-15 Neat Resin Subjected to Prior Aging in Argon at 288 $^{\circ}C$ for 50 h.

Moduli	$E = 2090\ MPa$, $E_t = 18\ MPa$
Isotropic Stress	$A = 22.3\ MPa$
Viscosity Function	$k_1 = 1.0e4\ s$, $k_2 = 35\ MPa$, $k_3 = 12$
Shape Function	$C_1 = 100\ MPa$, $C_2 = 1.1e3\ MPa$, $C_3 = 10$

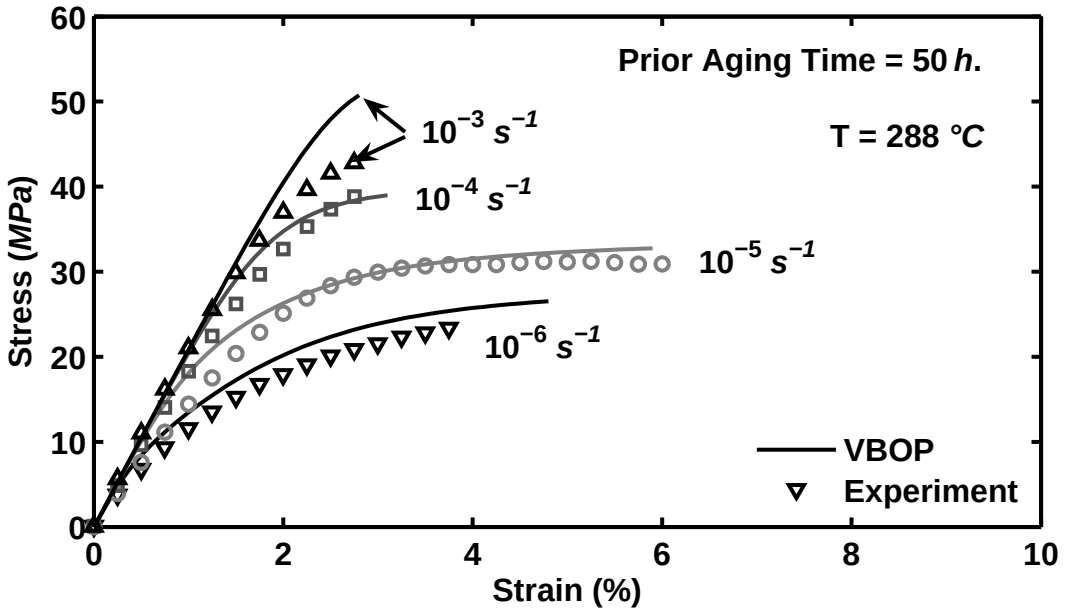

Figure 10.1: A Comparison Between Experimental Results and Simulated Stress-Strain Curves Obtained for PMR-15 Polymer Aged for 50 h at 288 $°C$ in Argon in Tensile Tests to Failure Conducted at Constant Strain Rates of 10^{-6}, 10^{-5}, 10^{-4}, and 10^{-3} s^{-1} at 288 $°C$. The Model Successfully Represents the Strain Rate Dependence of the Aged Material.

modulus, isotropic stress, and shape function parameter C_2 do indeed have a higher value than those for the unaged PMR-15 neat resin (see Table 7.1). The remaining parameters hold the same value as those for the unaged material.

The VBOP fit to the monotonic tensile loading data illustrated in Figure 10.1 shows a good representation of the experimental results. The stress-strain curves for the strain rate of 10^{-3} s^{-1} show an overprediction of stress. However, the fit is considered acceptable. Recall that the tension to failure results dictate the values of the elastic modulus, tangent modulus, and shape functions parameters.

Figure 10.2 shows stress drop during relaxation as a function of relaxation time for the prior strain rates of 10^{-6}, 10^{-5}, and 10^{-4} s^{-1}. Experimental results are shown

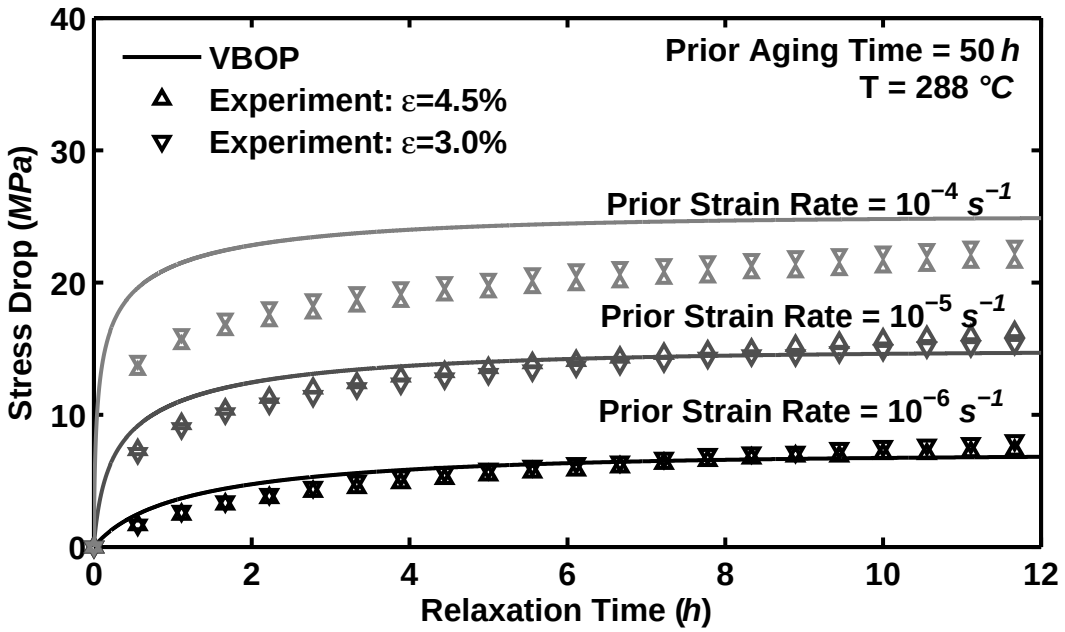

Figure 10.2: A Comparison Between Experimental Results and Simulated Stress Drop During Relaxation Obtained for PMR-15 Polymer Aged for 50 h at 288 $°C$ in Argon. Loading Prior to Relaxation is Conducted at Constant Strain Rates of 10^{-6}, 10^{-5}, and 10^{-4} at 288 $°C$. The Model Successfully Represents the Stress Drop During Relaxation for the Aged Material.

together with the VBOP simulations. The simulation of the stress drop at 4.5% strain successfully represents the behavior observed in the experimental results. Recall that the relaxation behavior dictates the isotropic stress value and the viscosity function parameters.

To validate the parameters determined in the characterization procedure for the PMR-15 subjected to 50 h of prior aging, VBOP predictions of the creep at 21 MPa were conducted. These creep periods were of 6 h duration following loading at constant strain rates of 10^{-6} and 10^{-4} s^{-1}. The predictions, shown in Figure 10.3, accurately capture the creep strain including the effect of the prior loading rate.

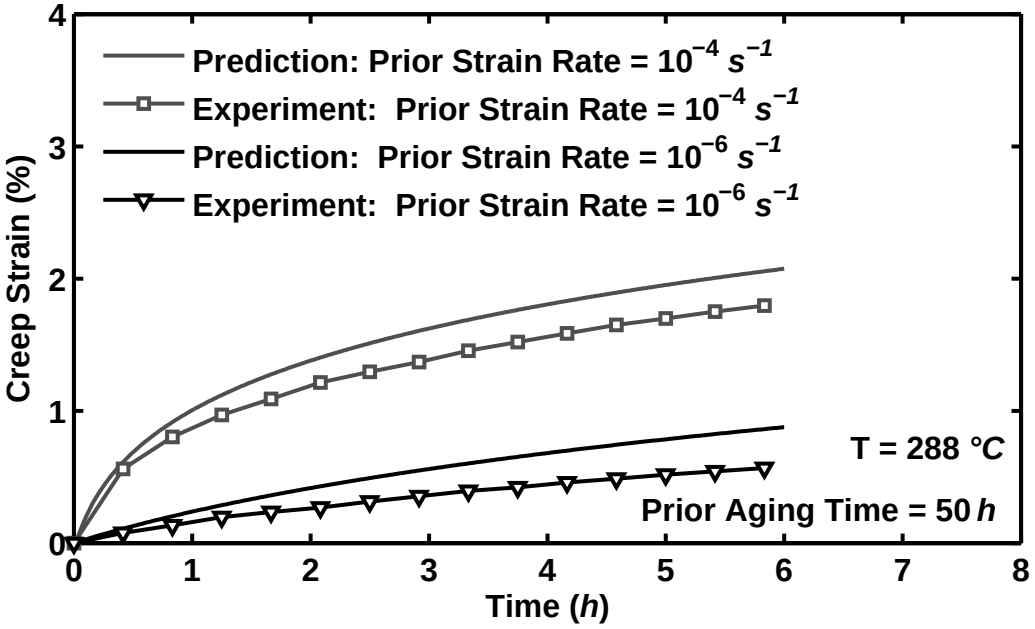

Figure 10.3: Comparison Between the Experimental Results and the Predicted Strain vs Time Curves Obtained for PMR-15 Polymer at 288 $^{\circ}C$ in Creep at 21 MPa. Prior Aging for 50 h at 288 $^{\circ}C$ in Argon. Prior Strain Rates are 10^{-6} and 10^{-4} s^{-1}.

Table 10.2: VBOP Parameters for PMR-15 Neat Resin Subjected to Prior Aging in Argon at 288 $^{\circ}C$ for 100 h.

Moduli	$E = 2180\ MPa$, $E_t = 30\ MPa$
Isotropic Stress	$A = 22.9\ MPa$
Viscosity Function	$k_1 = 1.0e4\ s$, $k_2 = 35\ MPa$, $k_3 = 12$
Shape Function	$C_1 = 100\ MPa$, $C_2 = 1.19e3\ MPa$, $C_3 = 10$

The systematic characterization procedure presented in Section 7.2 was employed to determine the VBOP parameters for the material aged for 100 h (see Table 10.2). The VBOP fit to the monotonic tension to failure data illustrated in Figure 10.4 shows a good representation of the experimental results. The VBOP fit to stress drop during relaxation at 4.5% strain in Figure 10.5 demonstrates that the VBOP successfully represents the material behavior observed in the experiments. To validate the model parameters determined for the PMR-15 subjected to 100 h of prior aging, VBOP predictions of the creep tests at 21 MPa are compared to experimental results. The predictions shown in Figure 10.6 accurately capture the creep strain including the effect of the prior loading rate.

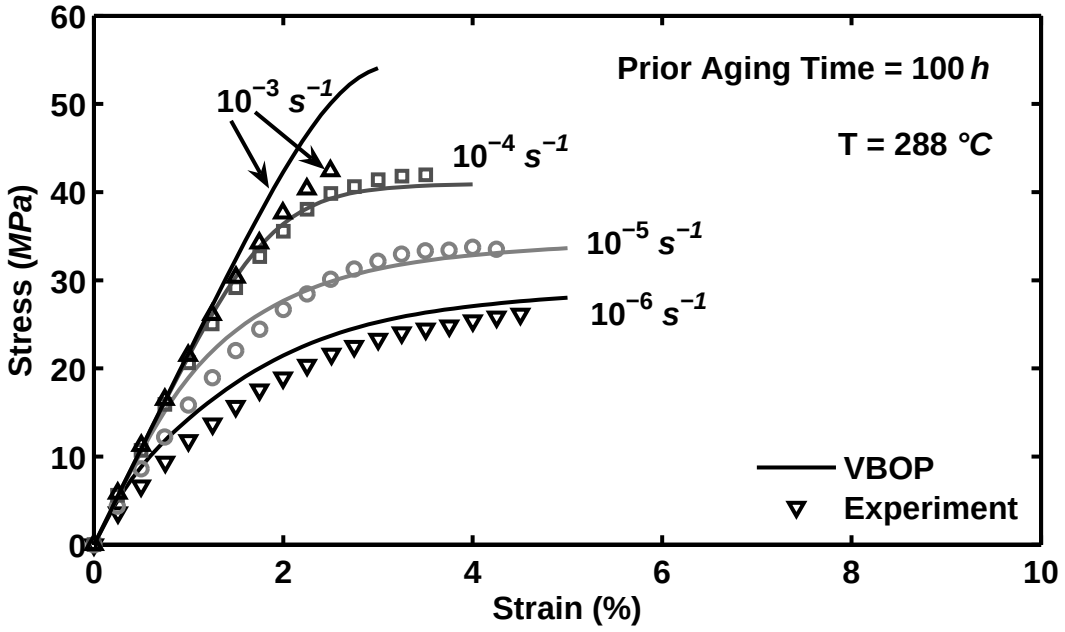

Figure 10.4: A Comparison Between Experimental Results and Simulated Stress-Strain Curves Obtained for PMR-15 Polymer Aged for 100 h at 288 $^{\circ}C$ in Argon in Tensile Tests to Failure Conducted at Constant Strain Rates of 10^{-6}, 10^{-5}, 10^{-4}, and 10^{-3} s^{-1} at 288 $^{\circ}C$. The Model Successfully Represents the Strain Rate Dependence of the Aged Material.

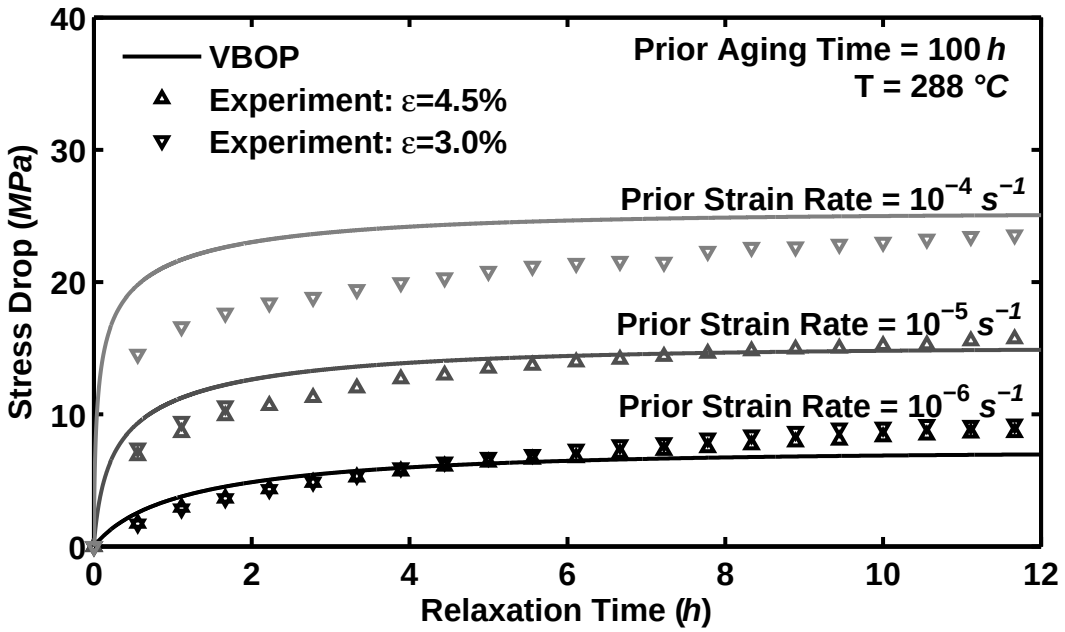

Figure 10.5: A Comparison Between Experimental Results and Simulated Stress Drop During Relaxation Obtained for PMR-15 Polymer Aged for 100 h at 288 $^{\circ}C$ in Argon. Loading Prior to Relaxation is Conducted at Constant Strain Rates of 10^{-6}, 10^{-5}, and 10^{-4} s^{-1} at 288 $^{\circ}C$. The Model Successfully Represents the Stress Drop During Relaxation for the Aged Material.

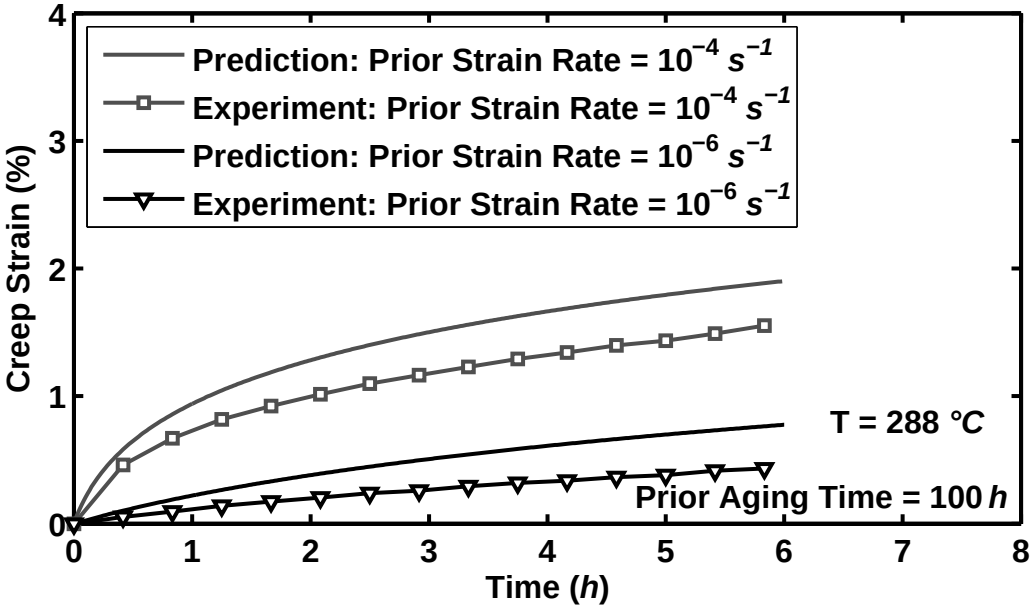

Figure 10.6: Comparison Between the Experimental Results and the Predicted Strain vs Time Curves Obtained for PMR-15 Polymer at 288 $^{\circ}C$ in Creep at 21 MPa. Prior Aging for 100 h at 288 $^{\circ}C$ in Argon. Prior Strain Rates are 10^{-6} and 10^{-4} s^{-1}.

Table 10.3: VBOP Parameters for PMR-15 Neat Resin Subjected to Prior Aging in Argon at 288 $^{\circ}C$ for 250 h.

Moduli	$E = 2200\ MPa$, $E_t = 40\ MPa$
Isotropic Stress	$A = 24\ MPa$
Viscosity Function	$k_1 = 1.0e4\ s$, $k_2 = 35\ MPa$, $k_3 = 12$
Shape Function	$C_1 = 100\ MPa$, $C_2 = 1.2e3\ MPa$, $C_3 = 10$

The model parameters obtained for the material aged for 250 h are shown in Table 10.3. The parameters show a continuation of the trends seen in the results for the material subjected to 50 and 100 h of prior aging. The VBOP fit to the monotonic tensile loading to failure data illustrated in Figure 10.7 shows a good representation of the experimental results. The VBOP fit to stress drop during relaxation in Figure 10.8 successfully represents the behavior observed in the experiments. Note, that in this case the fit was achieved with the modeling of relaxation at 4.5% strain for the prior strain rates of 10^{-6} and $10^{-5}\ s^{-1}$ and at 3% strain for the prior strain rate of $10^{-4}\ s^{-1}$. To validate the parameters determined in the characterization procedure for the PMR-15 subjected to 250 h of prior aging, VBOP predictions of the creep at 21 MPa were compared with experimental results. The predictions shown in Figure 10.9 accurately capture the creep strain including the effect of the prior loading rate.

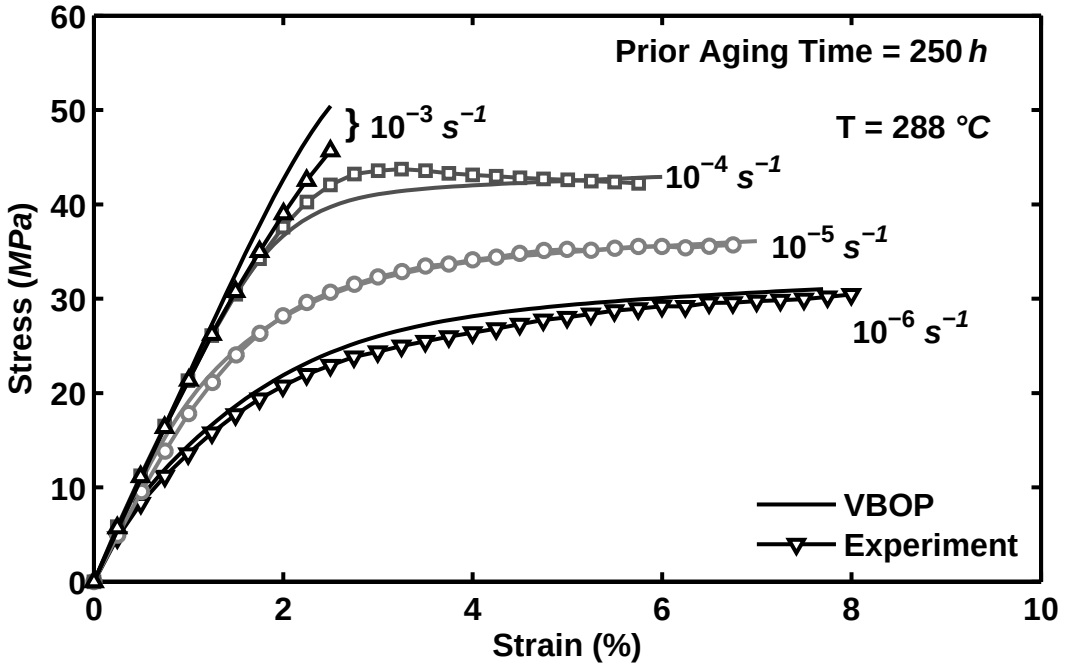

Figure 10.7: A Comparison Between Experimental Results and Simulated Stress-Strain Curves Obtained for PMR-15 Polymer Aged for 250 h at 288 $^{\circ}C$ in Argon in Tensile Tests to Failure Conducted at Constant Strain Rates of 10^{-6}, 10^{-5}, 10^{-4}, and 10^{-3} s^{-1} at 288 $^{\circ}C$. The Model Successfully Represents the Strain Rate Dependence of the Aged Material.

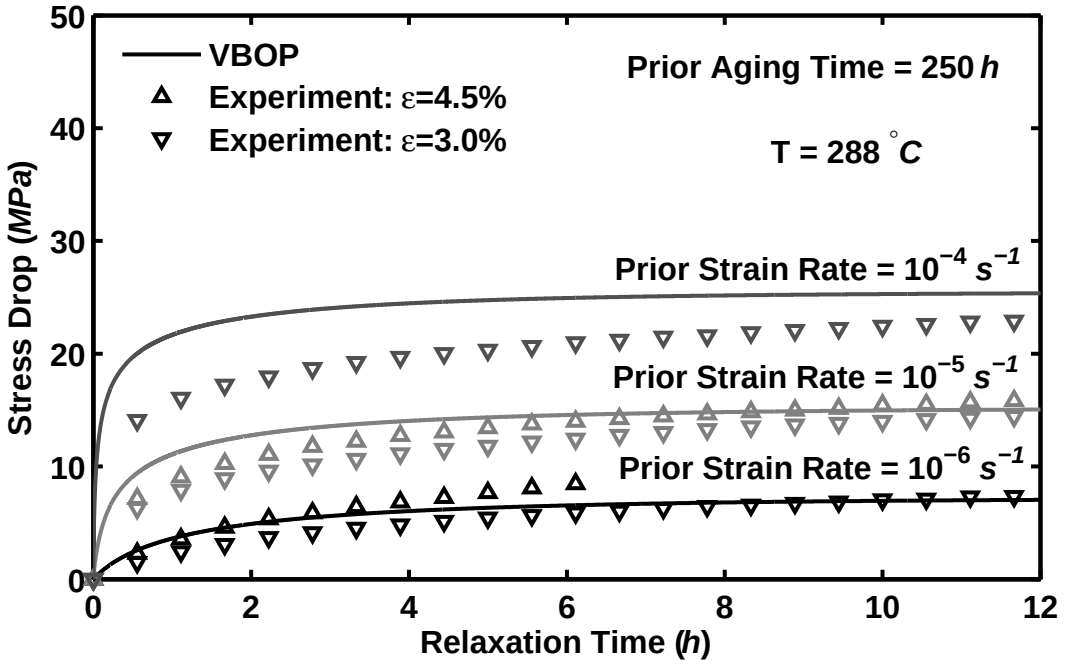

Figure 10.8: A Comparison Between Experimental Results and Simulated Stress Drop During Relaxation Obtained for PMR-15 Polymer Aged for 250 h at 288 $^{\circ}C$ in Argon. Loading Prior to Relaxation is Conducted at Constant Strain Rates of 10^{-6}, 10^{-5}, and 10^{-4} s^{-1} at 288 $^{\circ}C$. The Model Successfully Represents the Stress Drop During Relaxation for the Aged Material.

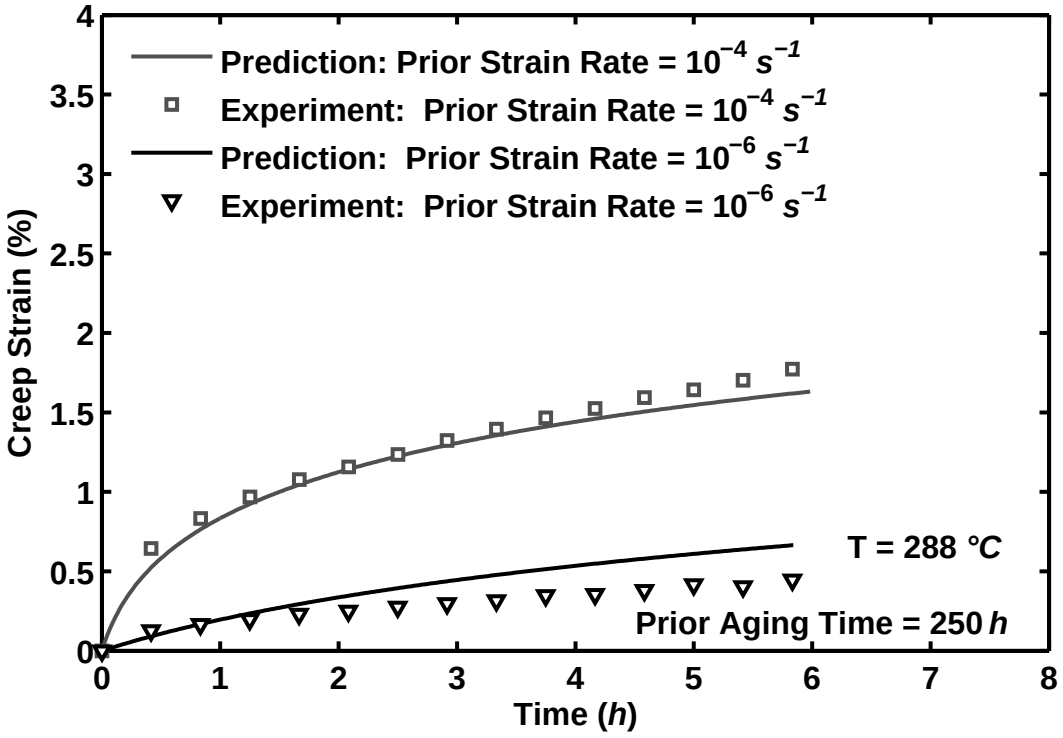

Figure 10.9: Comparison Between the Experimental Results and the Predicted Strain vs Time Curves Obtained for PMR-15 Polymer at 288 $^{\circ}C$ in Creep at 21 MPa. Prior Aging for 250 h at 288 $^{\circ}C$ in Argon. Prior Strain Rates are 10^{-6} and 10^{-4} s^{-1}.

Table 10.4: VBOP Parameters for PMR-15 Neat Resin Subjected to Prior Aging in Argon at 288 $^{\circ}C$ for 500 h.

Moduli	$E = 2230\ MPa$, $E_t = 44\ MPa$
Isotropic Stress	$A = 25.4\ MPa$
Viscosity Function	$k_1 = 1.0e4\ s$, $k_2 = 35\ MPa$, $k_3 = 12$
Shape Function	$C_1 = 100\ MPa$, $C_2 = 1.29e3\ MPa$, $C_3 = 10$

The model parameters obtained for the material aged for 500 h are shown in Table 10.4. The parameters show a continuation of the trends seen in the model parameters for the material subjected to 50–250 h of prior aging. The VBOP fit to the monotonic tensile loading to failure data illustrated in Figure 10.10 shows a good representation of the experimental results. Note that material subjected to the 500 h of prior aging exhibits extremely low ductility at the strain rate of $10^{-4}\ s^{-1}$, which is similar to that observed in the previous aging groups of material at the strain rate of $10^{-3}\ s^{-1}$. The VBOP fit to stress drop during relaxation in Figure 10.11 successfully represents the behavior observed in the experiments. Note, that in this case (as in the case of the material aged for 250 h), the fit was achieved with the modeling of relaxation at 4.5% strain for the prior strain rates of 10^{-6} and $10^{-5}\ s^{-1}$ and at 3% strain for the prior strain rate of $10^{-4}\ s^{-1}$. To validate the parameters determined for the PMR-15 subjected to 500 h of prior aging, VBOP predictions of the creep at 21 MPa were compared to experimental results. The predictions shown in Figure 10.12 accurately capture the creep strain including the effect of the prior loading rate.

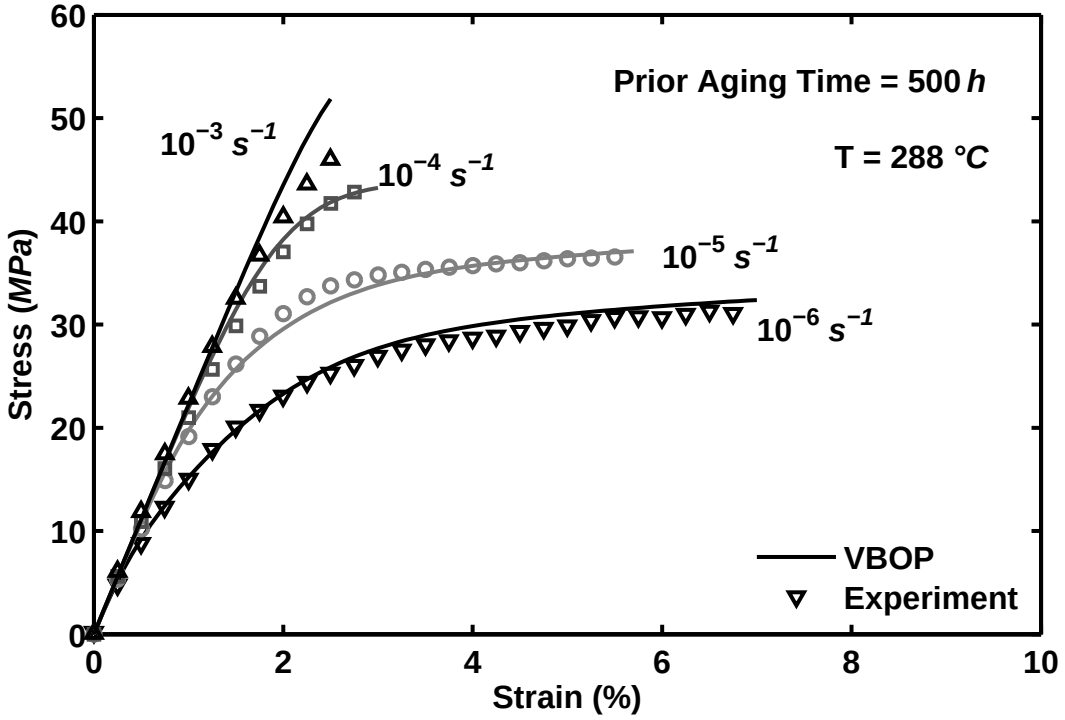

Figure 10.10: A Comparison Between Experimental Results and Simulated Stress-Strain Curves Obtained for PMR-15 Polymer Aged for 500 h at 288 $°C$ in Argon in Tensile Tests to Failure Conducted at Constant Strain Rates of 10^{-6}, 10^{-5}, 10^{-4}, and 10^{-3} s^{-1} at 288 $°C$. The Model Successfully Represents the Strain Rate Dependence of the Aged Material.

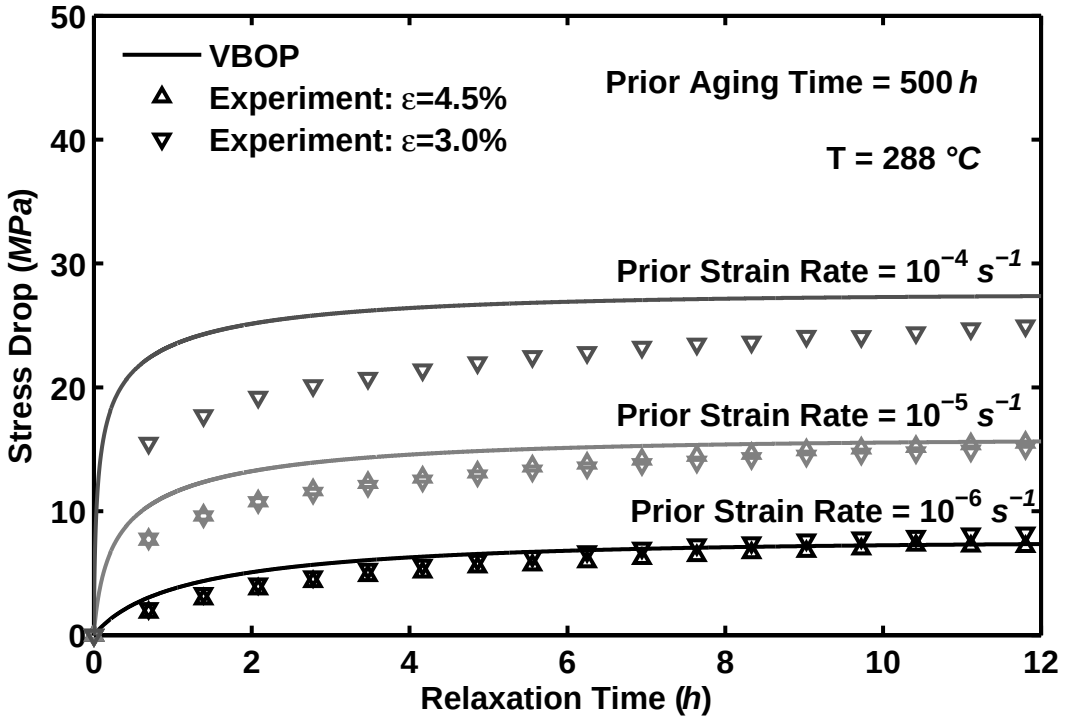

Figure 10.11: A Comparison Between Experimental Results and Simulated Stress Drop During Relaxation Obtained for PMR-15 Polymer Aged for 500 h at 288 $^{\circ}C$ in Argon. Loading Prior to Relaxation is Conducted at Constant Strain Rates of 10^{-6}, 10^{-5}, and 10^{-4} s^{-1} at 288 $^{\circ}C$. The Model Successfully Represents the Stress Drop During Relaxation for the Aged Material.

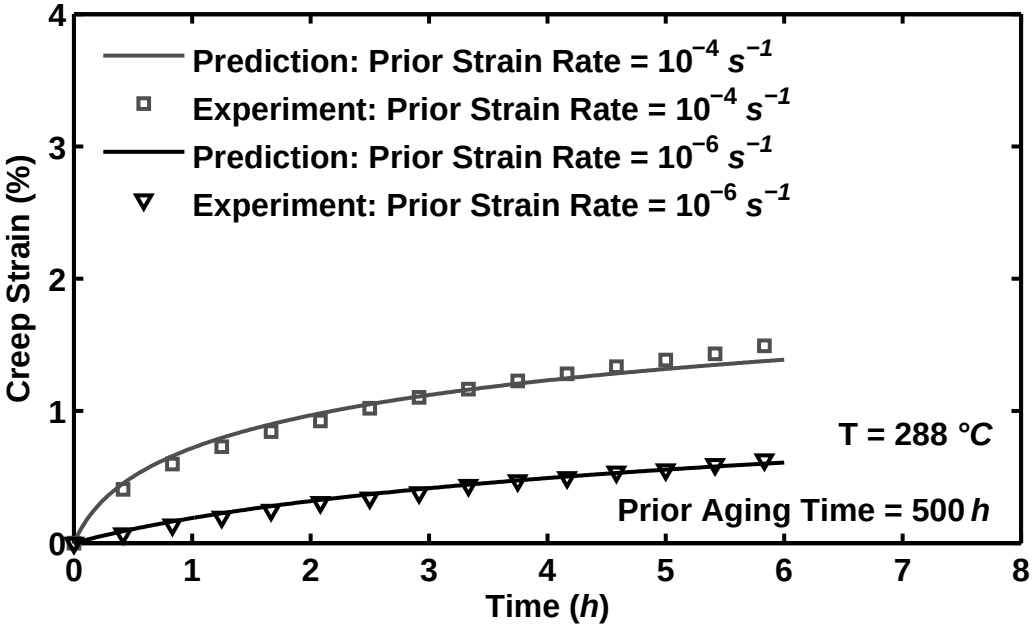

Figure 10.12: Comparison Between the Experimental Results and the Predicted Strain vs Time Curves Obtained for PMR-15 Polymer at 288 $^{\circ}C$ in Creep at 21 MPa. Prior Aging for 500 h at 288 $^{\circ}C$ in Argon. Prior Strain Rates are 10^{-6} and 10^{-4} s^{-1}.

Table 10.5: VBOP Parameters for PMR-15 Neat Resin Subjected to Prior Aging in Argon at 288 $^{\circ}C$ for 1000 h.

Moduli	$E = 2270\ MPa$, $E_t = 49\ MPa$
Isotropic Stress	$A = 26\ MPa$
Viscosity Function	$k_1 = 1.0e4\ s$, $k_2 = 35\ MPa$, $k_3 = 12$
Shape Function	$C_1 = 100\ MPa$, $C_2 = 1.3e3\ MPa$, $C_3 = 10$

The model parameters for the material aged for 1000 h are shown in Table 10.5. The parameters show a continuation of the trends seen in the model parameters for the material subjected to 50–500 h of prior aging. The VBOP fit to the monotonic tensile loading to failure data illustrated in Figure 10.13 shows a good representation of the experimental results. Note that material subjected to the 1000 h of prior aging exhibits extremely low ductility for all strain rates except at $10^{-6}\ s^{-1}$. The VBOP fit to stress drop during relaxation in Figure 10.14 successfully represents the behavior observed in the experiments. Note that due to the limited ductility and decreased capability for inelastic straining exhibited by the material aged for 1000 h, the constant strain rate test with a period of relaxation could be conducted only at the strain rate of $10^{-6}\ s^{-1}$. To validate the parameters determined for the PMR-15 subjected to 1000 h of prior aging, VBOP predictions of the creep at 21 MPa were compared to the experimental results. The predictions shown in Figure 10.15 accurately capture the creep strain including the effect of the prior loading rate.

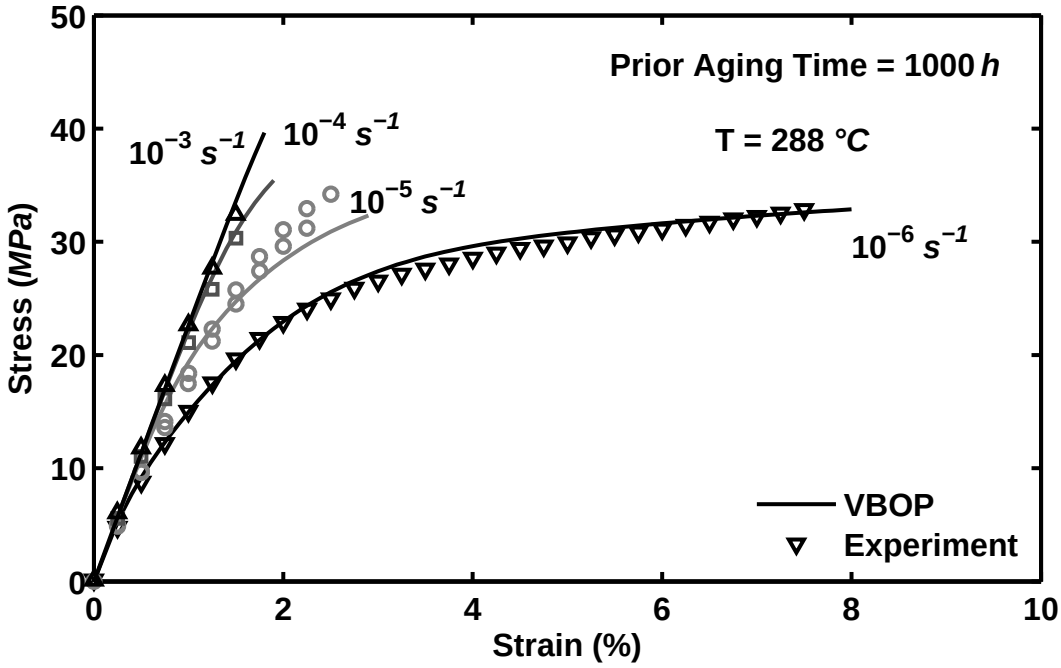

Figure 10.13: A Comparison Between Experimental Results and Simulated Stress-Strain Curves Obtained for PMR-15 Polymer Aged for 1000 h at 288 $^{\circ}C$ in Argon in Tensile Tests to Failure Conducted at Constant Strain Rates of 10^{-6}, 10^{-5}, 10^{-4}, and 10^{-3} s^{-1} at 288 $^{\circ}C$. The Model Successfully Represents the Strain Rate Dependence of the Aged Material.

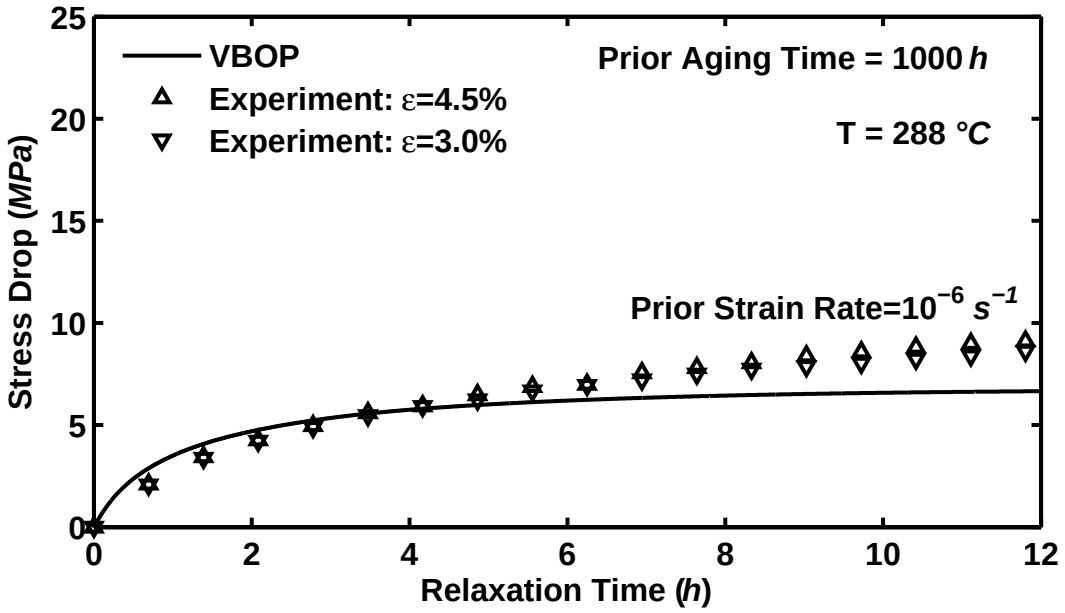

Figure 10.14: A Comparison Between Experimental Results and Simulated Stress Drop During Relaxation Obtained for PMR-15 Polymer Aged for 1000 h at 288 $^{\circ}C$ in Argon. Loading Prior to Relaxation is Conducted at Constant Strain Rate of 10^{-6} s^{-1} at 288 $^{\circ}C$. The Model Successfully Represents the Stress Drop During Relaxation for the Aged Material.

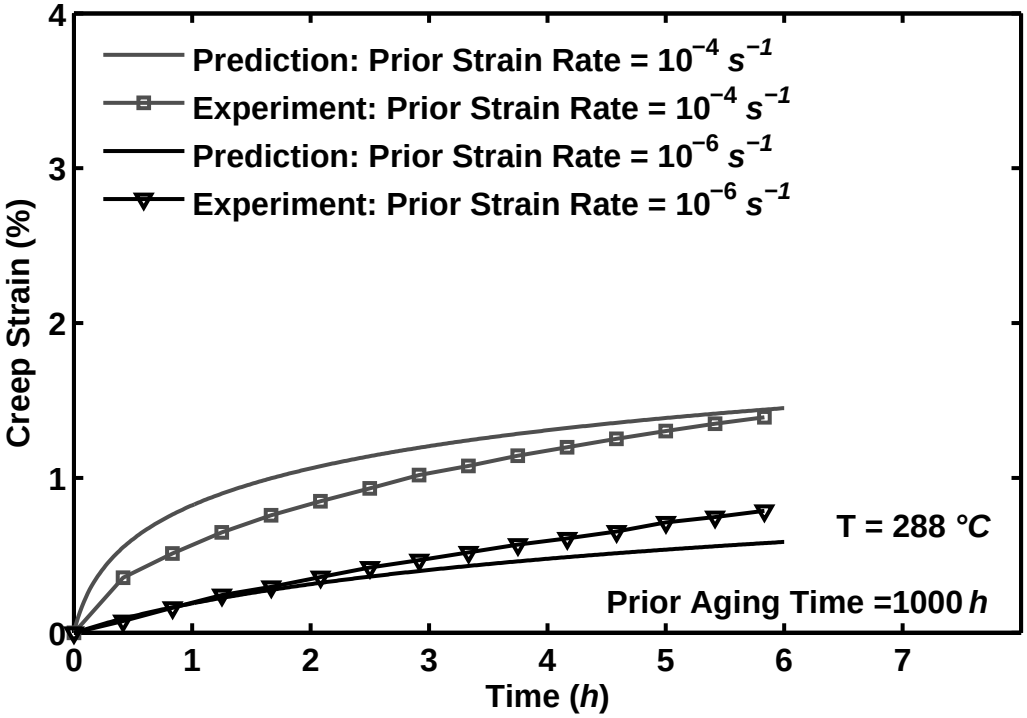

Figure 10.15: Comparison Between the Experimental Results and the Predicted Strain vs Time Curves Obtained for PMR-15 Polymer at 288 $^{\circ}C$ in Creep at 21 MPa. Prior Aging for 1000 h at 288 $^{\circ}C$ in Argon. Prior Strain Rates are 10^{-6} and 10^{-4} s^{-1}.

Table 10.6: Summary of the VBOP Parameters Dependent on Prior Aging Time for PMR-15 Polymer at 288 $^{\circ}C$ Subjected to Prior Aging in Argon for Various Durations.

	Prior Aging Time (h)						
Parameter	0	50	100	250	500	1000	2000
Elastic Modulus, E (GPa)	2.08	2.09	2.18	2.20	2.23	2.27	2.32
Tangent Modulus, E_t (MPa)	18	18	30	40	44	49	
C_2 (GPa)	1.0	1.1	1.19	1.20	1.29	1.3	
Isotropic Stress, A (MPa)	20	22.3	22.9	24	25.4	26.0	

The systematic characterization procedure provided the same values for the parameters of the VBOP not listed in Table 10.6 regardless of prior aging duration.

The only step of the systematic characterization procedure presented in Section 7.2 which can be performed for the material subjected to prior aging of 2000 h is the measurement of the elastic modulus. The elastic modulus for this aging duration is 2.32 GPa. The measurement of the other parameters is accomplished by examining the stress-strain behavior and relaxation behavior in the region of fully developed plastic flow. Recall that in the case of the PMR-15 polymer aged for 2000 h, the failure occurred in the quasi-linear regime. The predictions of the behavior of the PMR-15 subjected to prior aging for 2000 h is discussed in detail in Section 10.3.

10.2 Model Parameters as Functions of Aging Time

The parameters which depend on prior aging are presented versus aging duration in Table 10.6. In this section, these parameters are developed into functions of aging time.

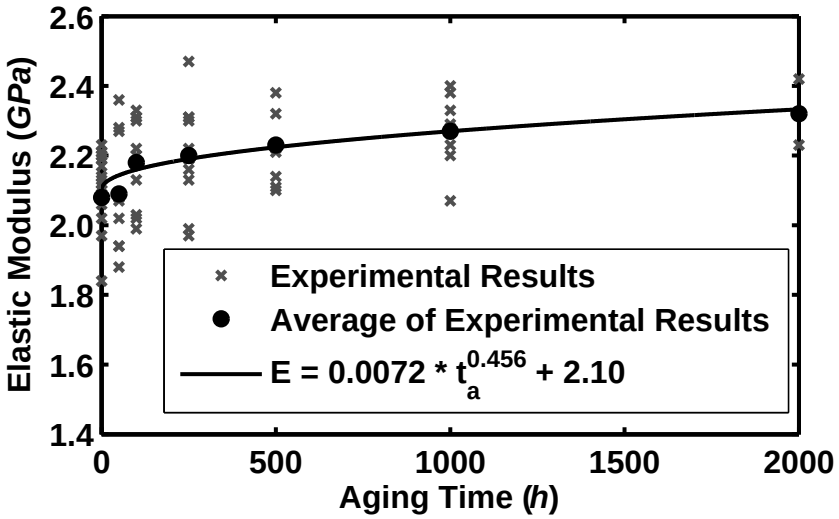

Figure 10.16: Elastic Modulus E at 288 $^{\circ}C$ as a Continuous Function vs Prior Aging Time for the PMR-15 Neat Resin Aged at 288 $^{\circ}C$ in Argon. Elastic Modulus Increases with Prior Aging Time.

10.2.1 Elastic Modulus – Effect of Aging. The elastic modulus increases with prior aging duration as shown in Figure 10.16. The graph in Figure 10.16 shows that the elastic modulus can be represented as an increasing function of aging duration using the equation

$$E = 0.0072\ t_a^{0.456} + 2.10, \tag{10.1}$$

where t_a is the prior aging time.

10.2.2 Tangent Modulus – Effect of Aging. The tangent modulus increases with prior aging time as shown in Figure 10.17. The graph in Figure 10.17 shows that the tangent modulus can be represented as an increasing function of prior aging time using the equation

$$E_t = 2.89\ t_a^{0.354} + 17.4. \tag{10.2}$$

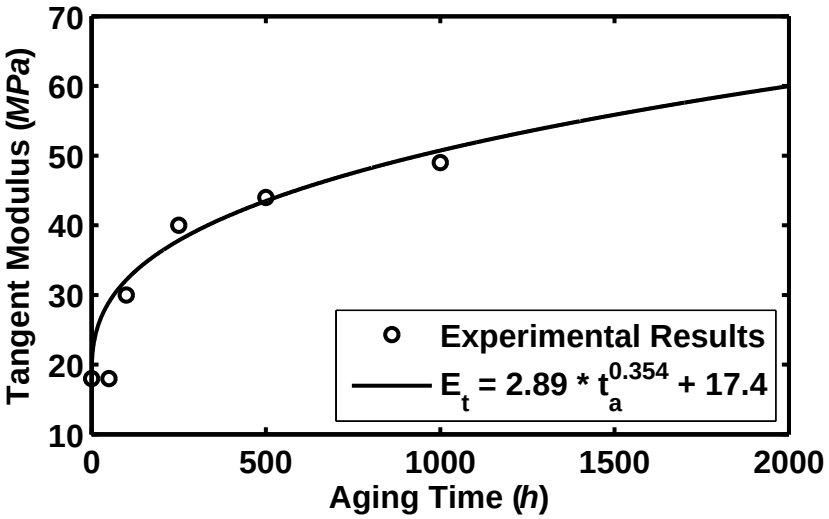

Figure 10.17: Tangent Modulus E_t at 288 $^\circ C$ as a Continuous Function vs Aging Time for the PMR-15 Neat Resin Aged at 288 $^\circ C$ in Argon. Tangent Modulus Increases with Prior Aging Time.

10.2.3 Isotropic Stress – Effect of Aging. The isotropic stress increases with prior aging time as shown in Figure 10.18. The graph in Figure 10.18 shows that the isotropic can be represented as an increasing function of prior aging time using the equation

$$A = 0.7022\ t_a^{0.3168} + 19.97. \tag{10.3}$$

10.2.4 Shape Function – Effect of Aging. The shape function parameter C_2 increases with prior aging time as shown in Figure 10.19. The graph in Figure 10.19 shows that C_2 can be represented as an increasing function of prior aging time using

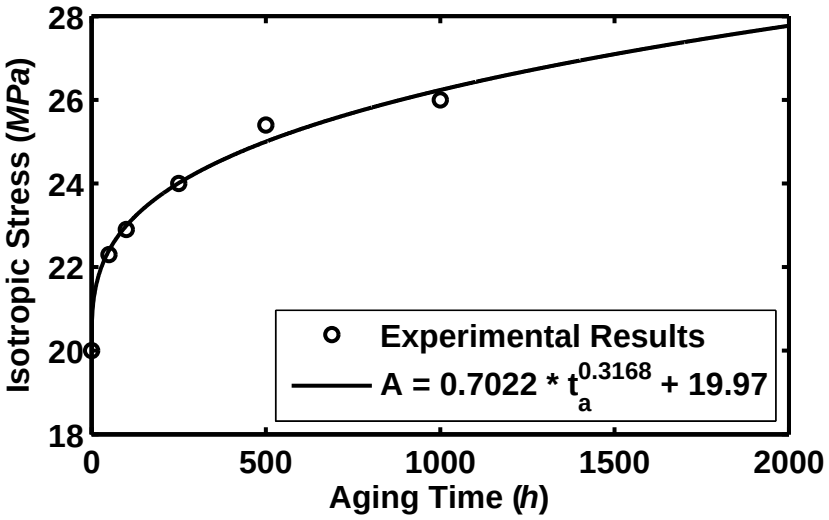

Figure 10.18: Isotropic Stress A at 288 $^{\circ}C$ as a Continuous Function vs Prior Aging Time for the PMR-15 Neat Resin Aged at 288 $^{\circ}C$ in Argon. Isotropic Stress Increases with Prior Aging Time.

the equation

$$C_2 = 0.0685\ t_a^{0.224} + 0.989. \tag{10.4}$$

The remaining VBOP parameters for the PMR-15 at 288 $^{\circ}C$ do not vary with prior aging time.

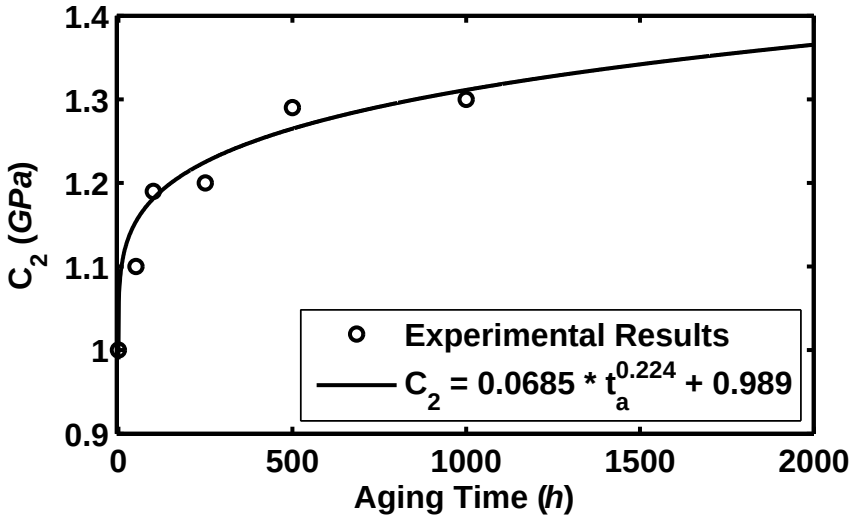

Figure 10.19: Shape Function Parameter C_2 at 288 $^\circ C$ as a Continuous Function vs Prior Aging Time for the PMR-15 Neat Resin Specimens Aged at 288 $^\circ C$ in Argon. The Parameter C_2 Increases with Prior Aging Time.

Table 10.7: VBOP Parameters for PMR-15 Neat Resin Subjected to Prior Aging in Argon at 288 $^{\circ}C$ for 2000 h.

Moduli	$E = 2320\ MPa$, $E_t = 60\ MPa$
Isotropic Stress	$A = 27.7\ MPa$
Viscosity Function	$k_1 = 1.0e4\ s$, $k_2 = 35\ MPa$, $k_3 = 12$
Shape Function	$C_1 = 100\ MPa$, $C_2 = 1.37e3\ MPa$, $C_3 = 10$

10.3 Predictions of Deformation Behavior of the PMR-15 Neat Resin Subjected to Prior Aging for 2000 h

To validate the model characterization procedure and the model formulation extended to capture the effects of prior aging, the model predictions obtained for PMR-15 polymer aged for 2000 h are compared with experimental results. The value of the elastic modulus was measured directly from the stress-strain curve of the PMR-15 aged for 2000 h to be $E = 2,320\ MPa$. However, the other three parameters which vary with prior aging time were calculated using Eq. (10.1)–(10.4) developed in the previous section. The parameters, calculated as $E_t = 60\ MPa$, $A = 27.7\ MPa$, and $C_2 = 1,370\ MPa$, for the material subjected to prior aging for 2000 h are summarized in Table 10.7. The predictions of the deformation behavior were performed using these calculated parameter values.

The predictions of the strain-controlled monotonic tension tests at 288 $^{\circ}C$ are shown in Figure 10.20. The predictions are in good agreement with the experimental data at all four strain rates. The model predicts quasi-linear stress-strain behavior to failure for the strain rates of 10^{-6} to $10^{-3}\ s^{-1}$.

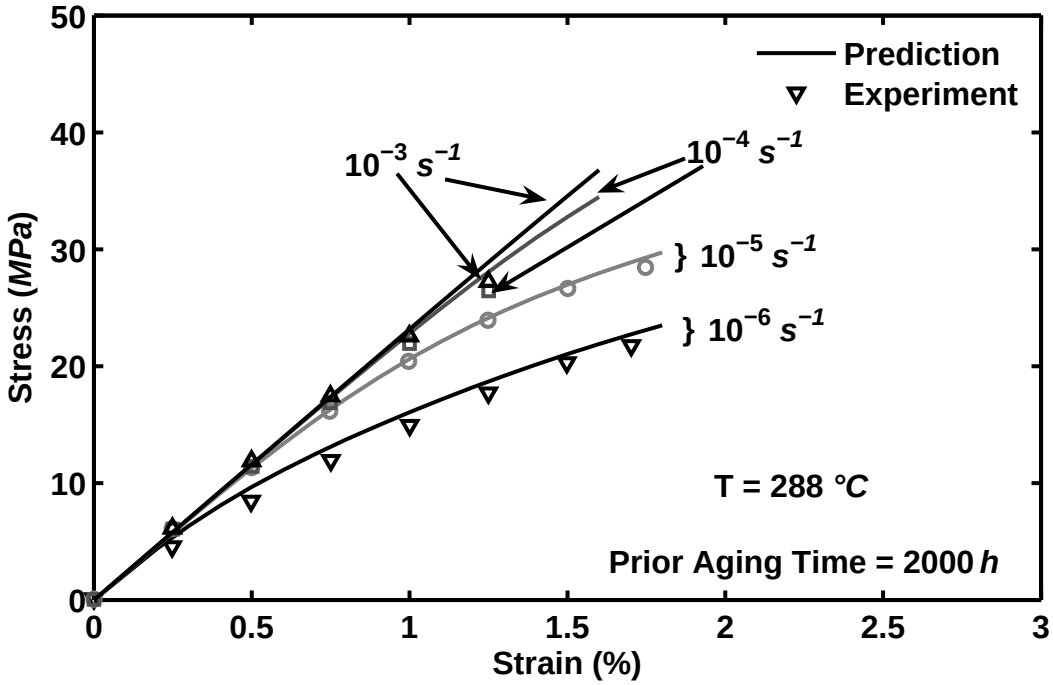

Figure 10.20: A Comparison Between Experimental Results and Predicted Stress-Strain Curves Obtained for PMR-15 Polymer Aged for 2000 h at 288 $°C$ in Argon in Tensile Tests to Failure Conducted at Constant Strain Rates of 10^{-6}, 10^{-5}, 10^{-4}, and 10^{-3} s^{-1} at 288 $°C$. The Model Successfully Predicts the Strain Rate Dependence of the Aged Material.

The predictions of the creep response at 21 MPa following loading at constant strain rates of 10^{-6} and 10^{-4} s^{-1} are shown in Figure 10.21. The predictions of the creep response also show good agreement with the experimental data. The model predicts the effect of the prior strain rate on creep.

The predictions in Figures 10.20 and 10.21 serve as an example of how the model parameters (E, E_t, A, and C_2) developed into functions of aging time in Section 10.2 can be used to predict the behavior of the PMR-15 at 288 $°C$ subjected to prior aging for durations ranging from 0 to 2000 h.

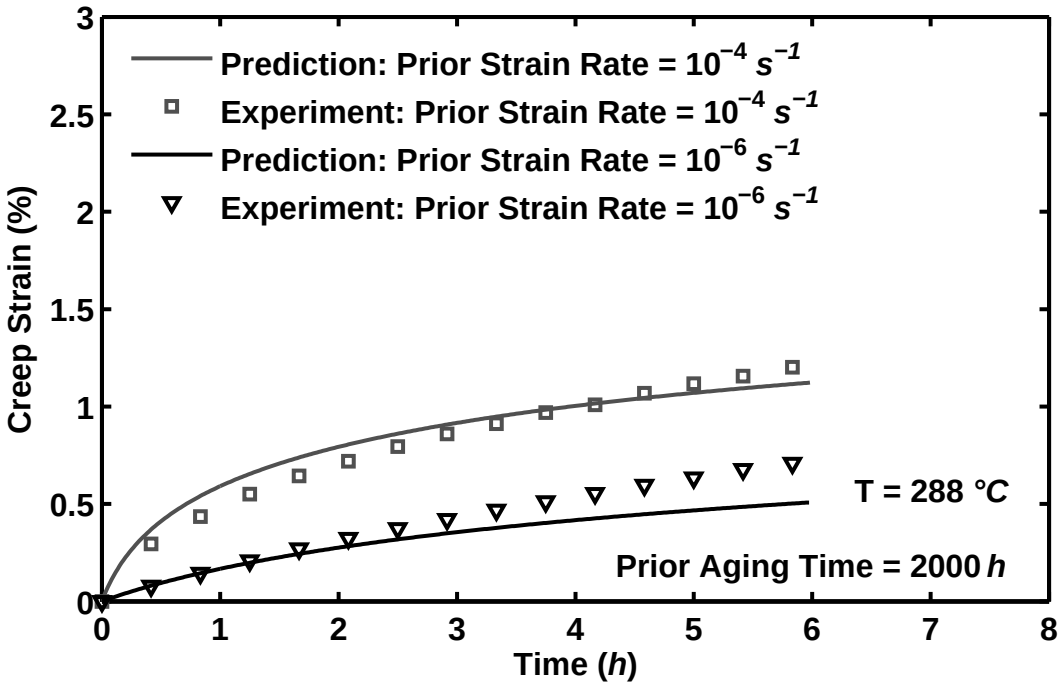

Figure 10.21: Comparison Between the Experimental Results and Predicted Strain vs Time Curves Obtained for PMR-15 Polymer at 288 $^{\circ}C$ in Creep at 21 MPa. Prior Aging for 2000 h at 288 $^{\circ}C$ in Argon. Prior Strain Rates are 10^{-6} and 10^{-4} s^{-1}. The Model Successfully Predicts the Creep Response of the Aged Material.

XI. Conclusions and Recommendations

11.1 Conclusions

The inelastic deformation behavior of unaged PMR-15 neat resin was investigated at 288 $^{\circ}C$. Experimental results revealed the rate dependence of the inelastic deformation. The unaged PMR-15 polymer exhibits positive nonlinear strain rate sensitivity during monotonic loading and unloading. In the inelastic flow region a unique stress-strain curve is obtained for a given strain rate for the unaged polymer. There is no strain rate history effect in the strain rate jump test. The recovery of strain at zero stress is strongly influenced by prior strain rate. The recovery rate increases with prior strain rate. Creep behavior is also profoundly affected by the prior strain rate. Creep rate at the same stress level increases with prior strain rate. Likewise, relaxation behavior is influenced by prior loading rate. Once the inelastic flow is fully established, the stress change during relaxation depends only on relaxation time and prior strain rate and is independent of the stress and strain at the beginning of relaxation. When a relaxation test is conducted during unloading, change in stress may be (1) negative (decrease in stress relative to start value), (2) positive (increase in stress), or (3) initially positive, but becoming negative after some time. These experimental investigations revealed several qualitative features of the inelastic deformation behavior of the PMR-15 neat resin that strongly suggest the usefulness of the overstress constitutive model.

The Viscoplasticity Based on Overstress for Polymers (VBOP) was chosen for constitutive modeling. Before the VBOP was employed, a systematic experimen-

tally based model characterization procedure was developed. The parameters and functions of the VBOP constitutive model have a clear physical meaning, and can therefore be measured experimentally. A limited set of experiments needed to characterize the VBOP parameters was identified in this effort. The developed characterization method relies on experimental data and eliminates the uncertain and time-consuming "guess-and-check" approach to determining model parameters. The model capabilities and the model characterization procedure were evaluated by comparing the model predictions with the experimental results obtained in tests that were not used for model characterization. The simulations of the deformation behavior of the unaged material under strain-controlled and stress-controlled tests histories were in good agreement with the experimental data. The model was unable to accurately predict the unloading stress-strain behavior of the PMR-15 polymer at 288 $^{\circ}C$.

The effects of prior aging in argon at 288 $^{\circ}C$ on the time dependent deformation behavior of the PMR-15 at 288 $^{\circ}C$ were examined by means of the monotonic tensile tests conducted at constant strain rates, constant strain rate tests with periods of relaxation, and creep at 21 MPa following loading in strain control. The experimental results clearly demonstrate that prior aging in argon influences the rate-dependent behavior of the PMR-15 polymer. The effects of prior aging on deformation behavior of the PMR-15 polymer at 288 $^{\circ}C$ include:

- an increase in the elastic modulus with an increase in prior aging time,
- an increase in the tangent modulus with an increase in prior aging time,

- a delay in the departure from quasi-linear behavior with an increase in prior aging time,
- an increase in the flow stress levels with an increase in prior aging time,
- a decrease in the material's capacity for inelastic straining with an increase in prior aging time,
- a reduction in strength for aging durations above 1000 h.

The VBOP parameters were determined for specimens subjected to prior aging of various durations using the developed model characterization procedure. Then the model parameters were extended as functions of prior aging time. The model parameters that were expanded as functions of prior aging time are elastic modulus, tangent modulus, isotropic stress, and the shape function parameter C_2. The viscosity function remains unaffected by prior aging. The VBOP parameters as functions of prior aging time were validated using the experimental results for PMR-15 neat resin subjected to 2000 h prior aging in both strain-controlled tension to failure tests and in creep at 21 MPa. The model extended to capture the effects of prior aging accurately predicted the behavior of the material subjected to prior aging for 2000 h.

11.2 Contributions

Experimentally, this was the first strain-controlled testing of the PMR-15 material and the first strain-controlled testing of any material in the AFIT materials lab.

There were several features of the unaged PMR-15 behavior demonstrated in the current research which were reasonably expected and similar to the behaviors seen in stress-controlled testing which include:

- positive, nonlinear strain rate sensitivity in monotonic loading,
- dependence of recovery behavior on the prior strain rate magnitude,
- dependence of creep rate on the prior strain (loading) rate.

The experiments which of course were only possible in strain control and therefore were conducted for the first time in this study were:

- the tests with periods of relaxation,
- the strain rate jump tests.

These tests allowed for the evaluation of the effect of prior strain rate on the relaxation behavior of the material as well as the evaluation of the effect of instantaneous changes in strain rate on the material behavior in loading.

This was the first assessment of the effects of prior aging on the strain-controlled behavior of the PMR-15. The effects of prior aging that were found were consistent with those already established in stress-controlled testing were:

- The elastic modulus increases with an increase in prior aging time.
- The tangent modulus increases with an increase in prior aging time.
- The departure from quasi-linear behavior is delayed with an increase in prior aging time.

- The flow stress levels increase with an increase in prior aging time.
- The material capacity for inelastic straining decreases with an increase in prior aging time.

This was the first study to examine if aging had an effect on the relaxation behavior of the PMR-15.

The novel modeling contributions of this research were:

- the introduction of a characterization scheme for determining the parameters of the VBOP,
- the first modeling of the PMR-15 behavior with a viscoplastic constitutive framework,
- the first modeling of a solid polymer behavior at high temperature with the VBOP model,
- the first extension of the VBOP framework in order to incorporate the effect of prior aging into the modeling of a structural material.

11.3 Recommendations for Future Research

Modifications to VBOP Formulation to Improve Predictions of the Unloading Stress-Strain Behavior. Future modeling efforts of the behavior of the PMR-15 neat resin may involve enhancements of the VBOP formulation to address the unloading stress-strain behavior. An alternative path of the equilibrium stress upon unloading may provide a more realistic description of the material's behavior. Currently the

equilibrium stress values produced upon unloading are too low. As a result the VBOP predicts the transition (during unloading) from downward relaxation to upward relaxation at a strain value that is small compared to that observed in experiments. Higher equilibrium stress values upon unloading to zero stress would also improve predictions of the strain recovery which is currently under-predicted by the VBOP.

It may also be possible to capture the unloading behavior more effectively by introducing a tendency to develop more plastic strain at higher values of overstress, through either the viscosity function or adopting a new form for the dependence of plastic strain rate upon overstress. A hyperbolic sine formulation is an example of an alternative form.

An improvement in the representation of the unloading behavior would also potentially improve prediction of relaxation and creep during unloading as well as recovery at zero stress and stress-strain response during re-loading.

Extension of Developed Methodology to Represent Inelastic Behavior of PMR-15 at Various Temperatures. The deformation of the PMR-15 neat resin is dependent not only on the duration of prior aging, but also on the test temperature. It is also dependent upon the temperature at which the prior aging occurs. The methodology developed in this research could be extended to represent the inelastic behavior of the PMR-15 at various temperatures ranging from room temperature to the glass transition temperature of the material. In particular, additional investigations at 204, 260, and 316 $^{\circ}C$ would be of interest because (along with the current results

at 288 $^{\circ}C$) they would complement thermal degradation studies conducted on the PMR-15 by NASA [6,72]. The extension of the VBOP parameters to account for test and prior aging temperature as well as for prior aging duration would significantly expand the predictive capabilities of the VBOP.

Applying the Tools Developed in this Research to Other High Temperature Polymers. The methods and tools developed in this research can also be applied to other high temperature polymers such as the BMI 5250-4 neat resin studied by Ruggles-Wrenn and Balaconis [62] at 191 $^{\circ}C$.

High temperature polymers to replace PMR-15 are also under development as researchers search for a replacement resin that would not exhibit the toxicity displayed by one of the monomers, methylenedianiline (MDA), used in the preparation of PMR-15 [2, 7, 55, 57]. As these replacement materials become available, the tools developed in this research should be used to evaluate and model the mechanical behavior of these materials.

Furthermore, this study investigates the PMR-15 neat resin which is used as a matrix material in high temperature PMC's. Similar studies should be conducted for the PMR-15 based composites to investigate the effects of prior aging and the interactions between the neat resin matrix and the reinforcement material. In addition, modeling efforts must ultimately be extended to accurately represent the rate dependent behavior of polymer based composite materials employed in critical load-bearing structures.

Appendix A. The VBOP Formulation Selected for Modeling the Deformation Behavior of the Unaged PMR-15 Neat Resin at 288 °C

This appendix provides a detailed explanation of modeling efforts carried out using several variants of the VBOP formulation. The goal of this appendix is to explain which specific VBOP formulation was chosen and why. The discussion includes simulations of the unaged PMR-15. These simulations were obtained with model parameters that were systematically determined using the characterization procedure developed in Section 7.2.

A.1 Full VBOP Formulation

The full formulation for the Viscoplasticity Based on Overstress for Polymers is reviewed here.

The uniaxial flow law:

$$\dot{\epsilon} = \dot{\epsilon}^{el} + \dot{\epsilon}^{in} = \frac{\dot{\sigma}}{E} + \frac{\sigma - g}{Ek} \tag{A.1}$$

Equilibrium stress evolution:

$$\dot{g} = \Psi \frac{\dot{\sigma}}{E} + \Psi \left[\frac{(\sigma - g)}{Ek} - \frac{(g - f)}{A} \left| \frac{(\sigma - g)}{Ek} \right| + \frac{(\dot{\sigma} - \dot{g})}{E} \right] + \left[1 - \frac{\Psi}{E} \right] \dot{f} \tag{A.2}$$

Kinematic stress evolution:

$$\dot{f} = \left[\frac{|\sigma|}{\Gamma + |g|}\right] E_t \frac{(\sigma - g)}{Ek} \tag{A.3}$$

Isotropic stress evolution:

$$\dot{A} = A_c[A_f - A] \left|\frac{\sigma - g}{Ek}\right| \tag{A.4}$$

Shape function:

$$\Psi = C_1^* + (C_2 - C_1^*)e^{-C_3|\epsilon^{in}|} \tag{A.5}$$

$$C_1^* = C_1 \left[1 + C_4 \left(\frac{|g|}{A + |f| + \xi\Gamma^\zeta}\right)\right] \tag{A.6}$$

Viscosity function:

$$k = k_1 \left(1 + \frac{\Gamma}{k_2}\right)^{-k_3} \tag{A.7}$$

Overstress Invariant:

$$\Gamma = |\sigma - g| \tag{A.8}$$

The systematic characterization procedure outlined in Section 7.2 was used to determine parameters for the full VBOP formulation for the unaged PMR-15 neat resin. This characterization procedure is briefly reviewed here.

The elastic modulus and tangent modulus were measured to be $E = 2100\ MPa$ and $E_t = 18\ MPa$. The next step is to determine the isotropic stress, the experimental

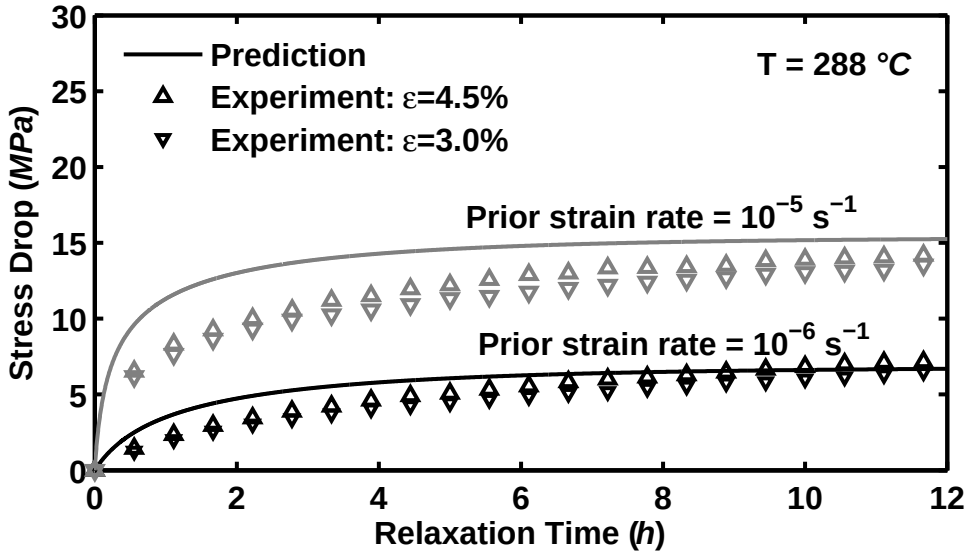

Figure A.1: A Comparison Between Experimental Results and Simulated Stress Drop During Relaxation for PMR-15 Polymer at 288 $^{\circ}C$. The Full VBOP Formulation is Used. Loading Prior to Relaxation is Conducted at Constant Strain Rates of 10^{-6} and 10^{-5} s^{-1} at 288 $^{\circ}C$.

results give an estimate of the equilibrium stress for the slowest prior loading rate as 13.9 MPa.

This value of the equilibrium stress at the strain of 4.5% was used to determine the isotropic stress from

$$A = \{g - E_t \epsilon\}, \tag{A.9}$$

where the brackets $\{n\}$ designate the asymptotic limit of n. For PMR-15 the isotropic stress $A = 13.1$ MPa was established.

The viscosity function is determined by a fit to the experimental stress drop during relaxation for prior strain rates of 10^{-6} and 10^{-5} s^{-1}, shown in Figure A.1. The viscosity function parameters were found to be $k_1 = 1.0e4$ s, $k_2 = 30$ MPa, and $k_3 = 15$.

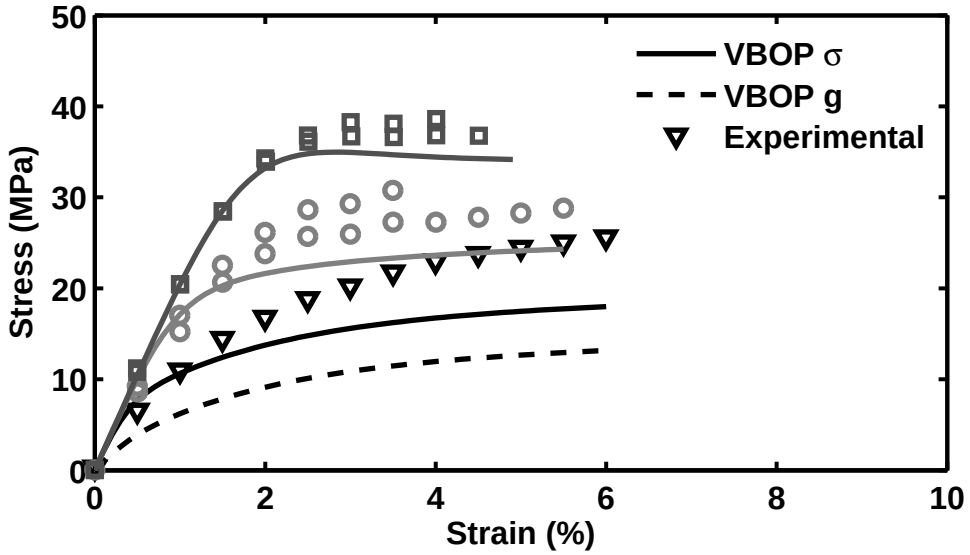

Figure A.2: A Comparison Between Experimental Results and Simulated Stress-Strain Curves for PMR-15 Polymer at 288 $^{\circ}C$. The Full VBOP Formulation is Used. Tensile Tests to Failure Conducted at Constant Strain Rates of 10^{-6}, 10^{-5}, and 10^{-4} s^{-1} at 288 $^{\circ}C$. The Model Under-Predicts the Equilibrium Stress and the Stress in the Region of Plastic Flow.

The shape function is determined by a fit to the knee of the stress-strain curves as illustrated in Figure A.2. The shape function parameters used for the simulations in the figure were $C_1 = 10\ MPa$, $C_2 = 600\ MPa$, $C_3 = 10$, $C_4 = 1$, $\xi = 1\ MPa^{-1}$, and $\zeta = 2$. A set of shape function constants that matched the data well was not found for this case. The results in Figure A.2 demonstrate the under-prediction of the stress and the equilibrium stress in the region of fully developed plastic flow. Different values of the shape function parameters varied the knee of the stress-strain curves, however the low prediction of equilibrium stress was hindering the ability to accurately predict the flow stress past the knee. Therefore, the equilibrium stress was

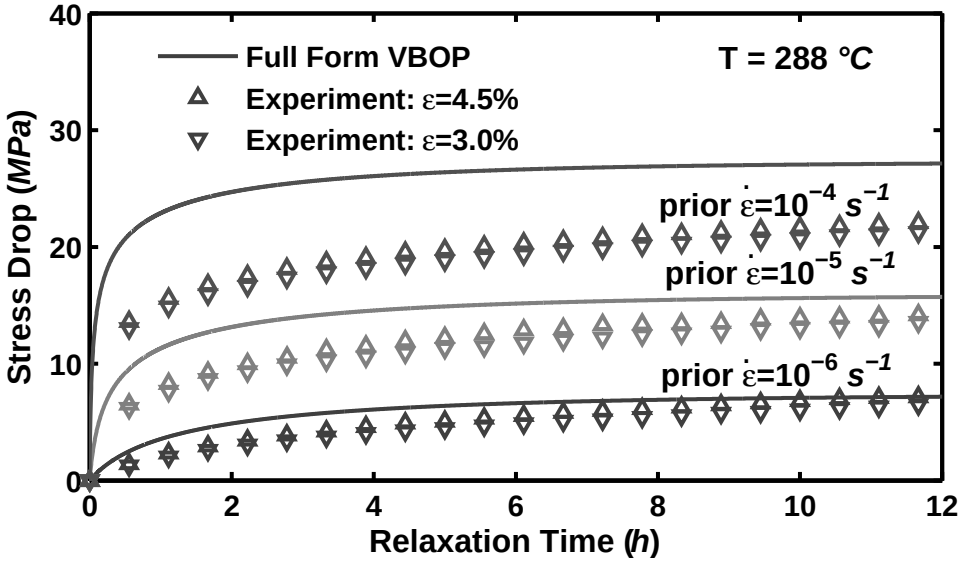

Figure A.3: A Comparison Between Experimental Results and Simulated Stress Drop During Relaxation for PMR-15 Polymer at 288 $°C$. The Full VBOP Formulation is Used, the Optimization Objective Function is Updated. Loading Prior to Relaxation is Conducted at Constant Strain Rates of 10^{-6}, 10^{-5}, and 10^{-4} s^{-1} at 288 $°C$. The Model Over Predicts the Stress Drop During Relaxation.

re-evaluated and the value was increased, resulting in an increase in the isotropic stress up to $A = 20\ MPa$, and the characterization of the viscosity function re-determined.

When iterating back on the flow chart based on initial unacceptable results following the determination of Ψ, one may also asses the regions to which the functions are being matched. For instance, in this case, the viscosity function is once again, determined by a fit to the experimental stress drop during relaxation. However, this time it is fit for the prior strain rates of 10^{-6}, 10^{-5}, and 10^{-4} s^{-1}, as shown in Figure A.3 to better capture the effect of the prior strain rate on the stress drop during relaxation. The viscosity function parameters were found to be $k_1 = 1.0e4\ s$,

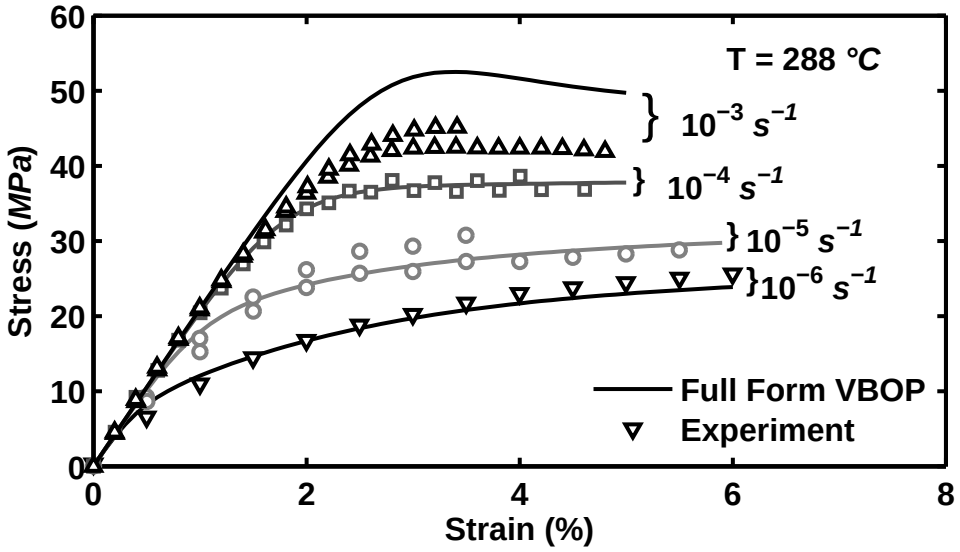

Figure A.4: A Comparison Between Experimental Results and Simulated Stress-Strain Curves for PMR-15 Polymer at 288 $^{\circ}C$. The Full VBOP Formulation is Used, the Optimization Objective Function is Updated. Tensile Tests to Failure Conducted at Constant Strain Rates of 10^{-6}, 10^{-5}, 10^{-4}, and 10^{-3} s^{-1} at 288 $^{\circ}C$. The Model Over Predicts the Stress at the Strain Rate of 10^{-3} s^{-1}.

$k_2 = 35\ MPa$, and $k_3 = 12$. With these parameters, the model over-predicts the stress drop during relaxation especially for the prior strain rate of 10^{-4} s^{-1}.

The shape function is determined by a fit to the knee of the stress-strain curve as illustrated in Figure A.4. The VBOP was fit to the experimental results at the strain rates of 10^{-6}, 10^{-5}, 10^{-4}, and 10^{-3} s^{-1} in this case. The shape function parameters were found to be $C_1 = 100\ MPa$, $C_2 = 750\ MPa$, $C_3 = 10$, $C_4 = 1$, $\xi = 1\ MPa^{-1}$, and $\zeta = 2$. The model simulations exhibit an overshoot in the beginning of the knee especially at the strain rate of 10^{-3} s^{-1}.

The C_1^* function embedded in the shape function was designed to match the unloading behavior of Nylon-66 which exhibits a reduced dependence upon strain rate

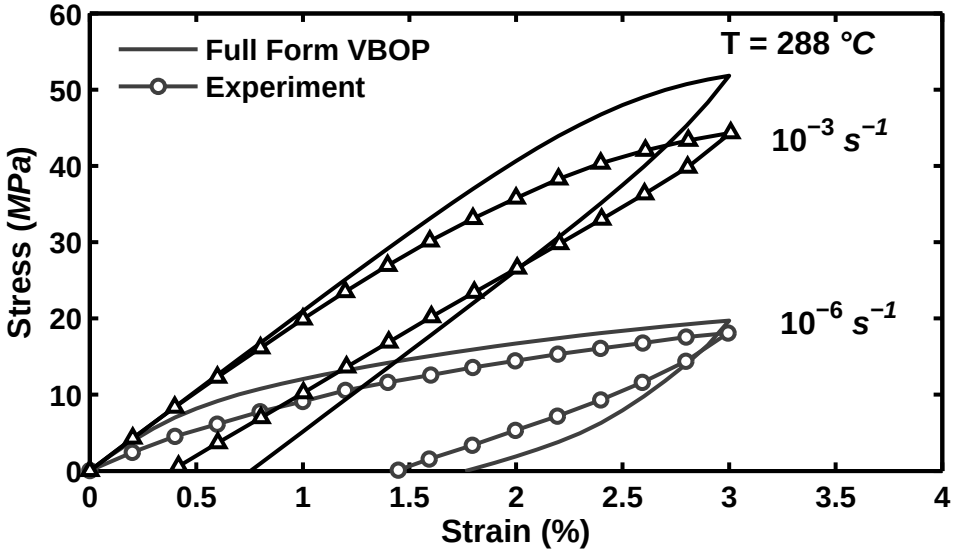

Figure A.5: A Comparison Between Experimental Results and Predicted Stress-Strain Curves for PMR-15 Polymer at 288 $^{\circ}C$. The Full VBOP Formulation is Used, the Optimization Objective Function is Updated. Loading/Unloading Tests Conducted at Constant Strain Rates of 10^{-6}, 10^{-5}, 10^{-4}, and 10^{-3} s^{-1}. C_1^* Term Does Not Contribute to the Unloading as Desired.

during unloading, and also to increase the curvature of the unloading stress-strain curve. Because the PMR-15 exhibits significant rate dependence during unloading as well as significant curvature, the C_1^* function was explored with parameter values ranging several orders of magnitude. Varying the values of the parameters C_4, ξ, and ζ did not improve the predictions of the unloading as desired. The predictions of the unloading behavior with the final values $C_1 = 100\ MPa$, $C_2 = 750\ MPa$, $C_3 = 10$, $C_4 = 1$, $\xi = 1\ MPa^{-1}$, and $\zeta = 2$ are illustrated in Figure A.5.

The full VBOP parameters for the PMR-15 are summarized in Table A.1.

Table A.1: VBOP Full Form Material Parameters for PMR-15 at 288 $^{\circ}C$.

Moduli	$E = 2100\ MPa$, $E_t = 18\ MPa$
Isotropic Stress	$A = 20\ MPa$
Viscosity Function	$k_1 = 1.0e4\ s$, $k_2 = 35\ MPa$, $k_3 = 12$
Shape Function	$C_1 = 100\ MPa$, $C_2 = 750\ MPa$, $C_3 = 10$, $C_4 = 1$, $\xi = 1\ MPa^{-1}$, $\zeta = 2$

The modeling efforts with the full VBOP formulation display the following discrepancies with the experimental results:

- Over-prediction of stress drop during relaxation.
- Over-prediction of knee in stress-strain curve.
- Room for improvement in predictions of unloading behavior.

The over-prediction of stress drop during relaxation can be addressed by modifying the growth law for the equilibrium stress. The $\Psi\frac{(\dot{\sigma}-\dot{g})}{E}$ term is intended to increase the stress drop during relaxation. Therefore, to reduce this quantity, the $\Psi\frac{(\dot{\sigma}-\dot{g})}{E}$ term is removed.

It was not immediately obvious what modifications would improve the prediction of the knee in the stress-strain curve. At the same time, the inclusion of the C_1^* term was complicating the model without adding to its predictive capability. Therefore, to decrease the unnecessary complexity of the model, the C_1^* term was removed. These changes are discussed in more detail in the following section.

A.2 Modified VBOP Formulation Dictated by Experimental Observations

The modifications to VBOP formulation based on experimental observations are outlined in this section. The two equations which change in form are the growth law for the equilibrium stress and the shape function.

The uniaxial flow law:

$$\dot{\epsilon} = \dot{\epsilon}^{el} + \dot{\epsilon}^{in} = \frac{\dot{\sigma}}{E} + \frac{\sigma - g}{Ek} \tag{A.10}$$

Equilibrium stress evolution:

$$\dot{g} = \Psi \frac{\dot{\sigma}}{E} + \Psi \left[\frac{(\sigma - g)}{Ek} - \frac{(g - f)}{A} \left| \frac{(\sigma - g)}{Ek} \right| \right] + \left[1 - \frac{\Psi}{E} \right] \dot{f} \tag{A.11}$$

Kinematic stress evolution:

$$\dot{f} = \left[\frac{|\sigma|}{\Gamma + |g|} \right] E_t \frac{(\sigma - g)}{Ek} \tag{A.12}$$

Isotropic stress evolution:

$$\dot{A} = A_c [A_f - A] \left| \frac{\sigma - g}{Ek} \right| \tag{A.13}$$

Shape function:

$$\Psi = C_1 + (C_2 - C_1)e^{-C_3|\epsilon^{in}|} \tag{A.14}$$

Viscosity function:

$$k = k_1 \left(1 + \frac{\Gamma}{k_2}\right)^{-k_3} \tag{A.15}$$

Overstress Invariant:

$$\Gamma = |\sigma - g| \tag{A.16}$$

The systematic characterization procedure was employed together with the new formulation to determine the model parameters for the PMR-15 neat resin at 288 $^{\circ}C$. The elastic modulus, tangent modulus, and isotropic stress values were not changed in the modified formulation. These values were still measured to be $E = 2100\ MPa$, $E_t = 18\ MPa$, and $A = 20\ MPa$.

The viscosity function was determined by a fit to the experimental stress drop during relaxation, shown in Figure A.6. The viscosity function parameters were found to be $k_1 = 1.0e4\ s$, $k_2 = 35\ MPa$, and $k_3 = 12$. The modification to the equilibrium stress did indeed decrease the prediction of the stress drop during relaxation, resulting in a more accurate representation of the experimental results.

The shape function is determined by a fit to the knee of the stress-strain curve as illustrated in Figure A.7. The shape function parameters were found to be $C_1 = 100\ MPa$, $C_2 = 1.0e3\ MPa$, and $C_3 = 10$. The modifications to the shape

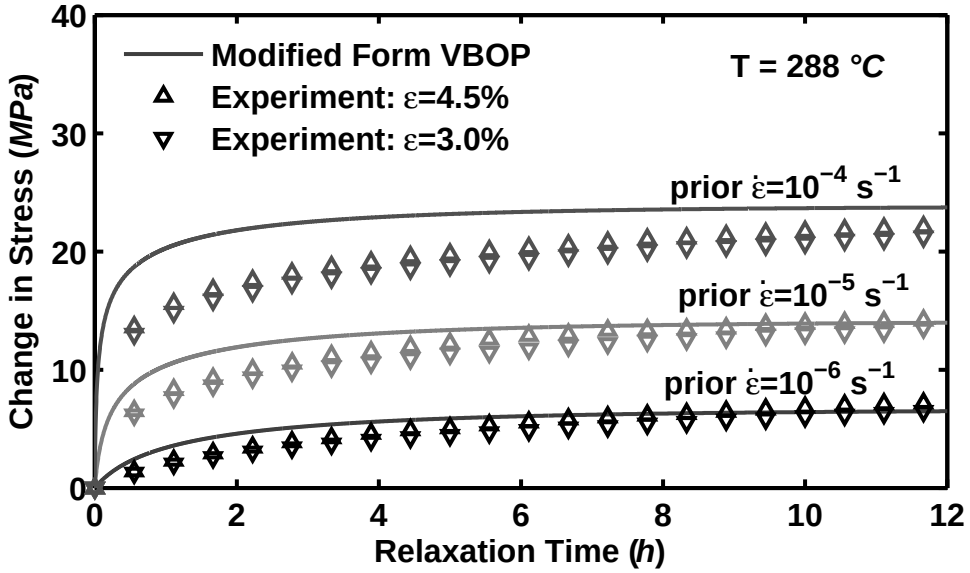

Figure A.6: A Comparison Between Experimental and Simulations Using the Modified Form VBOP Stress Drop During Relaxation Obtained for PMR-15 Polymer at 288 $^{\circ}C$. Loading Prior to Relaxation is Conducted at Constant Strain Rates of 10^{-6}, 10^{-5}, and 10^{-4} s^{-1} at 288 $^{\circ}C$. The Model Representation of the Stress Drop During Relaxation is More Accurate.

Table A.2: VBOP Modified Form Material Parameters for PMR-15 at 288 $^{\circ}C$.

Moduli	$E = 2100\ MPa$, $E_t = 18\ MPa$
Isotropic Stress	$A = 20\ MPa$
Viscosity Function	$k_1 = 1.0e4\ s$, $k_2 = 35\ MPa$, $k_3 = 12$
Shape Function	$C_1 = 100\ MPa$, $C_2 = 1.0e3\ MPa$, $C_3 = 10$

function not only simplify the VBOP formulation, they also more accurately capture the knee of the stress-strain curve.

The modified VBOP parameters for the PMR-15 are summarized in Table A.2.

The predictions of the unloading behavior of the PMR-15 are illustrated in Figure A.8. The model captures the qualitative effect of the strain rate on the unloading behavior. Unfortunately the model still does not reproduce the unloading behavior

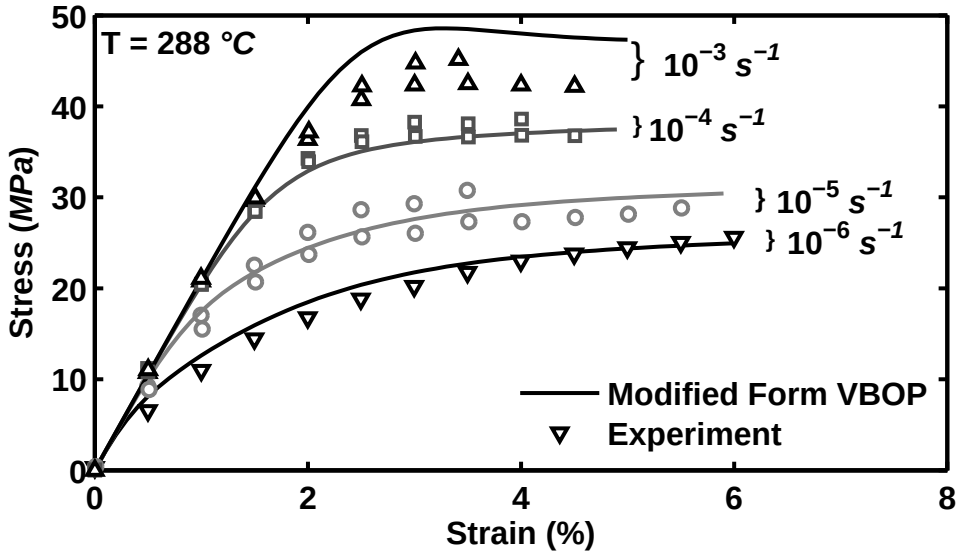

Figure A.7: A Comparison Between Experimental Results and the Simulated Stress-Strain Curves Obtained for PMR-15 Polymer at 288 $^{\circ}C$. Tensile Tests to Failure Conducted at Constant Strain Rates of 10^{-6}, 10^{-5}, 10^{-4}, and 10^{-3} s^{-1} at 288 $^{\circ}C$. The Modified Form of the VBOP is Used. The Model Representation of the Stress at the Strain Rate of 10^{-3} s^{-1} is More Accurate.

with the desired accuracy. Modifying the formulation to more accurately predict the unloading behavior is strongly suggested as a direction for future research.

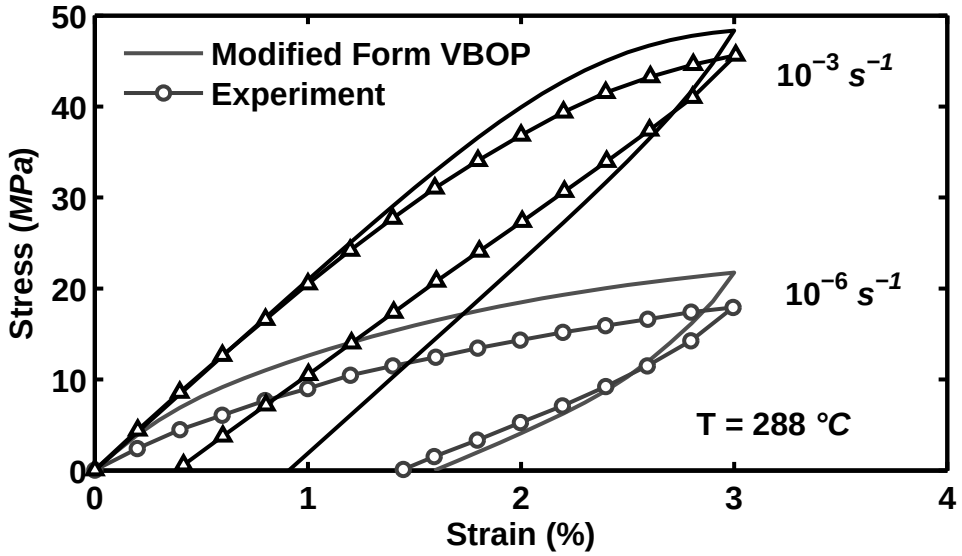

Figure A.8: A Comparison Between Experimental Results and Predicted Stress-Strain Curves Obtained for PMR-15 Polymer at 288 $^{\circ}C$. Loading and Unloading is Conducted at Constant Strain Rate Magnitudes of 10^{-6}, 10^{-5}, 10^{-4}, and 10^{-3} s^{-1} at 288 $^{\circ}C$. The Modified Form of the VBOP is Used.

Appendix B. Modeling Details

This appendix provides a description of the details surrounding the modeling of the material behavior using MATLAB.

B.1 Constitutive Equations for Stress-Controlled Loading

The state variable functions for stress-controlled loading in the MATLAB code are as follows.:

Y - State Variable Vector

Ydot - Derivative of the State Variable Vector

sig = Y(1) - Stress

g = Y(2) - Equilibrium Stress

eta = Y(3) - Strain

A = Y(4) - Isotropic Stress

f = Y(5) - Kinematic Stress

p = Y(6) - Accumulated Inelastic Strain

lr = Y(7) - Stress Load Rate

The MATLAB code developed in this research uses the following equations for modeling stress-controlled behavior (Note: comments are signified with %):

sigdot=lr;

%Look to the "materialparams" file to find the values of the various parameters.

$[E, Et, Ao, k1, k2, k3, C1, C2, C3]$ =materialparams();

```
%Calculate various functions and numbers.

L = abs(sig-g); %Overstress invariant

k = kfunction(L); %Viscosity Function k

etain=eta-sig./E; %Inelastic Strain (Total-Elastic)


psi = C1 + (C2-C1).*exp(-C3.*abs(etain)); %Shape Function

rin = (sig-g)./E./k; %Inelastic Strain Rate


%Derivatives

etadot = sigdot./E+rin; %Strain Rate


fdot = (abs(sig)./(L+abs(g)))*Et.*rin; %Kinetic Stress Rate


pdot = abs(rin); %Inelastic Strain Rate


%Equilibruim Stress Rate Equation

gdot = psi.*sigdot./E + psi.*(rin-(g-f)./A.*L./E./k)+(1-psi./E).*fdot;


%Repack Ydot

Ydot = [sigdot; gdot; etadot; 0; fdot; pdot;0];
```

B.2 Constitutive Equations for Strain-Controlled Loading

The state variable functions for strain-controlled loading in the MATLAB code are as follows:

Y - State Variable Vector

Ydot - Derivative of the State Variable Vector

sig = Y(1) - Stress

g = Y(2) - Equilibrium Stress

eta = Y(3) - Strain

A = Y(4) - Isotropic Stress

f = Y(5) - Kinematic Stress

p = Y(6) - Accumulated Inelastic Strain

lr = Y(7) - Strain Load Rate

The MATLAB code developed in this research uses the following equations for modeling strain-controlled behavior:

etadot=lr;

%Look to the "materialparams" file to find the values of the various parameters.

$[E, Et, Ao, k1, k2, k3, C1, C2, C3]$ =materialparams();

%Calculate various functions and numbers.

L = abs(sig-g); %Overstress invariant

k = kfunction(L); %Viscosity Function k

```
etain=eta-sig./E; %Inelastic Strain (Total-Elastic)

psi = C1 + (C2-C1).*exp(-C3.*abs(etain)); %Shape Function

rin = (sig-g)./E./k; %Inelastic Strain Rate

%Derivatives

sigdot = (etadot-rin).*E; %Stress Rate

fdot = (abs(sig)./(L+abs(g)))*Et.*rin; %Kinetic Stress Rate

pdot = abs(rin); %Inelastic Strain Rate

%Equilibruim Stress Rate Equation

gdot = psi.*sigdot./E + psi.*(rin-(g-f)./A.*L./E./k)+(1-psi./E).*fdot;

%Repack Ydot

Ydot = [sigdot; gdot; etadot; 0; fdot; pdot;0];
```

Appendix C. The Optimization Techniques Employed in Determining the Parameters of the Viscosity Function and the Shape Function

This appendix provides an explanation of optimization efforts carried out during this research effort. The optimization was conducted by means of the 'lsqcurvefit' command built into MATLAB. This routine does a least squares optimization or "curve fit" of the designated parameters to fit them to the desired experimental data.

C.1 Initial Optimization of Viscosity Function

Initially the least square optimization was used to fit the full VBOP formulation (discussed in section A.1) to the stress drop throughout relaxation for the prior strain rates of 10^{-6} and 10^{-5} s^{-1}. (At that point we did not yet have data for the stress drop after a prior strain rate of 10^{-4} s^{-1}.) This optimization elucidated the values of $k_1 = 1.98e+05$ s, $k_2 = 14.8$ MPa, and $k_3 = 6.04$. The simulations are compared to the experimental data in Figure C.1.

Once determining these viscosity function parameters, the evaluation of the shape function parameters was conducted using the loading followed by unloading experimental results. The simulations of loading followed by unloading exhibited unreasonable stiffness in the beginning of the stress-strain curve causing an unreasonable overshoot of simulation compared to the experimental data regardless of the shape function parameters employed for the two slower strain rates. An example simulation for shape function parameters of $C_1 = 400$, $C_2 = 1,060$ and $C_3 = 10$ are shown in

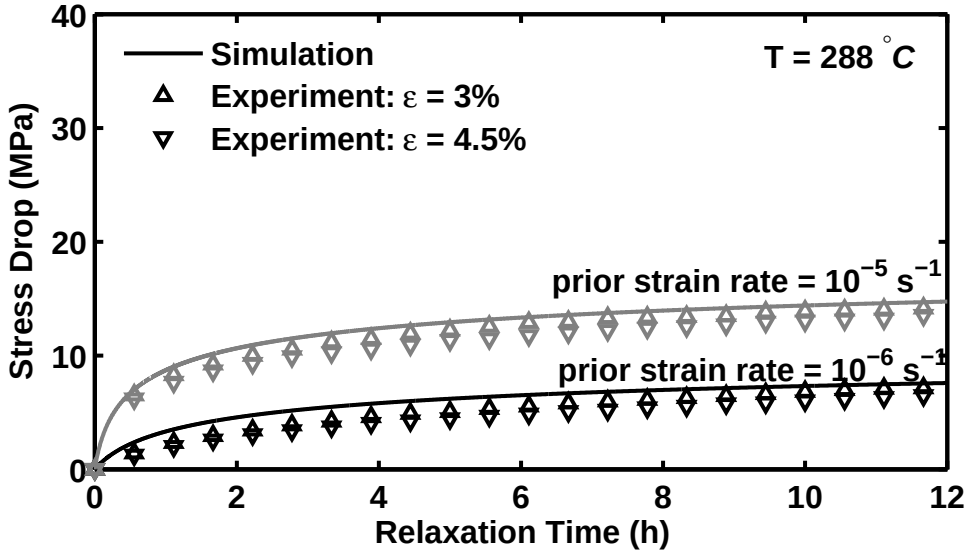

Figure C.1: Stress Decrease vs Relaxation Time for the PMR-15 Polymer at 288 $°C$. The Viscosity Function Parameters were Optimized Using a Least Square Curve Fit to the Stress Drop During Relaxation for Prior Strain Rates of 10^{-6} and 10^{-5} s^{-1}.

Figure C.2. At the two faster strain rates the simulations exhibit nearly linear behavior throughout the simulations. These unreasonable simulations were attributed to the high value of the k_1 parameter. Therefore, in the future optimizations the viscosity function parameters were fit to the stress drop values in the last two hours of relaxation. This slight decrease in simulation capability in stress-drop during relaxation allowed for a reasonable agreement for a wider range of loading histories (for example, monotonic loading and creep).

C.2 Refined Optimization of Viscosity Function

The optimization was then refined to fit to the VBOP simulations to the experimental stress values in the last two hours of the relaxation periods. The specific formulation of the VBOP employed was also altered to better fit the observed be-

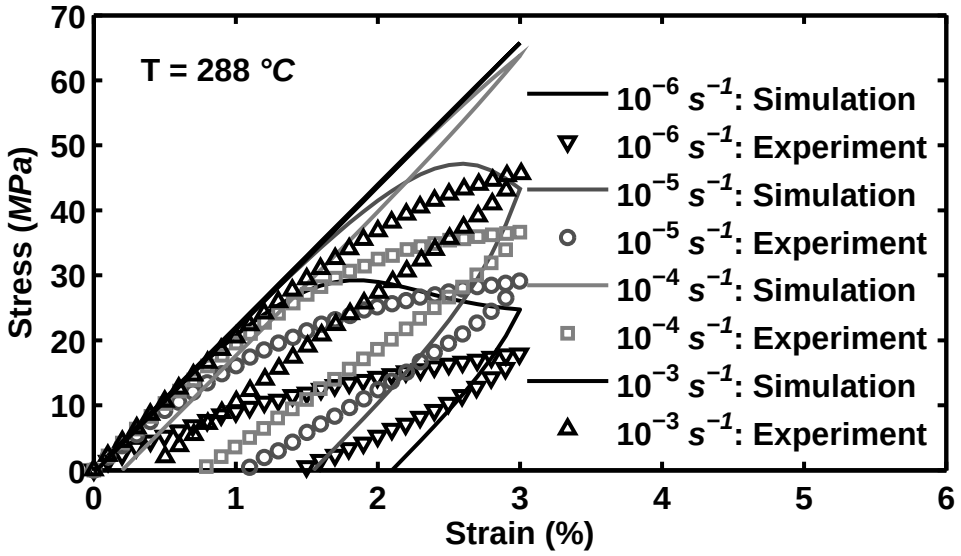

Figure C.2: A Comparison Between Experimental and Predicted Stress-Strain Curves Obtained for PMR-15 Polymer in Loading and Unloading at Constant Strain Rates of 10^{-6}, 10^{-5}, 10^{-4}, and 10^{-3} s^{-1} at 288 $°C$. The Shape Function Parameters Cannot Correct the Overshoot Caused by the High Value of k_1.

havior of the PMR-15. (For more details on the modification of the formulation see Appendix A.) The parameters of the viscosity function using this optimization were found to be $k_1 = 1.0e+04$ s, $k_2 = 35$ MPa, and $k_3 = 12$. The simulations are compared to the experimental results in Figure C.3.

C.3 Expansion to Optimization of Shape Function

Once the appropriate viscosity function parameters were determined, the shape function is found as the next step in the systematic characterization procedure shown in flowchart 7.3. The shape function parameters were also found using the 'lsqcurvefit' command built into MATLAB to fit the simulation to the knee of the stress-strain curves of the experimental data from the tension to failure results. The resulting

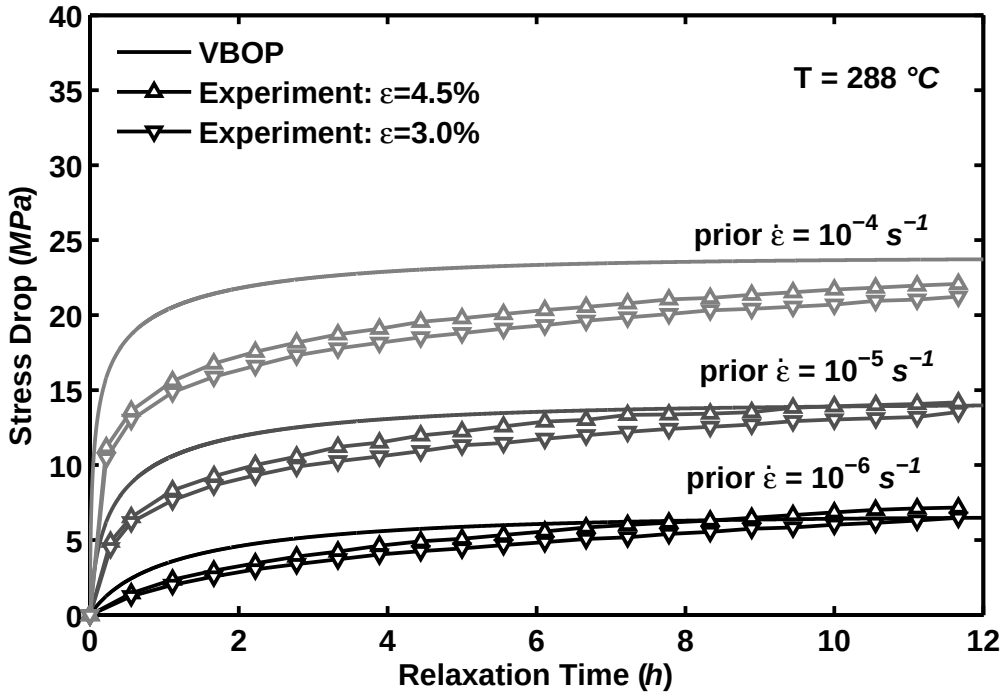

Figure C.3: Stress Decrease vs Relaxation Time for the PMR-15 Polymer at 288 $^{\circ}C$. The Viscosity Function Parameters were Optimized Using a Least Square Curve Fit to the Last Two Hours of Relaxation for the Prior Strain Rates of 10^{-6}, 10^{-5}, 10^{-4} s^{-1} .

shape function parameters were $C_1 = 100\ MPa$, $C_2 = 1,000\ MPa$, and $C_3 = 10$. The simulations are compared to the experimental results in Figure C.4.

C.4 Combined Optimization of Viscosity and Shape Function

As a final step in this study, the optimization procedure was expanded to a more sophisticated form. In this form, the Viscosity Function Parameters and the Shape Function Parameters were found simultaneously using both tension to failure results and stress drop during relaxation results.

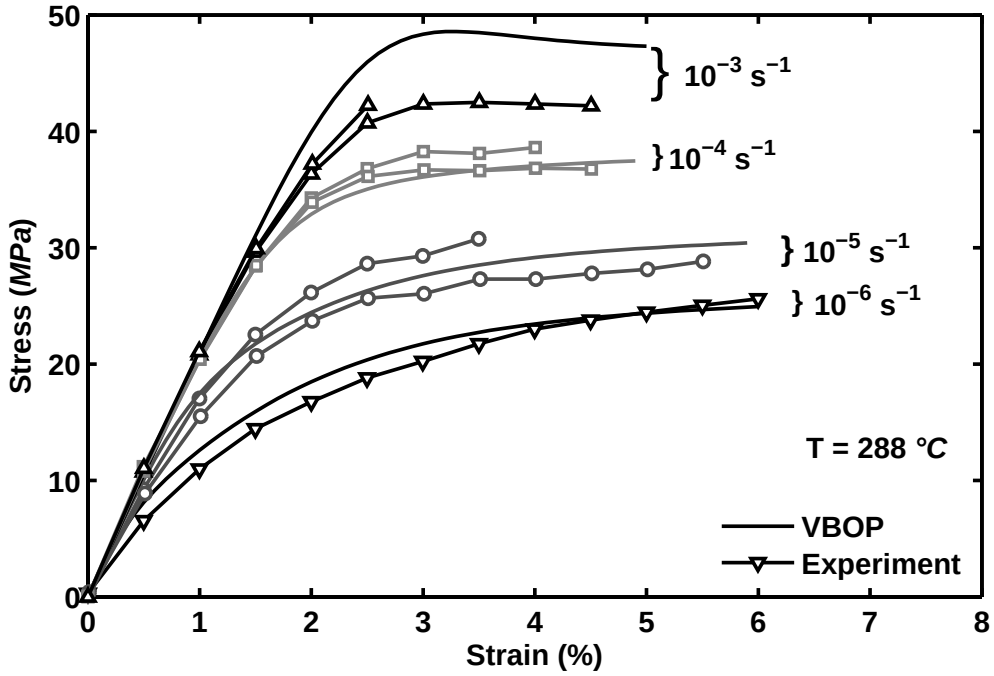

Figure C.4: A Comparison Between Experimental and Predicted Stress-Strain Curves Obtained for PMR-15 Polymer at Constant Strain Rates of 10^{-6}, 10^{-5}, 10^{-4}, and 10^{-3} s^{-1} at 288 $^{\circ}C$. The Shape Function Parameters were Optimized Using a Least Square Curve Fit.

The resulting parameters found by the optimization method were $k_1 = 1.1e4$ s, $k_2 = 34.5$ MPa, $k_3 = 12.4$, $C_1 = 100$ MPa, $C_2 = 944$ MPa, and $C_3 = 10$. These values are very similar to those found using the optimization in the individual steps of the characterization procedure (listed in sections C.2 and C.3). The simulations are compared to the experimental data in Figures C.5 and C.6. These optimized values validate the parameters that were found using the systematic characterization method in Chapter VII. In conclusion, either approach to finding the viscosity function and shape function parameters can be successfully employed.

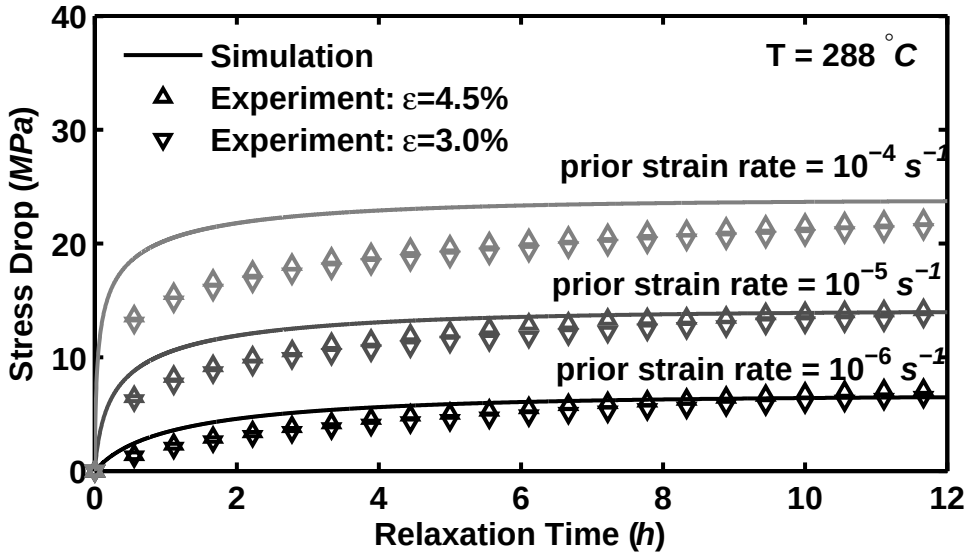

Figure C.5: A Comparison Between Experimental Results and Simulated Stress Drop During Relaxation for PMR-15 Polymer at 288 $^{\circ}C$. Loading Prior to Relaxation is Conducted at Constant Strain Rates of 10^{-6}, 10^{-5}, and 10^{-4} s^{-1} at 288 $^{\circ}C$. The Viscosity Function and Shape Function Parameters Were Found Simultaneously During the Optimization.

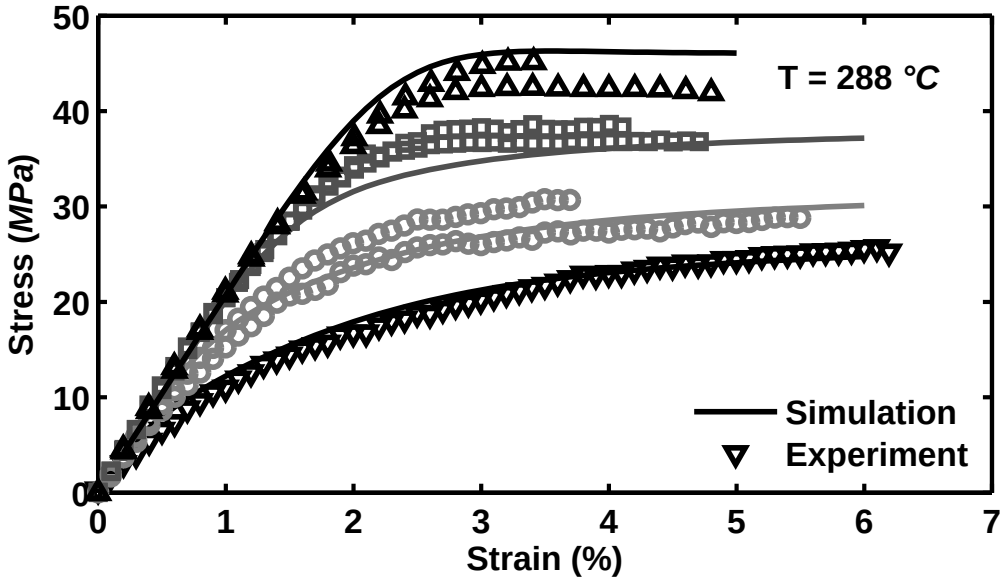

Figure C.6: A Comparison Between Experimental and Predicted Stress-Strain Curves Obtained for PMR-15 Polymer at Constant Strain Rates of 10^{-6}, 10^{-5}, 10^{-4}, and 10^{-3} s^{-1} at 288 $^{\circ}C$. The Viscosity Function and Shape Function Parameters Were Found Simultaneously During the Optimization.

Bibliography

1. Abdel-Tawab, Khaled I. and Y. Jack Weitsman. *A Continuum Model for Viscoelasticity, Damage, and Permanent Deformation with Application to Swirl-Mat Polymeric Composites*. Contract MAES96-3.0-CM, Office of Naval Research, Department of Mechanical and Aerospace Engineering and Engineering Science, The University of Tennessee, Knoxville, TN, July 1996.

2. Badir, Ashraf, Brian Shonkwiler, and Ramesh Talreja. *Fatigue Property Characterization of T650-35/AMB21 Laminates Under Room and Elevated Temperature*. Technical Report AIAA 2002-1679, American Institute of Aeronautics and Astronautics, 2002.

3. Balaconis, John G. *Some Aspects of the Mechanical Response of BMI 5250-4 Neat Resin at* 191 $^{\circ}C$*: Experiment and Modeling*. Master's thesis, Department of Aeronautics and Astronautics, Air Force Institute of Technology, Wright-Patterson Air Force Base, Ohio, 2006.

4. Bordonaro, Christine M. and Erhard Krempl. "Effects of Strain Rate on the Deformation and Relaxation Behavior of 6/6 Nylon at Room Temperature". *Polymer Engineering and Science*, 32(16):1066–1072, 1992.

5. Bordonaro, Christine Marie. *Rate Dependent Mechanical Behavior of High Strength Plastics: Experiment and Modeling*. Ph.D. thesis, Department of Mechanical Engineering, Aeronautical Engineering and Mechanics, Rensselaer Polytechnic Institute, Troy, NY, 1995.

6. Bowles, K.J., D.S. Papadopoulos, L.L. Ingrahm, L.S. McCorkle, and O.V. Klah. *Longtime Durability of PMR-15 Matrix Polymer at 204, 260, 288, and 316* $^{\circ}C$. TM 210602, NASA/Glenn Research Center, 2001.

7. Broeckert, Joseph L. *Effects of Prior Aging at Elevated Temperature in Air and in Argon Environments on Creep Response of PMR-15 Neat Resin at* 288 $^{\circ}C$. Master's thesis, Department of Aeronautics and Astronautics, Air Force Institute of Technology, Wright-Patterson Air Force Base, Ohio, 2007.

8. Cardon, A.H., Y. Qin, and C. Van Vossole. "Durability Analysis of Polymer Matrix Composites for Structural Applications". *Computers and Structures*, 76(1-3):35–41, April 2000.

9. Cernocky, E. P. and E. Krempl. "A Non-Linear Uniaxial Integral Constitutive Equation Incorporating Rate Effects, Creep, and Relaxation". *Internat. J. Non-Linear Mechanics*, 14(3):183–203, 1979. ISSN 0091-4037.

10. Cernocky, E.P. and E. Krempl. *A Theory of Viscoplasticity Based on Infinitesimal Total Strain*. Contract RPI CS 78-3, Rensselaer Polytechnic Institute, May 1978.

11. Colak, Ozgen U. "Modeling Deformation Behavior of Polymers with Viscoplasticity Theory Based on Overstress". *International Journal of Plasticity*, 21:145–160, 2005.

12. Colak, Ozgen U. and Necmi Dusunceli. "Modeling Viscoelastic and Viscoplastic Behavior of High Density Polyethylene (HDPE)". *J Eng Mater Technol, Trans ASME*, 128:572–578, 2006.

13. Dusunceli, Necmi and Ozgen U. Colak. "High Density Polyethylene (HDPE): Experiments and Modeling". *Mech Time-Depend Mater*, 10:331–345, 2006.

14. Elahi, M. and Y.J. Weitsman. *Some Aspects of the Deformation Response of Swirl-Mat Composites*. Contract ORNL/TM-13521, Oak Ridge National Laboratories, Oak Ridge, Tennessee, October 1999. Managed by Lockheed Martin Energy Research Corp. for the U.S. Department of Energy under contract DE-AC05-96OR22464.

15. Falcone, C. M. and M.B. Ruggles-Wrenn. "Rate Dependence and Short-Term Creep Behavior of a Thermoset Polymer at Elevated Temperature". *Journal of Pressure Vessel Technology, Trans ASME*, In press.

16. Falcone, Christina M. *Some Aspects of the Mechanical Response of PMR-15 Neat Resin at* 288 $^{\circ}C$*: Experiment and Modeling*. Master's thesis, Department of Aeronautics and Astronautics, Air Force Institute of Technology, Wright-Patterson Air Force Base, Ohio, 2006.

17. Findley, William N., James S. Lai, and Kasif Onaran. *Creep and Relaxation of Nonlinear Viscoelastic Materials*, volume 18 of *Applied Mathematics and Mechanics*. North-Holland, New York, 1976.

18. Flügge, Wilhelm. *Viscoelasticity*. Springer-Verlag, New York, second revised edition, 1975.

19. Hall, R., G. Schoeppner, K. Pochiraju, G. Tandon, E. Iarve, and E. Mollenhauer. "Progress Toward Thermodynamic Environmental Durability Modeling of High Temperature Polymer Matrix Composites". *Proceedings of the 5th International Conference on Mechanics of Time Dependent Materials*, October 2005.

20. Ho, Kwangsoo. *Application of the Viscoplasticity Theory Based on Overstress to the Modeling of Dynamic Strain Aging of Metals and to the Modeling of the Solid Polymers, Specifically to Nylon 66*. Ph.D. thesis, Department of Mechanical Engineering, Aeronautical Engineering and Mechanics, Rensselaer Polytechnic Institute, Troy, NY, 1998.

21. Ho, Kwangsoo. "Modeling of Nonlinear Rate Sensitivity by Using an Overstress Model". *CMES*, 2(3):351–364, 2001.

22. Ho, Kwangsoo and Erhard Krempl. "Modeling of Positive, Negative and Zero Rate Sensitivity by Using the Viscoplasticity Theory Based on Overstress(VBO)". *Mech Time-Depend Mater*, 4:21–42, 2000.

23. Ho, Kwangsoo and Erhard Krempl. "Extension of the Viscoplasticity Theory Based on Overstress (VBO) to Capture Non-Standard Rate Dependence in Solids". *International Journal of Plasticity*, 18:851–872, 2002.

24. Hu, Yafei, Zihui Xia, and Fernand Ellyin. "Deformation Behavior of an Epoxy Resin Subject to Multiaxial Loadings. Part I: Experimental Investigations". *Polymer Engineering and Science*, 43(3):721–733, 2003.

25. Khan, Fazeel. *The Deformation Behavior of Solid Polymers and Modeling with the Viscoplasticity Theory Based on Overstress*. Ph.D. thesis, Department of Mechanical Engineering, Aeronautical Engineering and Mechanics, Rensselaer Polytechnic Institute, Troy, NY, 2002.

26. Khan, Fazeel. "Loading History Effects on the Creep and Relaxation Behavior of Thermoplastics". *J Eng Mater Technol, Trans ASME*, 128:564–571, 2006.

27. Khan, Fazeel and Erhard Krempl. "Pre-Necking and Post-Necking Relaxation and Creep Behavior of Polycarbonate: A Phenomenological Study". *Polymer Engineering and Science*, 44:1783–1791, 2004.

28. Khan, Fazeel and Erhard Krempl. "Amorphous and Semicrystalline Solid Polymers: Experimental and Modeling Studies of Their Inelastic Deformation Behaviors". *J Eng Mater Technol, Trans ASME*, 128:64–72, 2006.

29. Kitagawa, Masayoshi and Tomohiko Matsutani. "Effect of Time and Temperature on Nonlinear Constitutive Equation in Polypropylene". *Journal of Materials Science*, 23(11):4085–4090, November 1988.

30. Kitagawa, Masayoshi, Dexin Zhou, and Jianhui Qiu. "Stress-Strain Curves for Solid Polymers". *Polymer Engineering and Science*, 35(22):1725–1732, November 1995.

31. Krempl, E. "Models of Viscoplasticity: Some Comments on Equilibrium (Back) Stress and Drag Stress". *Acta Mechanica*, 69(1-4):25–42, December 1987.

32. Krempl, E. and V. V. Kallianpur. "Some Critical Uniaxial Experiments for Viscoplasticity at Room Temperature". *J Mech Phys Solids*, 32(4):301–314, 1984.

33. Krempl, E., J.J. McMahon, and D. Yao. "Viscoplasticity Based on Overstress with a Differential Growth Law for the Equilibrium Stress". *Nonlinear Constitutive Relations for High Temperature Application-1984, Symposium Proceedings*, 25–50. NASA, Lewis Research Center, June 1985. NASA Conference Publication 2369.

34. Krempl, Erhard. "Cyclic creep: an Interpretive Literature Survey". *Weld. Res. Counc. Bull.*, (195):63–123, June 1974.

35. Krempl, Erhard. "An Experimental Study of Room-Temperature Rate-Sensitivity, Creep and Relaxation of AISI Type 304 Stainless Steel". *J. Mech. Phys. Solids*, 27(5):363–375, 1979.

36. Krempl, Erhard. "Viscoplasticity Based on Total Strain. The Modelling of Creep with Special Considerations of Initial Strain and Aging". *J Eng Mater Technol, Trans of the ASME*, 101(4):380–386, October 1979.

37. Krempl, Erhard. "The Role of Aging in the Modeling of Elevated Temperature Deformation". B. Wilshire and D.R.J. Owen (editors), *Creep and Fracture of Engineering Materials and Structures, Proceedings of the International Conference*, 201–211. Pineridge Press, University College, Swansea, Wales, March 1981.

38. Krempl, Erhard. "The Role of Servocontrolled Testing in the Development of the Theory of Viscoplasticity Based on Total Strain and Overstress". R.W. Rohde and J.C. Swearengen (editors), *Mechanical Testing for Deformation Model Development, ASTM STP 765*, 5–28. American Society for Testing and Materials, 1982.

39. Krempl, Erhard. "From the Standard Linear Solid to the Viscoplasticity Theory Based on Overstress". S.N. Atluri, G. Yagawa, and T.A. Cruse (editors), *Computational Mechanics '95 Theory and Applications, Proceedings of the International Conference on Computational Engineering Science*, volume 2, 1679–1684. Springer, Hawaii, July-August 1995.

40. Krempl, Erhard. *Unified Constitutive Laws of Plastic Deformation*, chapter A Small-Strain Viscoplasticity Theory Based on Overstress, 281–318. Academic Press, San Diego, 1996.

41. Krempl, Erhard. "Viscoplastic Model for High Temperature Applications". *International Journal of Solids and Structures*, 37:279–291, 2000.

42. Krempl, Erhard and Christine M. Bordonaro. "A State Variable Model for High Strength Polymers". *Polymer Engineering and Science*, 35(4):310–316, 1995.

43. Krempl, Erhard and Kwangsoo Ho. "An Overstress Model for Solid Polymer Deformation Behavior Applied to Nylon 66". R.A. Schapery and C.T. Sun (editors), *Time Dependent and Nonlinear Effects in Polymers and Composites; Proceedings of the ASTM Symposium, Atlanta, GA; UNITED STATES; 4-5 May 1998*, volume 1357 of *ASTM STP*, 118–137. American Society for Testing and Materials, West Conshohocken, PA, 2000.

44. Krempl, Erhard and Kwangsoo Ho. *Deformations of Materials*, volume 1 of *Handbook of Materials Behavior Models*, chapter Inelastic Compressible and Incompressible, Isotropic Small Strain Viscoplasticity Theory Based on Overstress (VBO), 336–348. Academic Press, San Diego, 2001.

45. Krempl, Erhard and Fazeel Khan. "The Rate (Time)-Dependent Behavior: An Overview of Some Properties of Metals and Solid Polymers". *International Journal of Plasticity*, 19:1069–1095, July 2003.

46. Kujawski, D., V. Kallianpur, and E. Krempl. "An Experimental Study of Uniaxial Creep, Cyclic creep and Relaxation of AISI Type 304 Stainless Steel at Room Temperature". *J. Mech. Phys. Solids*, 28:129–148, 1980.

47. Kujawski, D. and E. Krempl. "The Rate (Time)-Dependent Behavior of Ti-7Al-2Cb-1Ta Titanium Alloy at Room Temperature Under Quasi-Static Monotonic and Cyclic Loading". *Journal of Applied Mechanics, Transactions ASME*, 48(1):55–63, March 1981.

48. Ladrido, Christine G. *Effect of Prior Aging on Fatigue Response of IM7/BMI 5250-4 Composite at* 191 $^{\circ}C$. Master's thesis, Department of Aeronautics and Astronautics, Air Force Institute of Technology, Wright-Patterson Air Force Base, Ohio, 2007.

49. Lemaitre, Jean and Jean-Louis Chaboche. *Mechanics of Solid Materials*. Cambridge University Press, Cambridge, 1990.

50. Liu, M.C.M. and E. Krempl. "A Uniaxial Viscoplastic Model Based on Total Strain and Overstress". *Journal of the Mechanics and Physics of Solids*, 27(5-6):377–391, 1979.

51. Maciucescu, Luca. *A Simplified Viscoplasticity Theory Based on Overstress for Low to High Homologous Temperature and Quasi-Static to Dynamic Applications*. Ph.D. thesis, Department of Mechanical Engineering, Aeronautical Engineering and Mechanics, Rensselaer Polytechnic Institute, Troy, NY, 2002.

52. Marias, C. and G. Villoutreix. "Analysis and Modeling of the Creep Behavior of the Thermostable PMR-15 Polyimide". *Journal of Applied Polymer Science*, 69:1983–1991, 1998.

53. McClung, A.J.W. and M.B. Ruggles-Wrenn. "Strain Rate Dependence and Short-Term Relaxation Behavior of a Thermoset Polymer at Elevated Temperature: Experiment and Modeling". *Journal of Pressure Vessel Technology, Trans ASME*, In press.

54. McClung, A.J.W. and M.B. Ruggles-Wrenn. "The Rate (Time)-Dependent Mechanical Behavior of the PMR-15 Thermoset Polymer at Elevated Temperature". *Polymer Testing*, 27:908–914, 2008.

55. Meador, Dr. Michael A. ""Green" High-Temperature Polymers". Online, March 30 2007. Http://www.grc.nasa.gov/WWW/RT1997/5000/5150delvigs.htm.

56. MTS Systems Corporation. *Model 793.00 System Software: User Information and Software Reference*. Eden Prairie, MN, 2001.

57. NASA. "DMBZ Polyimides Provide an Alternative to PMR-15 for High-Temperature Applications". Online, July 12 2007. Http://www.grc.nasa.gov/WWW/RT1995/5000/5150c.htm.

58. Papanicolaou, G.C., S.P. Zaoutsos, and A.H. Cardon. "Prediction of the Non-Linear Viscoelastic Response of Unidirectional Fiber Composites". *Composites Science and Technology*, 59(9):1311–1319, 1999.

59. Ruggles, M.B., S. Cheng, and E. Krempl. "The Rate-Dependent Mechanical Behavior of Modified 9 wt. % Cr-1 wt. % Mo steel at 538 $^{\circ}C$". *Materials Science & Engineering A*, A186(1-2):15–21, 1994.

60. Ruggles, M.B. and E. Krempl. "The Influence of Test Temperature on the Ratchetting Behavior of Type 304 Stainless Steel". *J Eng Mater Technol, Trans of the ASME*, 111(4):378–383, October 1989.

61. Ruggles, M.B. and E. Krempl. "Rate-sensitivity and Short Term Relaxation Behavior of AISI Type 304 Stainless Steel at Room Temperature and at 650 $^{\circ}C$; Influence of Prior Aging". *Journal of Pressure Vessel Technology, Trans ASME*, 113(3):385–391, August 1991.

62. Ruggles-Wrenn, M.B. and J.G. Balaconis. "Some Aspects of the Mechanical Response of BMI 5250-4 Neat Resin at 191 $^{\circ}C$: Experiment and Modeling". *Journal of Applied Polymer Science*, 107:1378–1386, 2008.

63. Ruggles-Wrenn, M.B. and J.L. Broeckert. "Effects of Prior Aging at 288 $^{\circ}C$ in Air and in Argon Environments on Creep Response of PMR-15 Neat Resin". *Journal of Applied Polymer Science*, In press.

64. Schapery, R. A. "On the Characterization of Nonlinear Viscoelastic Materials". *Polymer Engineering and Science*, 9(4):295–310, 1969.

65. Schapery, R. A. "Nonlinear Viscoelastic and Viscoplastic Constitutive Equations with Growing Damage". *International Journal of Fracture*, 97:33–66, 1999.

66. Schoeppner, G.A., G.P. Tandon, and E.R. Ripberger. "Anisotropic Oxidation and Weight Loss in PMR-15 Composites". *Composites Part A: Applied Science and Manufacturing*, 38(3):890–904, March 2007.

67. Shearer, J. Lowen, Bohdan T. Kulakowski, and John F. Gardner. *Dynamic Modeling and Control of Engineering Systems*. Prentice Hall, Upper Saddle River, N.J., second edition, 1997.

68. Shen, Xinghe, Zihui Xia, and Fernand Ellyin. "Cyclic Deformation of an Epoxy Polymer. Part I: Experimental Investigations". *Polymer Engineering and Science*, 44(12):2240–2246, 2004.

69. Smith, L.V. and Y.J. Weitsman. "Inelastic Behavior of Randomly Reinforced Polymeric Composites under Cyclic Loading". *Mech Time-Depend Mater*, 1(3):293–305, 1998.

70. Tachibana, Yukio and Erhard Krempl. "Modeling of High Homologous Temperature Deformation Behavior Using the Viscoplasticity Theory Based on Overstress (VBO): Part III - A Simplified Model". *J Eng Mater Technol, Trans ASME*, 120(3):193–196, July 1998.

71. Tandon, G.P., K.V. Pochiraju, and G.A. Schoeppner. "Modeling of Oxidative Development in PMR-15 Resin". *Polymer Degradation and Stability*, 91(8):1861–1869, August 2006.

72. Tsuji, Luis C., Hugh L. McManus, and Kenneth J. Bowles. *Mechanical Properties of Degraded PMR-15 Resin*. TM 208487, NASA/Lewis Research Center, 1998.

73. Weitsman, Y. "Coupled Damage and Moisture-Transport in Fiber-Reinforced, Polymeric Composites". *International Journal of Solids and Structures*, 23(7):1003–1025, 1987.

74. Weitsman, Y. "A Continuum Damage Model for Viscoelastic Materials". *Journal of Applied Mechanics, Trans ASME*, 55(4):773–780, 1988.

75. Westberry, Candice M. *Rate Dependence and Short-Term Creep Behavior of PMR-15 Neat Resin at* 23 *and* 288 $^{\circ}C$. Master's thesis, Department of Aeronautics and Astronautics, Air Force Institute of Technology, Wright-Patterson Air Force Base, Ohio, 2005.

76. Xia, Zihui and Fernand Ellyin. "Time-Dependent Behaviour and Viscoelastic Constitutive Modelling of an Epoxy Polymer". *Polymers and Polymer Composites*, 6(2):75–83, 1998.

77. Xia, Zihui, Yafei Hu, and Fernand Ellyin. "Deformation Behavior of an Epoxy Resin Subject to Multiaxial Loadings. Part II: Constitutive Modeling and Predictions". *Polymer Engineering and Science*, 43(3):734–748, 2003.

78. Xia, Zihui, Xinghe Shen, and Fernand Ellyin. "Cyclic Deformation of an Epoxy Polymer. Part II: Predictions of Viscoelastic Constitutive Models". *Polymer Engineering and Science*, 45(1):103–113, 2005.

79. Yamada, H. and C.Y. Li. "Stress Relaxation and Mechanical Equation of State in Austenitic Stainless Steels". *Metallurgical Transactions*, 4:2133–2136, Sept. 1973.

80. Yao, D. and E. Krempl. "Viscoplasticity Theory Based on Overstress. The prediction of Monotonic and Cyclic Proportional and Nonproportional Loading Paths of an Aluminum Alloy". *Int J Plast*, 1(3):259–274, 1985.

81. Zaoutsos, S.P., G.C. Papanicolaou, and A.H. Cardon. "On the Non-Linear Viscoelastic Behaviour of Polymer-Matrix Composites". *Composites Science and Technology*, 58(6):883–889, 1998.

82. Zhang, Yunfa, Zihui Xia, and Fernand Ellyin. "Evolution and Influence of Residual Stresses/Strain of Fiber Reinforced Laminates". *Composites Science and Technology*, 64:1613–1621, 2004.

83. Zhang, Yunfa, Zihui Xia, and Fernand Ellyin. "Nonlinear Viscoelastic Micromechanical Analysis of Fibre-Reinforced Polymer Laminates with Damage Evolution". *International Journal of Solids and Structures*, 42:591–604, 2005.

REPORT DOCUMENTATION PAGE

Form Approved
OMB No. 0704–0188

1. REPORT DATE *(DD–MM–YYYY)*	2. REPORT TYPE	3. DATES COVERED *(From — To)*
15–10–2008	Doctors's Dissertation	Oct 2005 — Oct 2008

4. TITLE AND SUBTITLE

Extension of Viscoplasticity Based on Overstress to Capture the Effects of Prior Aging on the Time Dependent Deformation Behavior of a High-Temperature Polymer: Experiments and Modeling

5a. CONTRACT NUMBER

5b. GRANT NUMBER

5c. PROGRAM ELEMENT NUMBER

6. AUTHOR(S)

Amber J.W. McClung

5d. PROJECT NUMBER

5e. TASK NUMBER

5f. WORK UNIT NUMBER

7. PERFORMING ORGANIZATION NAME(S) AND ADDRESS(ES)

Air Force Institute of Technology
Graduate School of Engineering and Management
2950 Hobson Way
WPAFB OH 45433-7765

8. PERFORMING ORGANIZATION REPORT NUMBER

AFIT/DS/ENY/08-D15

9. SPONSORING / MONITORING AGENCY NAME(S) AND ADDRESS(ES)

N/A

10. SPONSOR/MONITOR'S ACRONYM(S)

11. SPONSOR/MONITOR'S REPORT NUMBER(S)

12. DISTRIBUTION / AVAILABILITY STATEMENT

Approved for public release; distribution unlimited.

13. SUPPLEMENTARY NOTES

14. ABSTRACT The inelastic deformation behavior of PMR-15 neat resin, a high-temperature thermoset polymer, was investigated at 288 °C. The experimental program was designed to explore the influence of strain rate on tensile loading, unloading, and strain recovery behaviors. In addition, the effect of the prior strain rate on the relaxation response of the material, as well as on the creep behavior following strain controlled loading were examined. The experimental data were modeled with the Viscoplasticity Based on Overstress (VBO) theory. A systematic procedure for determining model parameters was developed and the model was employed to predict the response of the material under various test histories. Additionally the effects of prior aging at 288 °C in argon on the time (rate)-dependent behavior of the PMR-15 polymer were evaluated in a series of strain and load controlled experiments. Based on experimental results, the VBO theory was extended to capture the environmentally induced changes in the material response. Several of the VBO material parameters were expanded as functions of prior aging time. The resulting model was used to predict the high-temperature behavior of the PMR-15 polymer subjected to prior aging of various durations.

15. SUBJECT TERMS

polymer, PMR-15, creep, recovery, relaxation, prior strain rate, prior loading history, nonlinear viscoplastic theory, aging, argon

16. SECURITY CLASSIFICATION OF:			17. LIMITATION OF ABSTRACT	18. NUMBER OF PAGES	19a. NAME OF RESPONSIBLE PERSON
a. REPORT	b. ABSTRACT	c. THIS PAGE			Marina B. Ruggles-Wrenn, PhD
U	U	U	UU	217	19b. TELEPHONE NUMBER *(include area code)* (937)255-3636x4641